Dissertation

submitted to the

Combined Faculty of Natural Sciences and Mathematics

of the Ruperto Carola University of Heidelberg, Germany

For the degree of

Doctor of natural sciences

Presented by

Andrey Bolbat

Diploma of the Specialist in bioorganic chemistry from Moscow State University;

Born in 18.10.1991, Volnovakha, Ukraine;

Oral examination: 04.06.2019.

Genetically encoded FRET sensor to detect double-stranded RNA during viral infection

Referees: Prof. Dr. Edward Lemke

Prof. Dr. Ralf Bartenschlager

Table of contents

Abstract

Förster resonance energy transfer (FRET) is a quantum effect of energy transfer from the donor chromophore to the acceptor one via non-radiative dipole-dipole coupling when those chromophores are positioned close enough and in the right orientation to each other. Genetically encoded FRET sensors consist of donor and acceptor fluorescent protein pair (usually CFP/YFP) and a protein based sensing domain in between which responds to the presence or the activity of desired molecule via conformational change resulting in change of FRET efficiency. In this thesis, I developed a genetically encoded FRET sensor for detecting double stranded RNA (dsRNA) during viral infection. The response of eukaryotic cells to infection by RNA viruses is based to a large extent on the regulation by protein kinase R. Protein kinase R (PKR, RNA-regulated protein kinase, eIF2α kinase 2) becomes activated via homodimerisation in the presence of double-stranded RNA produced during replication of RNA viruses (or if endogenously present). Active PKR phosphorylates its target – mostly α subunit of eIF2 – and inhibits the translation of viral proteins. PKR is a two domain protein which consists of an N-terminal double-stranded RNA binding domain (RBD) and a C-terminal catalytic domain separated by a 100-amino acid unstructured region. The idea exploited in the current project is based on the ability of the N-terminal PKR domain to undergo a conformational change when binding double-stranded RNA, hence functioning as a sensor for double-stranded RNA. The fluorescent sensor is completed by the addition of the fluorescent proteins mTurquoise and cp173Venus forming a FRET pair. I successfully tested the sensor termed KPR1 *in vitro* as well as in HeLa Kyoto cells against double-stranded RNA and found a high FRET increase upon binding. The sensor responded well to the presence of self-replicating subgenomic Hepatitis C Virus RNA replicon in Huh7 cells. The data on detection of full Hepatitis C infection was inconclusive.

Zusammenfassung

Förster-Resonanzenergietransfer (FRET) ist ein quantenmechanischer Effekt des Energietransfers von einem Donor-Chromophor auf einen Akzeptor-Chromophor durch strahlungslose Dipol-Dipol Kopplung, wenn diese Chromophore nahe genug beieinander liegen und die richtige Orientierung haben. Genetisch kodierte FRET Sensoren bestehen aus einem Paar fluoreszierender Proteinen, dem Donor und Akzeptor (üblicherweise CFP/YFP) und einer dazwischenliegenden Protein-basierten Sensordomäne, die auf die Anwesenheit oder die Aktivität eines Moleküls durch Konformationsänderung reagiert, die in einer Änderung der FRET Effizienz resultiert.

In dieser Dissertation entwickelte ich einen genetisch kodierten FRET Sensor für die Detektion doppelsträngiger RNA (dsRNA) während viraler Infektion. Die Antwort eukaryontischer Zellen auf die Infektion durch RNA-Viren basiert hauptsächlich auf der Regulation der Proteinkinase R. Proteinkinase R (PKR, RNA-regulierte Proteinkinase, eIF2α kinase 2) wird durch Homodimerisierung aktiviert in der Anwesenheit doppelsträngiger RNA, die während der Replikation von RNA-Viren erzeugt wird (oder falls endogen vorhanden). Die aktivierte PKR phosphoryliert das Zielprotein – meist handelt es sich dabei um die α-Untereinheit von eIF2 – und inhibiert the Translation viraler Proteine. PKR ist aus zwei Domänen aufgebaut, die aus einer N-terminalen doppelsträngigen RNA Bindedomäne (RBD) und einer C-terminalen katalytischen Domäne bestehen, getrennt durch eine unstrukturierte Region mit der Länge von 100 Aminosäuren. Das gegenwärtige Projekt basiert auf der Fähigkeit der N-terminalen PKR-Domäne, konformationelle Umlagerungen bei Bindung doppelsträngiger RNA zu untergehen und so als Sensor für doppelsträngige RNA zu fungieren. Der fluoreszierende Sensor wird vervollständigt durch die fluoreszierenden Proteine mTurquoise und cp173Venus, die ein FRET-Paar bilden. Erfolgreich testete ich den Sensor KPR1 *in vitro* und in HeLa Kyoto Zellen in Anwesenheit doppelsträngiger RNA und fand einen deutlichen FRET-Anstieg infolge der Bindung. Der Sensor zeigte eine gute Antwort auf die Anwesenheit des selbst-replizierenden subgenomischen Hepatitis C Virus RNA Replicons in Huh7 Zellen. Die Daten für die Detektion einer vollständigen Hepatitis C Infektion blieben jedoch uneindeutig.

Introduction

Motivation and scientific background

Studying the biology of viral infection and virus-host interactions has been an important research area for a long time. Understanding the impact of viral infection on the cell and collecting comprehensive data about every stage of infection (cell entry, replication and the release of newly formed viral particles) is key for developing a cure from the pathogens.

Viruses are commonly classified according to the type of their genetic material and their method of replication (Baltimore classification) (Matthews and Maurin, 1979, King et al., 2018):

1) double-stranded DNA viruses (*Adenoviruses*, *Herpesviruses*);
2) positive sense single-stranded DNA viruses (*Parvoviruses*);
3) double-stranded RNA viruses (*Reoviruses*);
4) positive sense single-stranded RNA viruses (*Picornaviruses*, *Togaviruses*, *Flaviviridae*, Hepatitis C Virus (HCV), Dengue virus (DENV));
5) negative sense single-stranded RNA viruses (Orthomyxoviruses, Rhabdoviruses);
6) single-stranded RNA-RT viruses (Retroviruses);
7) double-stranded DNA-RT viruses (Hepadnaviridae).

The tools currently used to investigate viral infection (many of which are also incompatible with live cell research) exhausted themselves in terms of the information which can be collected. There is a growing request for new tools which can provide information with precise temporal and spatial resolution and based on observation and manipulation of intact live cells. In this work I aimed to contribute to the pool of newly emerging tools helping the virologists to understand pathogen-host interactions better. My interest was among RNA viruses (with the example of Hepatitis C Virus (HCV) which is arguably the best

studied RNA viruses). I decided to focus on the replication stage of the virus and produce a tool which is compatible with live cell research.

RNA-viruses

As was previously mentioned, viruses can be classified according to the type and polarity of nucleic acid molecules in the viral particle. RNA viruses include positive-sense single-stranded RNA viruses (class IV), negative-sense single-stranded RNA viruses (class V, also included ambisense RNA viruses), double-stranded RNA viruses (class III) and retroviruses (class VI). Viral particle usually contains from one to dozen copies of the nucleic acid genome together with viral proteins like polymerase or protease to help viral replication inside the cell. In the following paragraph I will mostly focus on the replication features of RNA viruses.

Positive-sense single-stranded RNA viruses form the largest group of RNA viruses. These viruses contain a single-stranded RNA molecule as a genome which is similar to cellular mRNA and thereby can be translated by the host cell machinery (Koonin and Dolja, 1993) Virion often contains viral RNA-dependent RNA polymerase enzymes (RNA replicase) to produce a negative strand which will be used as a template for the production of new positive-sense single-stranded RNAs destined to be packaged into the new viral particle (although the presence of the replicase in a viral particle is not necessary, it can be produced from a viral positive-sense RNA) (Figure 1a). Viral RNA positive strand is translated into a single protein polypeptide which later is processed by viral proteases and sometimes host enzymes to form several vital viral proteins (polymerase, protease, various structure proteins). RNA of positive-sense viruses can be infectious by itself even without the presence of a full viral particle since it encodes all the necessary proteins for the formation of a new virion. The infection power is obviously less than of a full virus but this ability of a positive-sense viral RNA is used in research to study viruses. All viral RNA

molecules have a conserved region which is called internal ribosome entry side (IRES) in their 5'-UTR (untranslated) region. It is a complicated three- or four-way secondary structure containing many RNA loops and used for host ribosome recognition and initiation of translation. The replication of these type of viruses involves the presence of double-stranded RNA intermediates of negative-sense RNA templates and a positive-sense future viral RNAs. The ratio of positive-sense RNAs to negative sense RNAs is understandably steered towards positive-sense ones (for instance, 10 times for Hepatitis C Virus).

Negative-sense viral RNA is complementary to mRNA and thus must be converted to positive-sense RNA by an RNA-dependent RNA polymerase (RNA replicase) before translation (Li et al., 2015) (Figure 1b). Other than that, this type of viruses is similar to the positive-sense single-stranded RNA viruses in many ways. One of the differences is that purified RNA of a negative-sense virus is not infectious by itself as it needs to be transcribed into positive-sense RNA. It is also for the same reason essential that a viral particle contains replicase enzyme inside a virion. There are reports that the amount of double-stranded RNA intermediate during the replication of a virus can be much lower than that of positive-sense RNA viruses (Weber et al., 2006).

An interesting type of single-stranded RNA viruses are ambisense RNA viruses (Nguyen and Haenni, 2003). They resemble negative-sense RNA viruses, except they also translate genes from the positive strand. Bunyaviruses have 3 single-stranded RNA fragments containing both positive-sense and negative-sense sections; arenaviruses are also single-stranded RNA viruses with an ambisense genome, as they have 2 fragments that are mainly negative-sense except for part of the 5'-ends of the large and small segments of their genome.

The double-stranded viruses represent a diverse group of viruses that vary widely in host range (humans, animals, plants, fungi, and bacteria), genome segment number (one to twelve), and virion organization (Wickner, 1993,

Targett-Adams et al., 2008). Partly because of that, their viral particle organization and RNA can vary significantly. The 5'-part of double-stranded RNA genome may be naked, capped or covalently linked to a viral protein. Upon infection, the genomic double-stranded RNA is transcribed in mRNAs that will both serve for translation and/or replication. mRNAs translation produces the proteins necessary for viral proliferation. Replication occurs in the host cytoplasm and converts mRNA to double-stranded genomic RNA. The double-stranded RNA is a kind of molecule that cells do not produce, and eukaryotes have various antiviral systems that detect and inactivate double-stranded RNA. To circumvent this defenses, many double-stranded RNA viruses are replicating their RNA inside the capsids (Figure 1c).

Retroviruses (Group VI) have a single-stranded RNA genome but, according to ICTV (International Committee on Taxonomy of Viruses), are not considered RNA viruses because they use DNA intermediates to replicate (Telesnitsky, 2010). Following the cell entry of a viral particle, the conversion of viral RNA genome in the cytoplasm begins. First, a complementary DNA strand is produced on top of the single-stranded viral RNA through the virion RNA-dependent DNA-polymerase (reverse transcriptase). After that, reverse transcriptase builds another DNA strand on top of the newly produced while getting rid of the old RNA template. This double-stranded DNA intermediate forms a so-called preintegration complex (PIC) with viral and some of the host proteins. PIC enters the nucleus (with a still unclear mechanism) where viral integrase inserts viral cDNA into the genome. Transcription and translation of viral DNA follows, producing single polypeptide which is digested by viral protease into proteins required for retrovirus proliferation. The most famous representative of the retrovirus class is HIV.

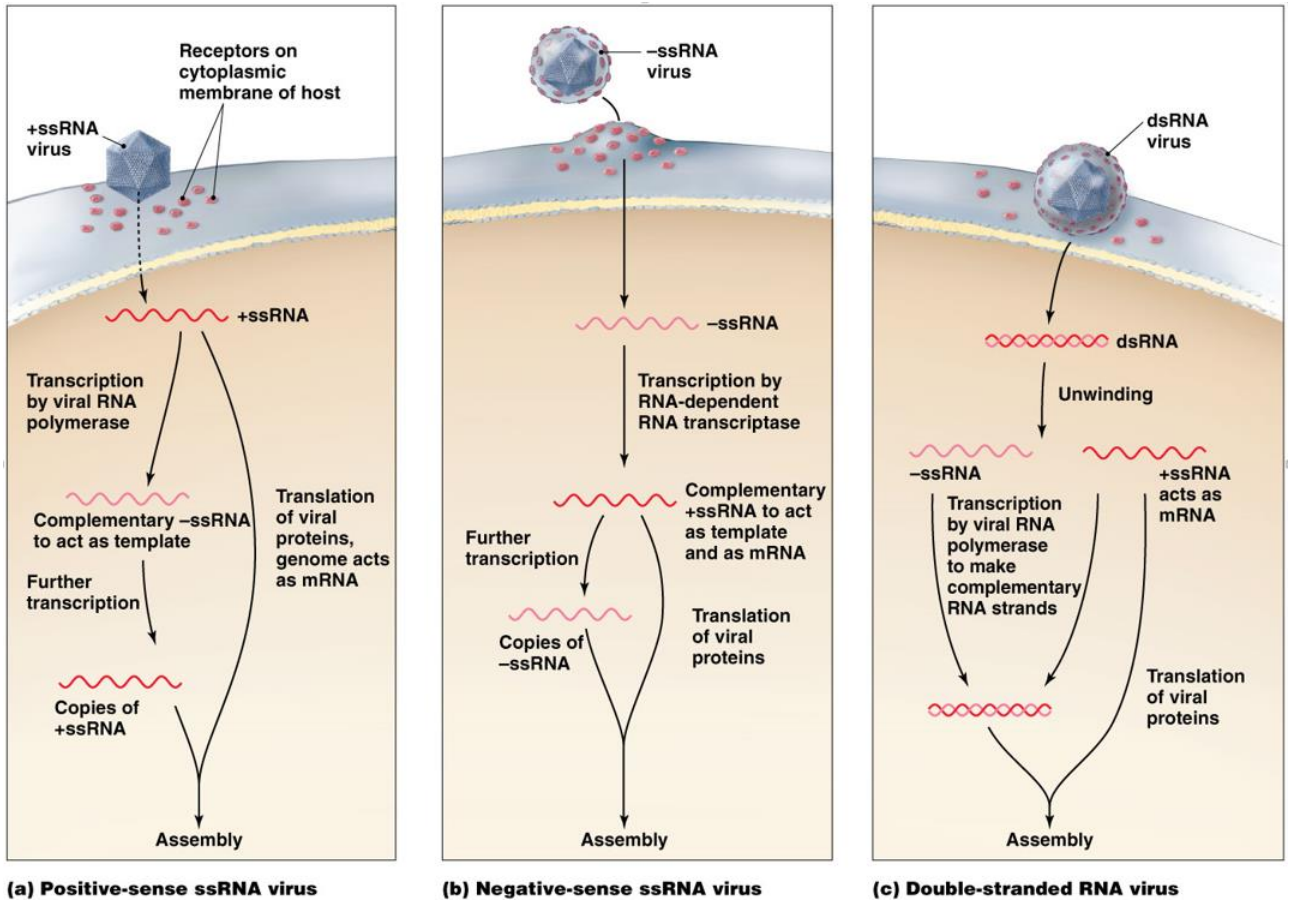

Figure 1. Replication of different RNA viruses (adapted from © Pearson Education, Inc)

Common for all RNA viruses is the fact that they have a much higher mutation rate compared to DNA viruses. Viral RNA polymerases are often inaccurate and lack proof-reading mechanisms like DNA polymerases have (especially reverse transcriptase of retroviruses). This is one reason why it is difficult to make effective vaccines to prevent diseases caused by RNA viruses. Another distinct feature of RNA viruses is that they produce double-stranded RNA intermediate during replication which has a very well-characterized cellular response represented mostly by the protein kinase R mediated pathway.

Hepatitis C Virus

I aimed to focus on HCV, an RNA virus. Hepatitis C Virus is a major causative agent of acute and chronic liver diseases in the world with an estimated

71 million affected patients worldwide (Luxenburger et al., 2018). Hepatitis C Virus is an enveloped, positive-sense single-stranded RNA virus. There are excellent reviews about the clinical relevance of Hepatitis C Virus (Modi and Liang, 2008), about treatment and therapies (Kaufmann et al., 2018, Kohli et al., 2014), immunological (Irshad et al., 2008), epidemiological (Memon and Memon, 2002), or inhibitor studies (Chen and Njoroge, 2009)

I will focus mostly on the replication-relevant part of HCV biology. Hepatitis C Virus is a positive-sense single-stranded RNA virus. The genome is ~9600 nucleotides which encodes a polypeptide proteolytically processed into distinct viral proteins (Figure 2). Translation begins via a ~340 nt long 5'-UTR region where IRES is located. The translated polypeptide is cut by viral protease into 9 distinct proteins.

The first cleavage product is a core protein (c) forming the majority of nucleocapsid. Next are two envelope proteins E1 and E2. These are highly glycosylated type I transmembrane proteins which are forming 2 types of heterodimeric complexes: disulfide linked or non-covalently linked. E2 protein also was shown to bind cellular protein kinase R and inhibit it. Protein p7 is a highly hydrophobic polypeptide of unknown function.

The remaining HCV genome encodes non-structural (NS) proteins named from 2 to 5. Most of these NS proteins are required for the replication of the virus. NS2 and the N-terminal part of NS3 translate into the NS2/3 protease which catalyzes cleavage at NS2/3 site. NS3 carries protease activities (cleavage of NS3/4A, SN4A/B, NS4B/5A, NS5A/B) and NTPase/helicase activity necessary for replication. NS4A is a cofactor of NS3 and is important for proteolytic activity of NS3, NS4B function is currently unclear. NS5A is a much phosphorylated protein and has a regulatory role in the replication of HCV and also involved in resistance to anti-viral interferons. NS5B is a RNA-dependent RNA-polymerase (Bartenschlager and Lohmann, 2000).

Liver is the main site of HCV replication. Virus attachment to the host cell during the infection involves the CD81 host receptor and the E2 HCV protein. Once inside the cytoplasm, HCV RNA is immediately translated. After the polypeptide has been synthesized and processed into essential viral proteins, a negative-sense strand is produced on top of the HCV genome to serve as a template for replication of new RNA. The amount of positive-sense RNA inside a cell can be estimated to be up to 50000 per cell, and the negative-sense RNA template around 10 times less. Viral RNA is transferred to the ER where the budding of new virions begins.

Since HCV activity is mostly found in the liver, different types of hepatocyte cell lines (primary and immortalized) has been tried for Hepatitis C research. All efficient infectious HCV cell culture systems employ the human hepatoma cell line Huh7 or cell lines derived from Huh7, such as the Huh7.5 cell line, which are typically cultured in monolayers in cell culture flasks (Seipp et al., 1997, Sainz et al., 2009). Moreover, only a single HCV genotype isolate 2a (JFH1) can recapitulate the complete viral life cycle in cell culture.

The common way of studying Hepatitis C is to use RNA clones from the HCV genome (Lohmann et al., 1999). HCV is a positive-sense virus, meaning isolated viral RNA is infectious and can be used in appropriate cell lines. The infectivity of genome or subgenome clones is lower but usage of RNA instead of the full virus can be very convenient. The more widespread approach is to use not a full HCV clone, but rather subgenomic replicons coding proteins from NS2-NS5B or NS3-NS5B. The advantage is the lack of structural protein genes which makes formation of a new viral particle impossible and hence the experiment is more safe and easy to perform. These subgenomic replicons are perfect to study the replication stage of the virus, often by introducing a fluorescent protein gene into RNA (usually NS5 protein is labeled).

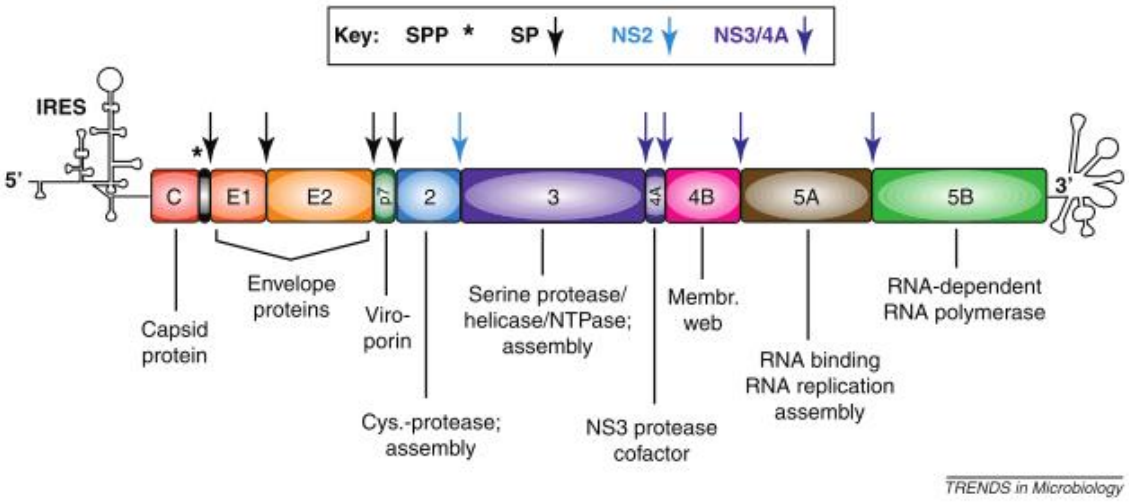

Figure 2. Schematic representation of the HCV genome (~9.6 kb, ~5kb structural genes, ~4.6 kb – replication genes). *Adopted from (Bartenschlager and Lohmann, 2000).*

For the same safety, simplicity and convenience reasons artificial HCV particles can be use. So-called trans-complementary particles (TCPs) are produced by introducing subgenomic replicon mentioned above into the Huh7 cell line which stably expresses HCV structural proteins. The newly formed TCPs has all the properties of the full HCV, but the genome RNA consists only of replication proteins (from NS2 to SN5B) and is therefore unable to produce new particles after infecting the host cells. The advantage of TCPs over isolated subgenomic RNA replicons is better infectivity (more efficient way of introduction of the replicating RNA into the cell).

Cellular response to the infection of RNA viruses

Cellular response to a viral infection can affect many different aspects of the cell and trigger a very complicated cascade of reaction. In case of RNA viruses secreted Interferon I (INF1) induces responses which involve NFκB-mediated activation of transcription of stress proteins, induction of apoptotic proteins (mostly proteases) and, most importantly, inhibition of translation involving protein kinase R (Figure 3).

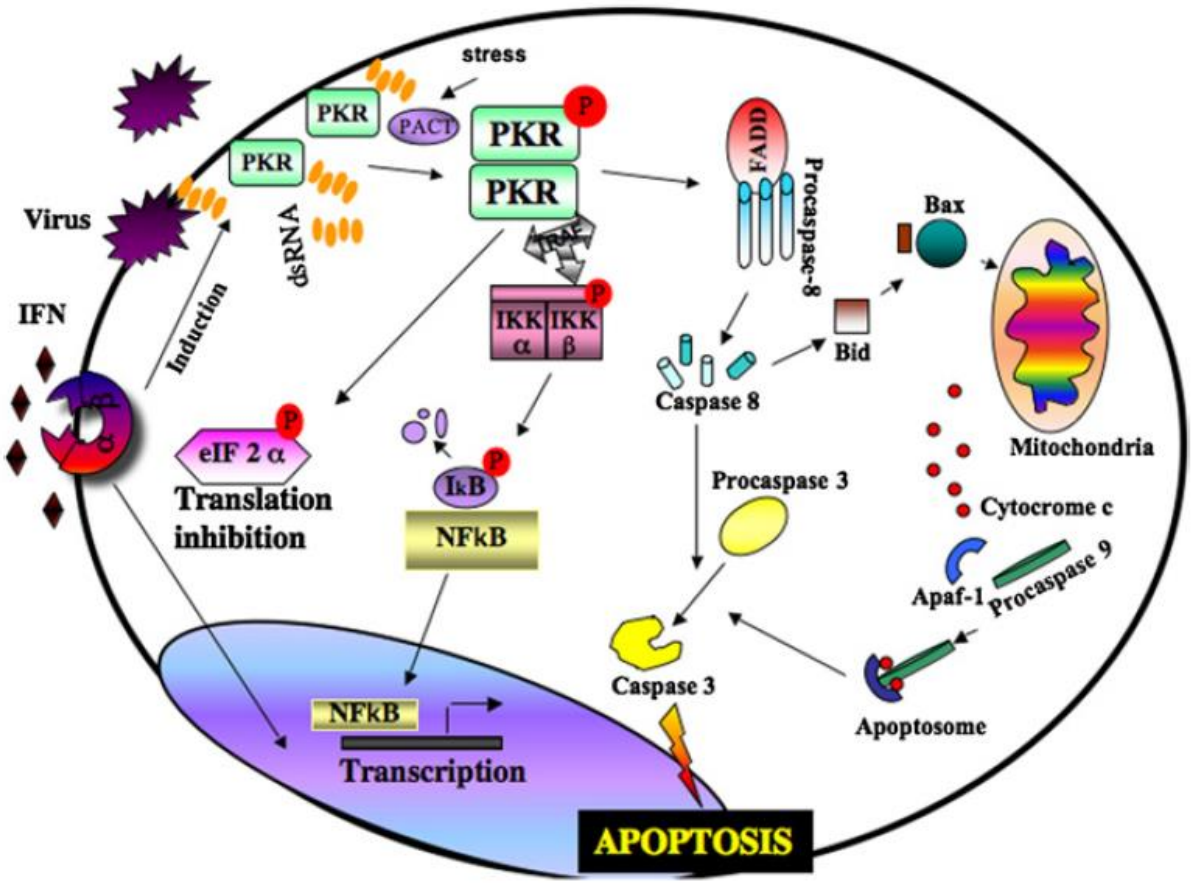

Figure 3. PKR: induction, activation and its role in different cellular pathways. *Adopted from (Garcia et al., 2007)*

The most well-known, robust and studied path – inhibition of translation, is activated via the presence of double-stranded RNA inside the cell. Double-stranded RNA is a replication intermediate for all RNA viruses (Appleby et al., 2015). Presence of double-stranded RNA triggers protein kinase R (PKR, EIF2AK2)-mediated stress response. PKR is a part of the family of four stress kinases (HRI or EIF2AK1, PKR or EIF2AK2, PERK or EIF2AK3 and GCN2 or EIF2AK4) which are involved in cellular stress-response (de Haro et al., 1996). HRI kinase is activated during iron deficiency (Burwick and Aktas, 2017), PERK is involved during protein misfolding and ER stress (Liu et al., 2015), GCN2 is related to amino acid starvation (Castilho et al., 2014), while PKR is known for its anti-viral activity.

PKR is present in the cytoplasm in low quantities in the latent state. RNA infection causes interferon to induce PKR production inside the cell. The kinase on by itself is not biologically active. During the infection, PKR can bind specifically and sequence-independently double-stranded RNA intermediate. Two molecules bind on top of double-stranded RNA which causes dimerization of two PKR monomers and subsequently trans-autophosphorylation in multiple serine and threonine sites. The activated kinase can later phosphorylate its downstream target, eIF2α subunit of eukaryotic initiation factor 2 (eIF2α), which, in turn, causes stalling of translation (initiation of translation to be precise). Phosphorylation of eIF2α prevents GDP dissociation from eIF2 in the ternary complex eIF2B/eIF2/GDP and inhibits the recycling of GTP/GDP prior to assembly of the 43S initiation complex (Figure 4).

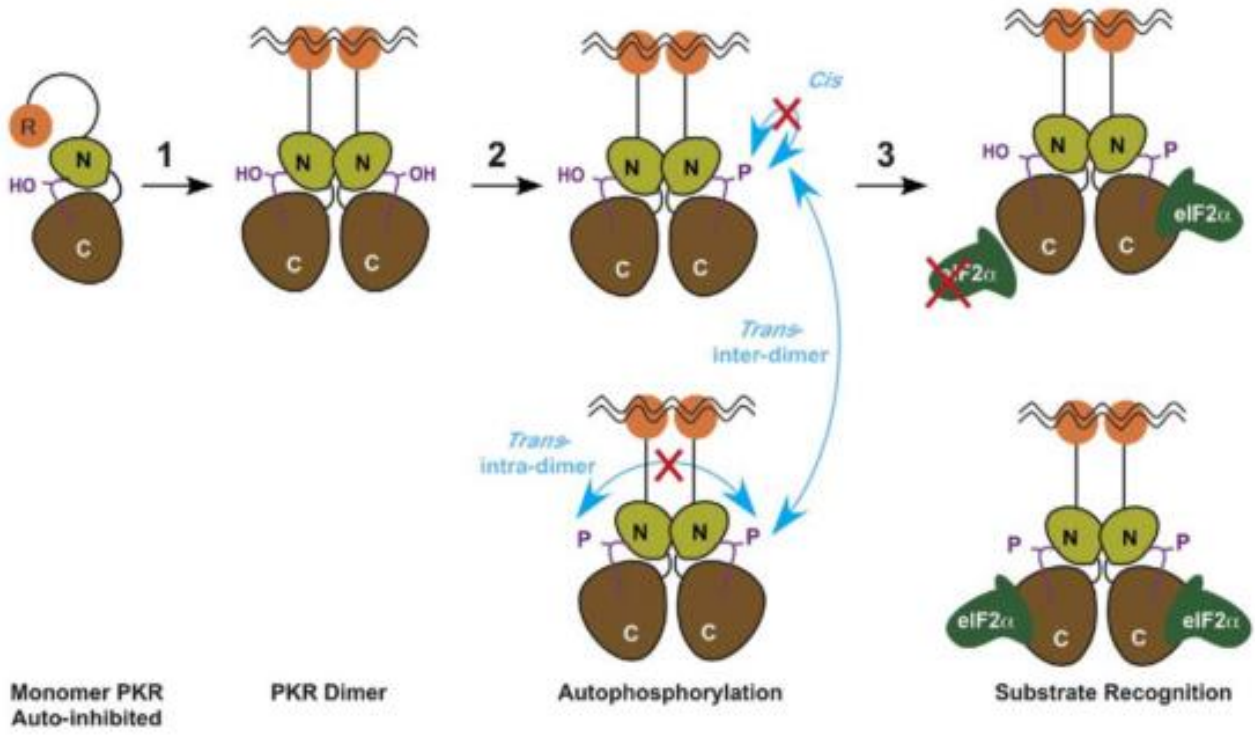

Figure 4. Model of PKR activation pathway. *Adapted from (Dey et al., 2005)*

Translation halt if not reversed leads to cellular death via apoptosis. This state is often associated with the formation of the so-called stress-granules, which are complexes (or rather aggregates) of untranslated both viral and produced

mRNAs together with several of cellular and viral proteins. (Ruggieri et al., 2012, Roth et al., 2017). Stress-granules formation and oscillation are a great indicator of the state of viral infection.

Evading anti-viral host response by RNA viruses is to large extend relying on blockading PKR by masking it with the viral proteins or causing its degradation inside the cell. (Dzananovic et al., 2018)

I am going to focus more closely on two most noticeable and well-studied members of the anti-viral response to the infection: PKR and eIF2α, which can be promising targets for the development of a sensor.

PKR structure and biology

PKR (protein kinase R) is a 68kDa serine/threonine kinase. It is encoded in humans in the EIF2K2 gene. Apart from the involvement in the anti-viral response, dysregulation of PKR is more and more often found to be associated with neurodegeneration like Alzheimer's disease (Bullido et al., 2008), Huntington's disease (Peel et al., 2001), Parkinson disease (Bando et al., 2005), memory and learning (Segev et al., 2013, Segev et al., 2015), metabolic disorders (Segev et al., 2016) and cancer (Garcia-Ortega et al., 2017).

PKR is a 551 amino acid protein which consist of two domains: an N-terminal double-stranded RNA binding domain and a C-terminal catalytic domain, separated by a long ~100 amino acid unstructured region which is acting as a flexible linker (Meurs et al., 1990) (Figure 5a). Full PKR was never crystalized, but structures of separate domains have been investigated.

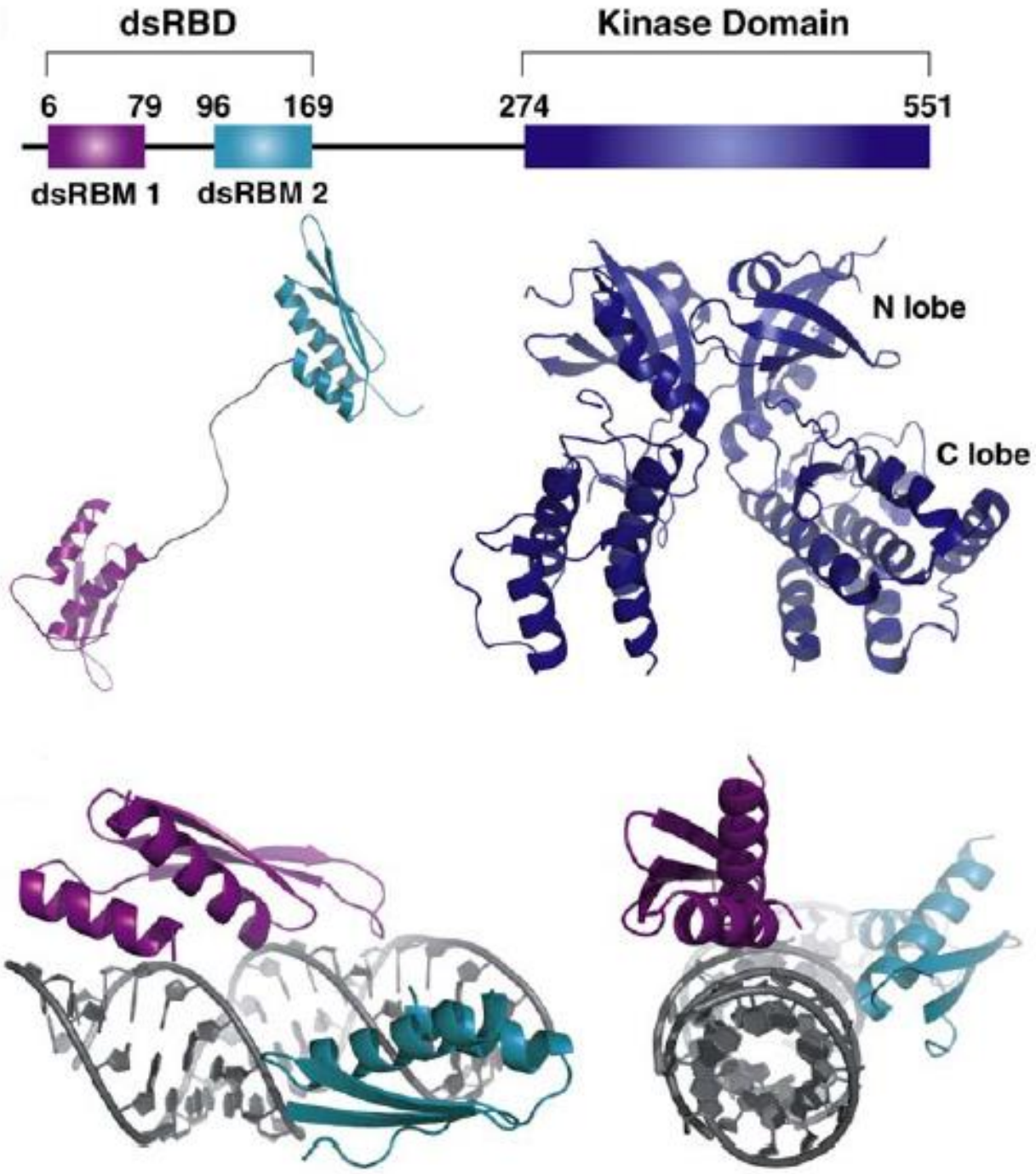

Figure 5. Schematic representation of the secondary structure of PKR (a), structure of N-terminal domain of PKR (b), structure of dimeric C-terminal catalytic domain (c) and complex of N-terminal domain of PKR with dsRNA from different views (d)

Insight into the structure of the N-terminal domain of PKR was obtained with the help of 2D NMR in solution (Sambasivarao Nanduri, 1998). The N-

terminal domain of PKR is also called dsRNA-binding domain of PKR, which indicates the primary function of this part of the kinase (Figure 5b). This domain consists of 169 amino acids which includes two 73 amino-acid long dsRNA binding motifs (RBM1 and RBM2) of similar structure separated by a flexible 17 amino acid linker. The linker fits into the minor groove of the A-helix of dsRNA (Figure 5d). This unstructured linker region contains a high number of positively charged amino acids promoting the binding with the negatively charged phosphate backbone of the nucleic acid. The minimum calculated lengh of dsRNA duplex for efficient landing of PKR is between 11 and 13 nucleotides. The minimum length of dsRNA required for the dimerization of two PKR molecules is 30 nucleotides. The dimerization on top of the RNA is of parallel manner, where both N-termini and both C-termini are in the same plane. The N-terminal domain of PKR is well-known to be highly specific to dsRNA structures and able to differentiate it from dsDNA helixes or even RNA/DNA duplexes. This is partly due to the length of the perfect fit of the 17 amino acid linker to the minor groove of the A-helix, but also due to the ability of RBMs to recognize the 2'-OH group of the RNA.

The C-terminal domain of PKR holds catalytic functions. The domain consists of N- and C-lobes placed in an angle to each other (Dey et al., 2005, Dar et al., 2005) (Figure 4C). The N-lobe consists of 5 anti-parallel beta-strands and a canonical helix (amino acids 258-369), while the C-lobe has only 2 beta-strands and 8 alpha-helixes (amino acids 370-551). Dimerization of PKR causes autophosphorylation at multiple serine and threonine sites, only a couple of which are located in the unstructured region and the majority is located in the C-terminal domain. The most well characterized phosphorylation positions are Thr449 and Thr451. Both of the lobes of the catalytic domain are involved in the binding of eIF2α.

eIF2α structure and biology

eIF2α (eIF2S1) is a 36kDa part of a heterotrimeric eIF2 complex located in the cytoplasm. eIF2α is a phosphorylation target of many stress-induced kinases. The family of eIF2α kinases, as mentioned above, includes HRI, GCN2, PERK and PKR (Figure65).

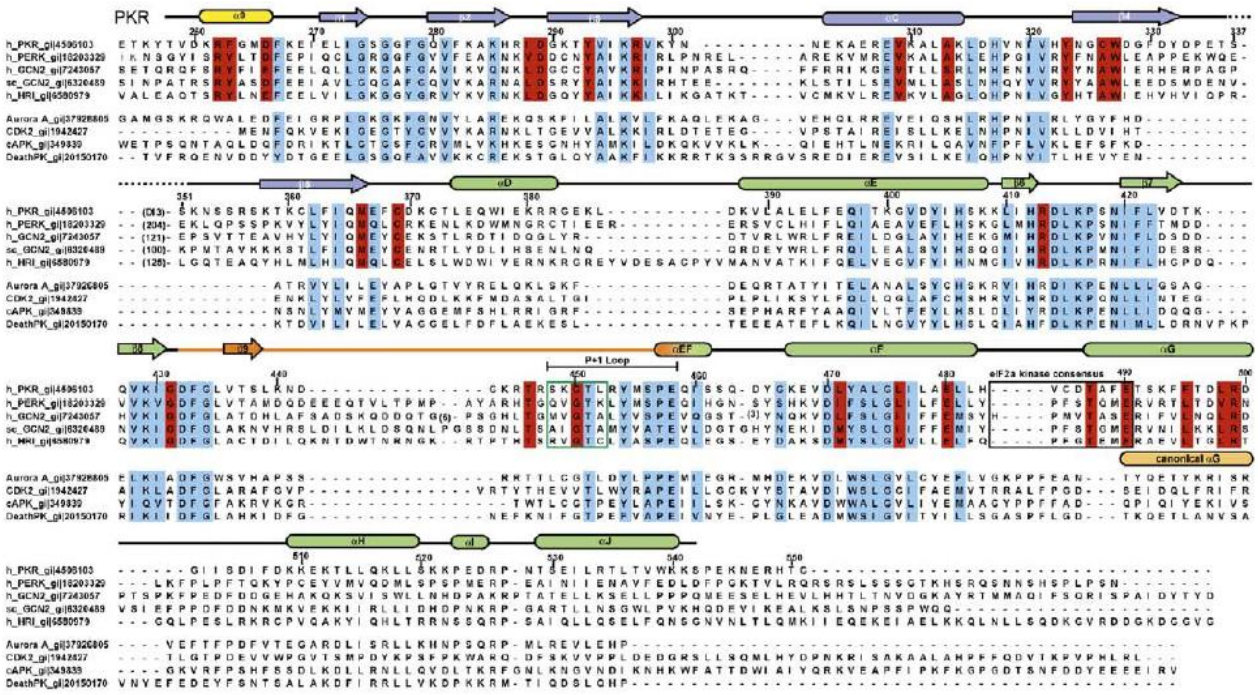

Figure 6. Secondary structure alignment of four eIF2α kinases

The eIF2α recognition mechanism is fully conserved across the eIF2α protein kinase family primarily relying on helix αG rather than conservation of residues on the contact surface. Sequence comparison reveals that all four members possess a short αF-αG helix linker and an atypically long helix αG.

The eIF2α structure consists of an S1 subdomain (residues 3–90) flanked on one surface by a C-terminal α-helical subdomain (residues 91–175). This subdomain contains the phosphorylation site and is involved in PKR binding. The remaining domain is forming the complex with eIF2B and GTP during the initiation of translation (Figure 7).

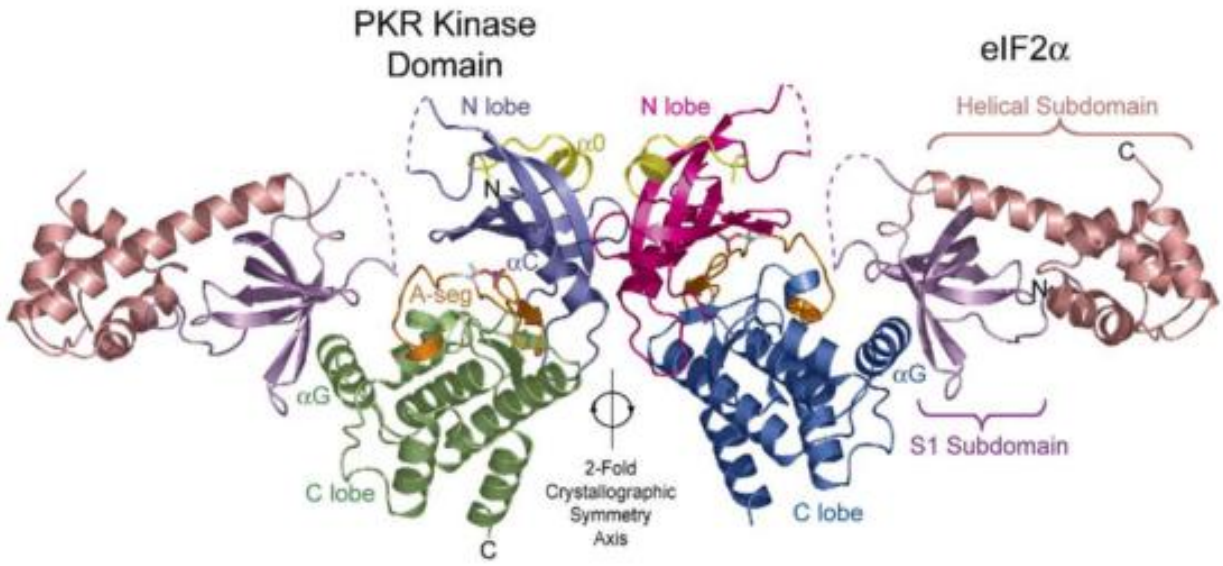

Figure 7. Ribbon model of a dimerized complex of eIF2α and the C-terminal domain of PKR.

eIF2α is phosphorylated in position Ser51. It has been shown that this Ser can be substituted for other amino acids such as Thr or Tyr and be equally phosphorylated (Lu et al., 1999). An eIF2α-derived target-peptide consists of 11 amino acids 45-56: *ILLSEL**S**RRRIR* (Mellor and Proud, 1991). The peptide itself is not a specific target to either of the four eIF2α kinases. It has been reported that abundant cellular kinases can cross-react with the peptide, most distinctly protein kinase A (PKA) (Proud et al., 1991). The specificity of the peptide recognition and phosphorylation comes from recognition of the helical structure on the C-terminus of S1 subdomain eIF2α far from the phosphorylation site (in terms of the secondary structure) containing a conserved amino acid sequence *KGYI*.

Genetically encoded FRET sensors

Optical sensors are powerful tools for live cell research as they permit to follow the location, concentration changes or activities of key cellular players such as lipids, ions and enzymes. Most of the current sensor probes are based on fluorescence which provides great spatial and temporal precision provided that high-end microscopy is used and that the timescale of the event of interest fits the

response time of the sensor. Many of the sensors developed in the past 20 years are genetically encoded. There is a diversity of designs leading to simple or sometimes complicated applications for the use in live cells. A highly comprehensive review of all kinds of optical sensors can be found in our review (Bolbat and Schultz, 2017).

We chose to focus on FRET because it allows for accurate ratiometric and spatiometric readout which can be helpful for studying viral infection. In brief, FRET is a phenomenon of energy transfer from one chromophore to another when they are in a very close proximity and provided the dipole moments of the chromophores are in the right orientation. Genetically encoded sensors are prepared by placing a protein-based sensing domain between a fluorescent protein FRET pair.

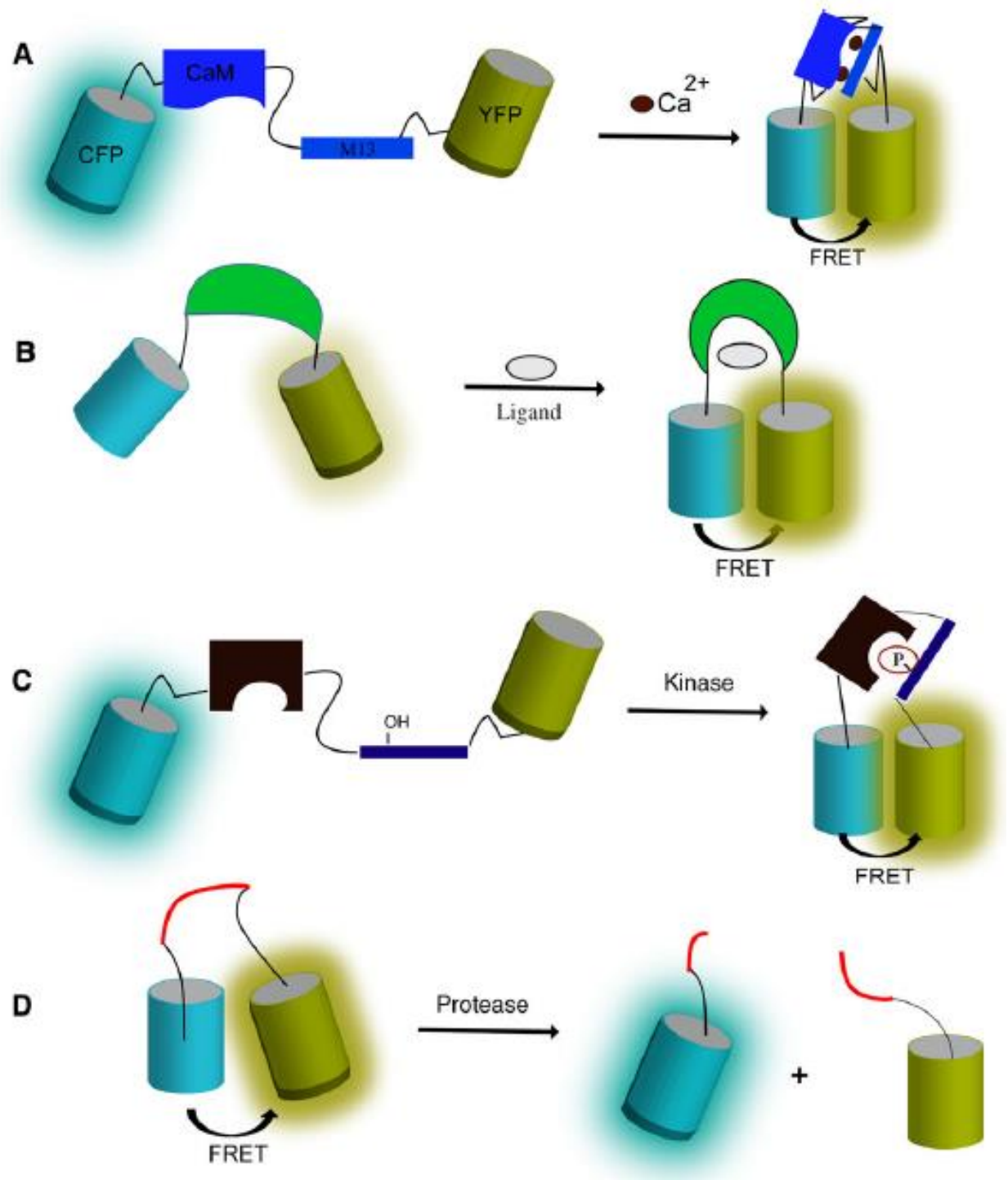

Figure 8. Some examples of the FRET sensor designs. *Adapted from (Bolbat and Schultz, 2017)*

The idea behind all FRET sensor types is to change the distance or the fluorophore orientation between fluorescent proteins in the presence of the analyte (Figure 8). One example of a sensor design is based on attaching

fluorescent FRET proteins to target proteins which are going to interact or dimerize in the presence of the substrate ("dimerization FRET"). Upon interaction fluorescent proteins are coming close to each other and a FRET readout appears. The opposite mechanism can be employed in protease FRET sensors, where a peptide target of protease is being cleaved and fluorescent proteins fall apart and the FRET readout disappears (Figure 8d).

Another design is sandwiching a protein or a single domain of a protein between two fluorescent FRET proteins. Upon binding of the analyte the protein will change its conformation to a more closed or more opened one, which leads to the increase or decrease of FRET efficiency (Figure 8b).

An example of a more complicated design approach are kinase activity FRET sensors. (Komatsu et al., 2011). In this case one builds a sensing domain out of the peptide target of a kinase connected via long polypeptide linker to a phospho-amino acid binding domain, followed by attaching fluorescent proteins on each side of the sensor. Upon activation of the kinase and phosphorylation the conformation of the sensor changes to a closed one which leads to appearance of a strong FRET readout (Figure 8a. 8c).

The fluorescent protein FRET pair is in the overwhelming majority of instances CFP/YFP because of an ideal fit of their spectrophotometric properties to each other. It is worth mentioning that novel developments of fluorescent proteins with improved spectrophotometric properties lead to possible alternatives in the choice of fluorescent protein FRET pair.

Aims and sensor design approaches

The goal of the current project was to develop a FRET sensor for detecting the infection of RNA viruses in live cells via fluorescent microscopy. PKR and eIF2α were selected as the design targets for potential FRET sensors. The first aim (**Aim 1**) was to develop a working sensor based on PKR or eIF2α. I designed

various different sensor models and I produced many FRET sensors. The majority of the developed sensors didn't work as intended or showed unacceptably small readouts. However, one FRET sensor model was successful for meeting the goals of the project. In this thesis I will describe the idea behind the working prototype (named KRP1) as well as the results obtained with it. I also will briefly mention the other ideas for the sensor design in this paragraph and discuss them in more detail in the discussion section of the thesis.

The working design for the FRET sensor was based on the N-terminal domain of PKR. The N-terminal domain of PKR, as described above, consists of 175 amino acids and two RNA-binding motifs. The hypothesis was that the N-terminal domain of PKR changes its conformation upon binding of double-stranded RNA, taking a more closed conformation. I placed a pair of fluorescent proteins on the N- and C-terminal ends of the PKR domain. The idea behind the sensor was that upon double-stranded RNA binding the N-terminal domain of PKR will "wrap" over the double-stranded RNA, fluorescent proteins at the termini will come closer together and FRET will increase (Figure 8). As fluorescent proteins, I chose cp173Venus and mTurquoise because this pair worked best in previous sensors designed in the lab (Piljic et al., 2011, Stein et al., 2013, Bulusu et al., 2017, Kuchenov et al., 2016).

The second aim of the thesis (**Aim 2**) was to optimize the sensor with the use of other fluorescent protein pairs from the library developed earlier in the lab (Piljic et al., 2011). This effective optimization approach is based on the use of circularly permutated fluorescent proteins. A circular permutation is a relationship between proteins whereby the proteins have a changed order of amino acids in their peptide sequence. The result is a protein structure with different connectivity, but overall similar three-dimensional structure. Different circularly permutated proteins possess different dipole moment of their fluorophore. Since FRET efficiency is dependent not only on the proximity but

also on the dipole orientation to each other (Ansbacher et al., 2012), varying the circularly permutated proteins in the same structure can yield significant improvements.

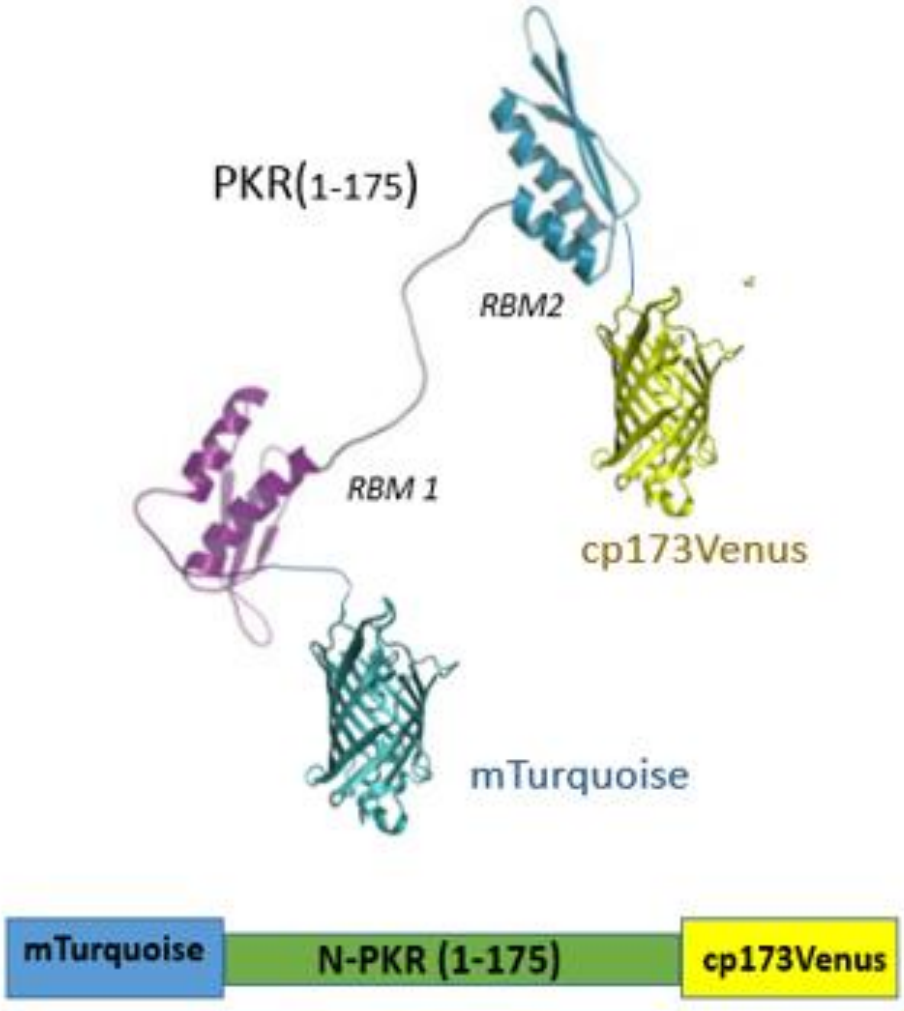

Figure 9. Schematic representation of the successful FRET sensor design.

The final aim (**Aim 3**) of the thesis was to test the ability of the sensor to detect the infection of host cells by RNA viruses. The target virus was chosen to be Hepatitis C. For full proof-of-concept, it was planned to use a subgenomic RNA_{HCV} replicon, trans-complementary particles and full viral infection. It was planned to compare the result to Dengue virus infection, as this virus is of the same family of positive-sense RNA viruses but with a much higher replication rate.

Moreover, for better understanding of the PKR and eIF2α biology I will discuss other sensor designs used during this work but weren't successful:

1. Sandwiching full PKR between the fluorescent protein FRET pair to detect presence of dsRNA;
2. Dimerization FRET with full PKR to detect presence of dsRNA;
3. Dimerization FRET with N-terminal PKR to detect presence of dsRNA;
4. Sandwiching eIF2α between fluorescent proteins to detect activity of PKR;
5. Sandwiching two subdomains of eIF2α (1-120 and 13-90) which involved in PKR binding and contain Ser51 phosphorylation site to detect activity of PKR;
6. 20 different eIF2α peptide-based phosphorylation sensors with various amino acid mutations.

Methods

Cloning

KRP1

KRP1 construct backbone was based on a pECFP-C1 (Clontech) vector. mTurquoise version of CFP was introduced between the NheI and BshTI restriction sites (instead of the ECFP in the vector). cp173Venus version of YFP was introduced between the MluI and BamHI restriction sites. PKR (1-175) was amplified from the full PKR via a polymerase chain reaction (PCR) and introduced between the BshTI and MluI restriction sites (which placed it between the two fluorescent proteins).

Optimization library

One set of plasmids for the sensor optimization was constructed by PCR amplification of different truncated versions of PKR (1-155, 1-195, 1-215, 1-235, 1-255, 1-275) form the full PKR sequence and introduction of them between the mTurquoise and cp173Venus via the BshTI and MluI restriction sites.

Another set of plasmids for optimization was constructed based on the previously reported library of plasmids (Piljic et al., 2011, Stein et al., 2013), substituting the existing sensing domain of Camk2a or DAPK1 with PKR (1-175) between the BshTI and MluI restriction sites.

Other versions of FRET sensors

Other FRET sensors were cloned in a similar fashion to KRP1. pECFP-C1 vector contained one of the CFP versions of the sensor between NheI and BshTI, one of the YFP versions between MluI and BamHI and the sensing domain between BshTI and MluI. As a sensing domain, I used full PKR sequence, full eIF2α, truncated eIF2α (1-120) and eIF2α (13-90), all amplified via PCR.

Dimerization FRET sensor

Full and truncated (1-175) versions of PKR were amplified via PCR and introduced into the pECFP-C1 or PECFP-N1 vectors (depending on the desired position of the fluorescent protein: N-terminal or C-terminal respectively) between BshTI and BamHI restriction sites. The ECFP was substituted with the Venus sequence via the restriction-free cloning to obtain a second monomer for the dimerization FRET.

Peptide based kinase activity sensor

The plasmid backbone was based on previously reported EEVEE-linker optimized FRET sensors AKAR3EV, EKAR3EV and PichuuEV (Komatsu et al., 2011). The phosphorylation target-peptide was substituted with one of the 20 different versions of eIF2α (45-56) peptide between NotI and BspMII restriction sites.

Cloning protocol

The PCR amplification of the desired sequence was performed with the appropriate primers (purchased form Sigma) in a 3-step amplification cycle using a Hot-Start High Fidelity DNA polymerase from ThermoFisher according to the manufacturer's protocol.

The purification of the product was performed via 1% agarose gel electrophoresis (with SYBR Safe visualization intercalating agent from ThermoFisher) and QIAquick Gel Extraction Kit form QIAGEN.

The restriction was done using Fast Digest restriction enzymes from ThermoFisher and the ligation was performed using T4 DNA ligase with a 10:1 insert/vector ratio for 1 h at room temperature.

The ligation mixture was transformed into the competent cells via heat shock according to the standard protocol. Chemically competent cells were prepared in the lab using an RbCl-based Super Competent Cells preparation method https://openwetware.org/wiki/RbCl_competent_cell).

The MiniPrep from the appropriate amount of bacterial culture was performed with QIAprep Spin MiniPrep Kit from QIAGEN, MidiPrep was done with the QIAGEN HiSpeed Plasmid Midi Kit and the MaxiPrep was done with the QIAGEN HiSpeed Plasmid Maxi Kit.

Cell culture

More than half of the live cell experiments were performed in HeLa Kyoto cells. HeLa Kyoto cells were a kind gift from Pepperkok lab (European Molecular Biology Laboratory, Germany). The cells were passaged and maintained at 37°C with 5% CO_2 in DMEM consisting of 3.5 g/l glucose and 1 mM sodium pyruvate (Gibco), supplemented with 10% FBS (Gibco), 2 mM L-Glutamine and 0.1 mg/mL of Primocin antibiotic (Invivogen) or a PenStrep (Penicillin/Streptomycin) mix (ThermoFisher). The cells were splitted 3 times per week in 1:5 ratio. HeLa cells were seeded in the desired dishes at 35% confluency. 6-well plates (Nunc) contained $3*10^5$ cells (2 ml x $1.5*10^5$/ml), 12-well plates (Nunc) contained $1*10^5$ cells (1 ml x $1*10^5$/ml), 24-well plates (Nunc) contained $5*10^4$ cells (500 µl x $1*10^5$/ml), 96-well plates (Nunc) contained $1*10^4$ (150 µl x $6.7*10^4$/ml), 8-well LabTeks (ThermoFisher) $3.5*10^4$ cells (250 µl x $1.4*10^5$/ml), 1-well LabTeks (ThermoFisher) $3*10^5$ cells (2 ml x $1.5*10^5$/ml). After 24 h when the cells reach 70% confluency they are used for the subsequent experiments.

Huh7 cells were a kind gift from Ruggieri lab in the Department of Infectious diseases of Heidelberg University. Huh7 cells were maintained in the same medium and conditions as HeLa cells. The cells were splitted 2 times per week in 1:6 ratio. Huh7 cells were seeded in the desired dishes at 50% confluency (due to a slower life cycle). 6-well plates (Nunc) contained $1.2*10^5$ cells (2 ml x $6*10^4$/ml), 12-well plates (Nunc) contained $4*10^4$ cells (1 ml x $4*10^4$/ml), 24-well plates (Nunc) contained $2*10^4$ cells (500 µl x $4*10^4$/ml), 8-well LabTeks

(ThermoFisher) $1.4*10^4$ cells (250 μl x $6.4*10^4$/ml). After 24 h when the cells reach 70-75% confluency they are used for the subsequent experiments.

Huh7 stable cell line expressing KRP1 or KRP2 (produced in the Ruggieri lab) were maintained in the same conditions and seeded to the same density as Huh7 cells.

Transfection

Lipofectamine 2000 was used for the transfection of HeLa cells. The transfection mixture was prepared in OptiMEM or Serum free DMEM (with equal efficiency). The ratio of DNA plasmid to the transfection reagent was 200 ng per 0.5 ul of Lipofectamine 2000. The protocol was followed according to the manufacturer's recommendations. The amount of DNA used in different experiments per well was following: 200 ng in 96-well plates, 400 ng in 8-well LabTeks, 800 ng in 24-well plates, 1.6 ng in 12-well plates, 3-4 ng in the 6-well plates. The medium containing the transfection reagent was changed after 6 h of transfection. 24 h later the expression level was checked under the Olympus U-RFL-T widefield fluorescent microscope.

Lipofectamine 3000 was used for the transfection of Huh7 cells. The protocol used was identical to the Lipofectamine 2000 transfection protocol with the only difference of adding p1000 efficiency reagent together with the plasmid DNA in the amount equal to the Lipofectamine 3000 reagent (according to the manufacturer's protocol).

Native cell lysis

Cells of choice (HeLa, HEK293T or Huh7) were seeded in 6-, 12- or 24-well plates at 35 % confluency. In 24 h when the confluency reached 70% cells were transfected with the desired sensor plasmid according to the previously described protocol. After the next 24 h the medium was aspirated and the cells were kept on ice for all the following steps. Cells were gently washed twice with

2, 1 or 0.5 (depending on the cell culture dish) ml of ice cold PBS. After aspirating the excess PBS, I added RIPA buffer from ThermoFisher (150 mM NaCl, 50 mM Tris, pH=8.0, 1% of NP-40, 0.5% sodium deoxycholate, 0.1% SDS, supplemented with cOmplte^{TM} protease and phosphatase inhibitor cocktail from Roche and 1 mM PMSF from Sigma) in the amount of 10% of the cell culture medium volume (200 µl, 100 µl or 50 µl depending on the cell culture dish). Due to the potential drying of the buffer after the 15 min incubation time, not more than 6 wells can be handled at the same time. After the 15 min incubation successful lysis procedure can be identified by eye because of the appearance of membrane remainings aggregating with each other. Cells were scrapped using cell scrappers (one scrapper per well) and the lysate was transferred in the 1.5 ml eppendorfs. The samples were centrifuged at 13,000 x g for 15 minutes at 4°C. Finally, the supernatant was transferred into the new tubes, aliquoted and stored at -40°C. If using the lysates within a week, aliquoting step can be omitted. The lysates can be stored at +4°C for 3 days or one week with 0.01% NaN_3 before significant protein degradation.

Fluorimetry

The lysates from the 6-well plates were transferred into the Fluorimeter Micro Square Cells (black cuvettes for fluorescence measurements) from Thomas Scientific. The excitation and emission spectra were collected in the JASCO FP-8300 spectrofluorometer.

Calibration was done by collecting the spectra of the blank solution (lysate of untransfected Hela or Huh7 cells in RIPA buffer). Obtained wavelength intensities were subtracted from the corresponding wavelength intensities in collected excitation or emission spectra.

The excitation and emission spectra of individual fluorescent proteins were measured before each experiment as a quality control to confirm the presence of these fluorescent proteins in the sensor.

The “FRET” excitation spectra were collected at a constant wavelength of the acceptor fluorescent protein. The appearance of two peaks (both acceptor and donor) indicates the presence of FRET.

The “FRET” emission spectra were collected at a donor fluorescent protein excitation wavelength. The appearance of two peaks (both donor and acceptor) indicates the presence of FRET and the ratio of the acceptor emission to donor emission in this mode is used as a FRET readout.

CFP/YFP FRET. mECFP/mTurquoise excitation spectra were collected in the range of 400-470 nm at a constant 475 nm emission wavelength, FRET (CFP/YFP) excitation spectra were collected in the range of 400-520 nm at a constant 527 nm emission maximum, Venus excitation spectra were collected in the range of 500-520 nm at a constant 527 nm emission maximum.

mECFP/mTurquoise emission spectra were collected in the range of 460-500 nm with the 435 nm excitation wavelength. FRET (CFP/YFP) emission spectra were collected in the range of 460-540 nm with the 435 nm excitation wavelength. Venus emission spectra were collected in the range of 520-540 nm with the 515 nm excitation wavelength.

GFP/RFP and YFP/RFP FRET. mClover3 (green) excitation spectra were collected in the range of 450-510 nm based on 518 nm emission maximum, Venus/SYFP2/YPet excitation spectra were collected in the range of 450-520 nm at a constant 527 nm emission maximum, FRET (GFP or YFP/RFP) excitation spectra were collected in the range of 450-585 nm at a constant 594 nm emission maximum, mScarlet excitation spectra were collected in the range of 540-585 nm at a constant 594 nm emission maximum.

mClover3 emission spectra were collected in the range of 510-560 nm with the 506 nm excitation wavelength. FRET (GFP or YFP/RFP) emission spectra were collected in the range of 510-610 nm with the 506 (green) or 518 (yellow)

nm excitation wavelength. mScarlet emission spectra were collected in the range of 575-610 nm with the 569 nm excitation wavelength.

Trypsin digestion. Before the treatment of the sensor with the substrate (separately) and in the end of the experiment I added 10 μM recombinant trypsin (Sigma) to the lysate as a control for FRET (which lead to the disappearance of the FRET peak and increase in the donor fluorescence).

In vitro analysis of the FRET sensor library

The measurements were done in Nunc F96-well black plates with the Tecan the Infinite m1000 pro plate reader.

The HeLa cells were seeded and grown in the 96-well plates till 70% confluency. The cells were transfected with each of the plasmid from the optimization library with Lipofectamine 2000 in quadruplicates and lysed after 24h. 100 ng of dsRNA or polyI:C was added in the two of the well per plasmid. The intensity of emitted fluorescence was measured at the 435 nm excitation in the range of 470-480 (CFP peak is at 475 nm) and 522-532 (YFP peak is at 527 nm). The background was measured in untransfected HeLa lysate and subtracted from the corresponding sensor measurements. The ratio from the corrected average YFP intensity to corrected average CFP intensity was taken as a FRET readout.

Plasmid DNA spotting

Spotting of DNA plasmid transfection mixture and the reverse transfection was performed according to the previously described protocols (Piljic et al., 2011, Kuchenov et al., 2016, Stein et al., 2013, Bulusu et al., 2017). Plasmids used in this assay were all obtained from the MaxiPrep. To prepare the transfection mixture, 9 μL of a 0.4 M sucrose solution in DMEM, 9 μL of DNA and 33 μL of Lipofectamine 2000 were mixed in a 96-well plate. After 20 min incubation at room temperature, 21.75 μL of solution of 0.29% gelatin in water was added to

the mixture, and 24 μL of the transfection cocktail was distributed in 384-well plates. Subsequently, a plate was centrifuged briefly up to 54×g at room temperature to straighten the surface of the samples and placed immediately in the contact printer. Before printing, LabTek dishes were washed with 70% ethanol to increase the hydrophobicity of the LabTek surface and, accordingly, to improve the shape of the spots. One-well LabTek dishes were printed with a "ChipWriter" contact printer equipped with solid pins. Using PTS 600 pins, the diameter of printed spots was about 400 μm and the spot-to-spot distance was 1.125 μm. Printed 1-well LabTek dishes were stored at room temperature in a gel-drying box in the presence of drying pearls. Each FRET construct from the "optimization library" was printed in quadruplicate per one LabTek. Before the experiment, HeLa were seeded in these 1-well LabTeks containing the plasmid "spots" at 30% confluency. When the confluency reached 60-65% 24 h later, the cells were imaged upon addition of dsRNA.

RNA transfection

Short dsRNA 30 bp duplex was obtained via annealing of ssRNA components purchased from Sigma. I used previously reported (Lemaire et al., 2008) ssRNA sequences: 5'-GGAGAACUUCAUGCCCGUCGGAUAAGACU-3' and 5'-AGUCCUUAUCCGAAGGGCAUGAAGUUCUCC-3'.

Long 200 bp dsRNA was obtained via annealing of the ssRNA components provided by the Ruggieri lab. The ssRNA components were the first 200 nucleotides of the Ampicillin sequence obtained via in vitro transcription.

Annealing was performed by mixing equal amounts of ssRNA in the annealing buffer (10 mM Tris, pH 7.5, 50 mM NaCl, 1 mM EDTA), placing the mixture at 95°C for 5 min and allowing it to cool down at room temperature on the bench.

PolyI:C of low molecular length (LMW), polyI:C of high molecular weight (HMW) and polyA:U were purchased from the Invivogen.

For the experiments in HeLa cells, 200-500 ng of dsRNA (in 15 µl of the Imaging Buffer (IB): 115 mM NaCl, 1.2 mM $CaCl_2$, 1.2 mM $MgCl_2$, 1.2 mM K_2HPO_4, 0.2% glucose and 20 mM HEPES, pH 7.4) was mixed for 20 min with 0.5-1.25 µl of Lipofectamine 2000 (in 15 µl of the Imaging Buffer (IB). Before the imaging under the microscope, the dsRNA mixture was added into the well of the 8-well LabTek chamber containing cells expressing the FRET sensor. The negative control experiment was performed with the addition of the "empty" transfection reagent (without dsRNA).

For the experiments in Huh7 cells, the Lipofectamine 3000 was used to transfect the dsRNA (additional p1000 reagent was premixed with the dsRNA before the addition to the Lipofectamine 3000). Other than that the protocol was identical to the one described above.

Single-stranded viral subgenomic RNA_{HCV} replicon was produced in the Ruggieri lab according to the previously described protocol (Schult et al., 2018) and kindly provided to me. 100-200 ng of dsRNA was premixed with 0.5 µl of p1000 (from Lipofectamine 3000 kit) in 10 ul of IB. After 10 min this solution was added to the 10 ul of IB containing 0.75 µl of Lipofectamine 3000. Following the 15 min incubation time, the dsRNA mixture was added into the well of the 8-well LabTek chamber containing Huh7 cell stably expressing the FRET sensor. The imaging began after 12 h of transfection.

Solutions containing ssRNA was kept in ice at all times. Before handling the ssRNA, the workplace was always treated with RNaseZap Decontamination Solution from ThermoFisher.

Stable cell line production

The stable cell line of Huh7 cells expressing the designed FRET sensor was produced by Philipp Klein from the Ruggieri lab. It was done based via lentiviral transduction described previously (Schult et al., 2018).

Infection

The infection with trans-complementary particles of HCV (TCP_{HCV}) and Dengue virus (DENV) was performed in the Biological Safety 3 lab at the Heidelberg University Clinic with the help of Philipp Klein from the Ruggieri lab according to the previously described protocols (Ruggieri et al., 2012, Chatel-Chaix et al., 2016, Schult et al., 2018).

Microscopy

All cell experiments were performed in the Imaging buffer: 115 mM NaCl, 1.2 mM $CaCl_2$, 1.2 mM $MgCl_2$, 1.2 mM K_2HPO_4, 0.2% glucose and 20 mM HEPES, pH 7.4. In all cases, LabTeks with the cells were placed in the microscope environmental box at 37°C (and no CO_2). The overwhelming majority of imaging experiments were performed using confocal fluorescent microscopes: Olympus FluoViev1200 and Zeiss LSM 789 NLO.

Olympus FV1200. Imaging was performed on a FluoView1200 (catalog #IX83; Olympus) confocal laser-scanning microscope at 37°C (incubator box made by the European Molecular Biology Laboratory), using Olympus 20× UPLSAPO (numerical aperture 0.75, air) objectives and FluoView software, version 4.2. The images were acquired with a Hamamatsu C9100-50 EM-CCD camera. The cyan and FRET channels was imaged using a 405-nm laser line (120 mW/cm2, 5%) with the 460-500 (cyan) nm and 510-560 (yellow) nm emission range respectively. The red channel was imaged using a 559-nm laser (120 mW/cm2, 2.0%) and a 643/50 emission filter. Images were acquired in 15-s intervals. The dual scanner setup allowed for simultaneous laser stimulation and

confocal imaging. This permitted the acquisition of cellular responses that occur during or immediately after laser stimulation.

Zeiss LSM 789 NLO. Confocal microscopy was performed using a Zeiss LSM 780 NLO confocal microscope at 37°C, equipped with a 20x Plan-Apochromat 20x/0.8 M27 objective. Definite Focus (Carl Zeiss) was used to minimize focus shifts during time-lapse experiments. Excitation and emission settings were similar to the ones described above.

At the end of each imaging experiment the control acceptor photobleaching was performed in several selected cells in the field of view. This lead to vanishing of acceptor fluorescence and increase in the donor fluorescence in the target cells as a proof of FRET.

Olympus IX83. All the imaging related to the reverse transfection experiments with the "optimization library" were performed in the widefield fluorescent microscope due to the speed of imaging (fluorescent lamp illumination of the whole specimen instead of scanning in the confocal mode) and higher intensity of fluorescence (due to the absence of the pinhole compared to the confocal microscopes). The microscope was equipped with a Hamamatsu ImagEM CCD camera and an environmental chamber using 20× 0.70 numerical aperture (NA) or 10× 0.40 NA and 436/20 excitation filter, a CFP/yellow fluorescent protein (YFP) dual-band beam splitter (51017bs; Chroma), and two emission filters (470/30 for CFP and 535/50 for YFP) that were controlled by a filter wheel. The images were captured with xCELLence software at 3 min interval.

Nikon Eclipse Ti. Infection experiments were performed in the Biological safety level 3 lab at the Heidelberg university clinic using a Nikon Eclipse Ti inverted microscope using a 40× Plan-Apo N.A. 0.95 objective (Nikon). Forty to 60 observation fields were defined, and image acquisition was performed at intervals of 1 h for 48-72 h by using the automated Nikon perfect focus system,

435 nm excitation with CFP and YFP filters, together with 570 nm excitation with mCherry filters. Images were analyzed with the Nikon NIS Element Advanced Research program and processed by using the image processing package Fiji.

Image analysis

Images were analyzed using FIJI, a distribution of ImageJ with the help of previously designed macro for FRET readout analysis - FluoQ (Stein et al., 2013). FIJI is the recommended ImageJ distribution for FluoQ, since the macro makes use of several plug-ins that come with FIJI, but not with plain ImageJ. The following processing options were chosen within the macro: the background was subtracted using ImageJ's built in function. A median filter (radius size = 2) was used to smooth the images. Before calculating the ratio channel, images were transformed to 32-bit float and a threshold was applied to remove low value pixels from analysis. Cells were segmented automatically by FluoQ using the histogram-based "Triangle" threshold algorithm to create a binary cell mask, the watershed algorithm to separate cell clumps, and finally the particle analyzer plug-in to define ROIs. FluoQ measured the mean pixel intensity of each ROI over time and saved all measured data and calculated parameter in a text file (EXPNAME_data set.txt) that was subsequently loaded into the R program in order to do the data analysis. Plots were produced using the gglot2 R package.

Western blot

HeLa cells were split and grown in 6-well plates or individual 35mm cell culture dishes to a confluency of 70%. After 24h they were transfected with target FRET sensors using Lipofectamine 2000 and cultured for 24 h. Cells were harvested using a cell scraper and lysed according to the previously described protocol.. Lysates (50 mg) were separated on NuPAGE 4-12% Bis-Tris protein gels (10-well, ThermoFisher) in the X-Cell SuperLock Mini-Cell and transferred to PVDF membranes (Immobilon-P, Millipore), with the help of X-Cell II Blot

modules the following the manufactures' protocol. Afterwards, the membranes were blocked using 5% skim milk in a standard PBS-T buffer (or 5% BSA in a standard TBS-T buffer when using the antibodies against phosphorylation). The primary antibodies were incubated in 5% skim milk overnight. The HRP-conjugated secondary antibodies were incubated for 1 h and imaged using a Bio-Rad imaging system

Antibodies used were purchased from:

1. Loading control Abcam mouse anti-βactin, ab 6276;
2. Primary Abcam rabbit anti-eIF2α (pS51), ab 32157;
3. Primary Abcam rabbit anti-PKR (pT446), ab 32036;
4. Primary ThermoFisher mouse anti-eIF2α, QF215110;
5. Primary ThermoFisher rabbit anti-PKR, 810467 a;
6. Secondary ThermoFisher goat anti-rabbit IgG (H+L), HRP conjugated, AB_10960844;
7. Secondary ThermoFisher goat anti-mouse IgG (H+L), HRP conjugated, AB_1185566.

Results

Fluorometric analysis of the FRET sensor

As was previously mentioned, in the sensor I exploited the ability of the N-terminal domain of PKR to bind dsRNA during the infection of RNA viruses. I cloned a FRET sensor which consists of mTurquoise (version of CFP), N-terminal domain of PKR (PKR1-175) and cp173Venus (version of YFP with a circular permutation). At first, sensor had to be proven to produce a FRET response in the presence of dsRNA. For that, I expressed KPR1 in HeLa cells, next day the cells were lysed in the native conditions and the lysate containing the expressed KPR1 was transferred to the cuvette for the fluorescent measurements. I decided to perform the measurements in the lysate, as oppose to purifying the KRP1 protein. The reason behind it is a more native environment of the sensor in the cell potentially including some internal double-stranded RNA molecules that the sensor can bind to. Another reason is the simplicity of the lysis procedure compared to the protein purification methodology.

To obtain the FRET readout, I collected emission spectra of the lysate containing KPR1 with or without the presence of the substrate (dsRNA) while exciting only mTurquoise (CFP, one of the exc. max - 435 nm). In this excitation mode, a presence of the second peak of corresponding to YFP indicates energy transfer during FRET. The ratio of the intensities of two peaks was taken as a FRET readout. Titrating the lysate with 30 bp dsRNA duplex (reported previously in PKR-RNA studies) resulted in the increase in FRET ratio (Figure 10). This experiment clearly indicates that upon the dsRNA binding, the sensor adapts a more close conformation, fluorescent proteins come closer together and the FRET increases. The maximum FRET ratio change for KPR1 was 42% (Figure 11).

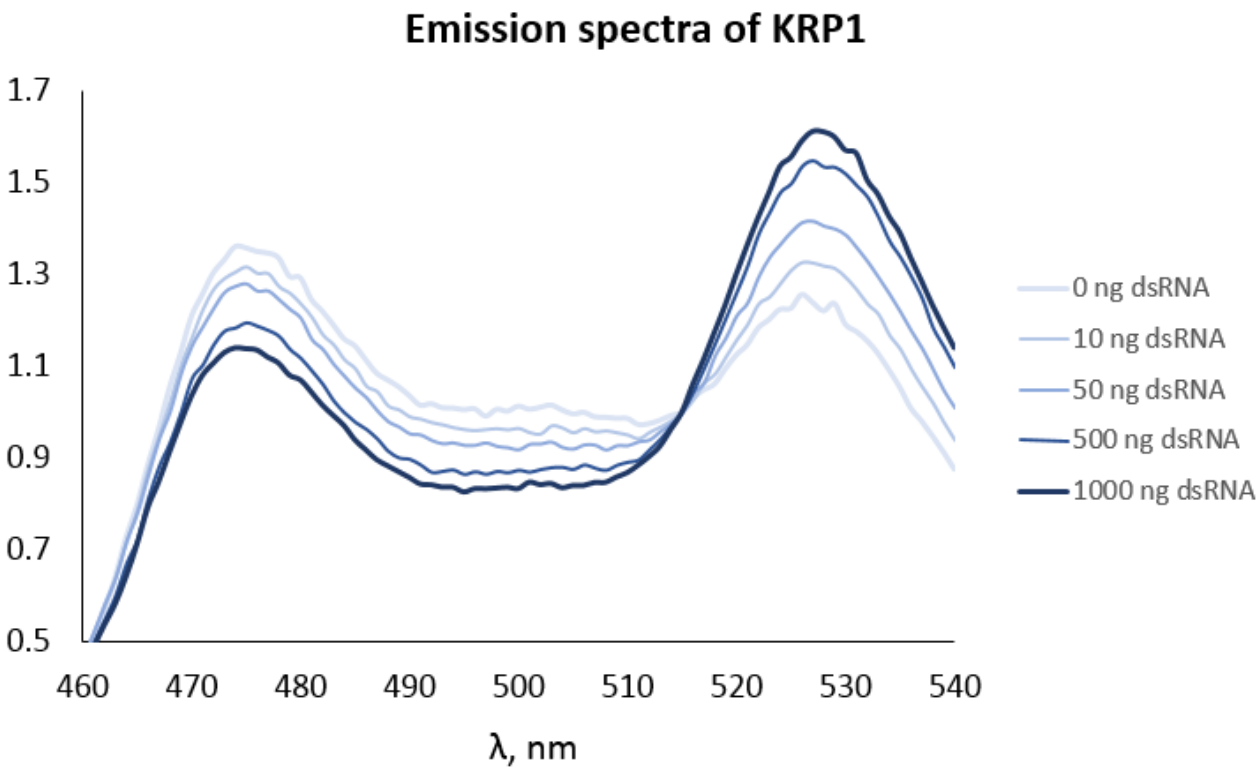

Figure 10. Emission spectra of KPR1 during the titration with dsRNA.

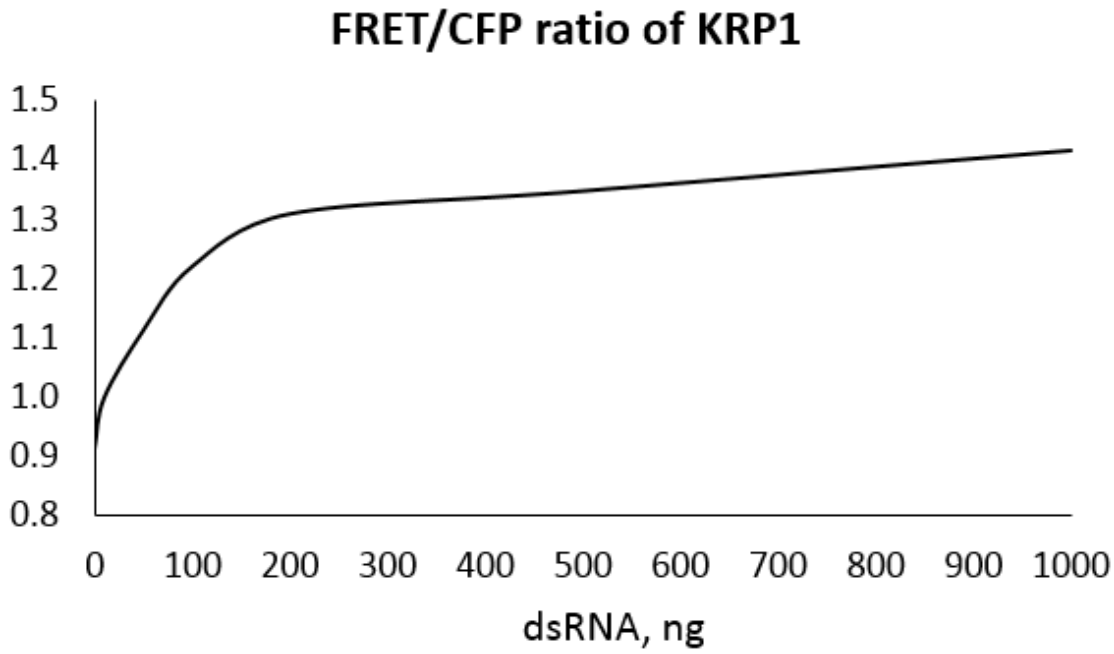

Figure 11. FRET ratio change against dsRNA amount.

To prove that the second peak appears due to FRET and not a cross-excitation of YFP, the lysate containing KPR1 or the lysate containing KPR1 after addition of saturating amount of dsRNA was treated with trypsin. We observed that the beta-barrel structure of the fluorescent proteins and also proteins' chromophores are more resistant to the trypsin digestion, we observed FRET to vanish due to the separation of FPs of KPR1 from each other (Figure 12).

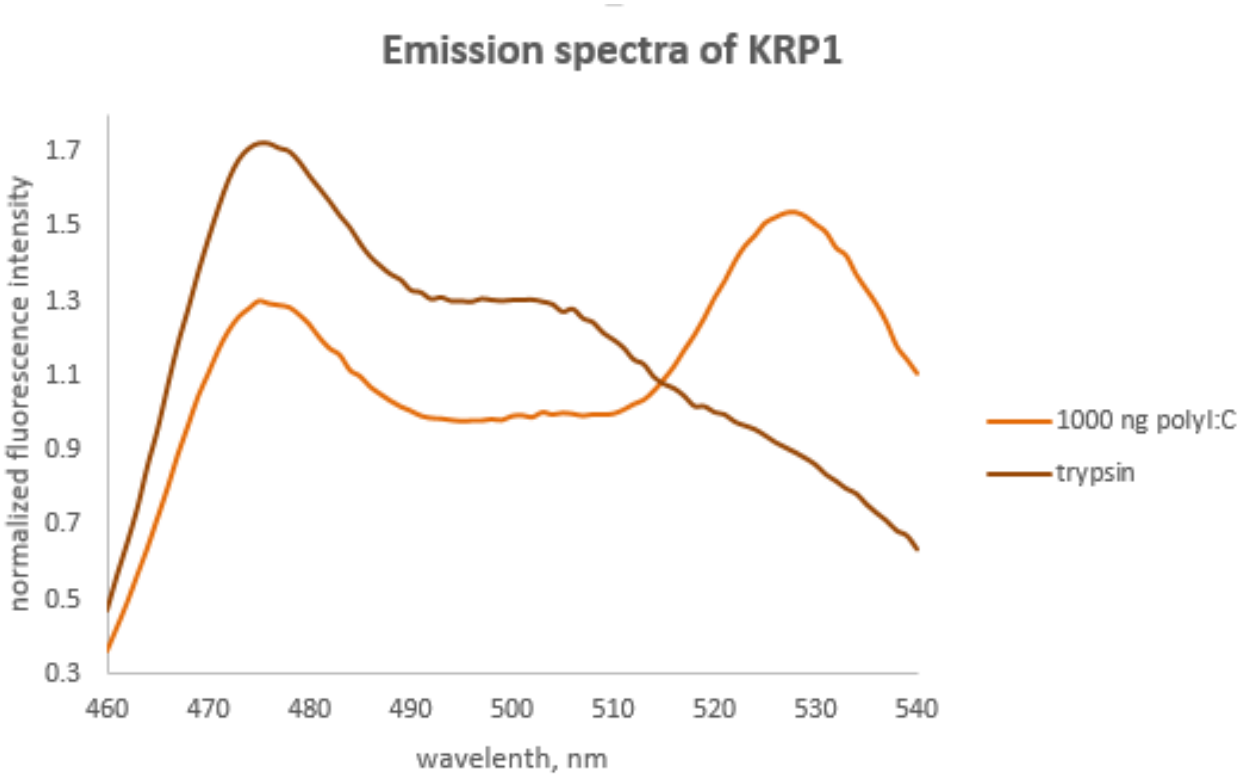

Figure 12. Emission spectra of KRP1 before and after the addition of trypsin.

PKR was reported to bind RNA sequence-independently. To test that we treated the lysate containing KPR1 with polyI:C mix. PolyI:C is a polymer mix of a varying lengh (LMW – low molecular weight: 100-1000 bp duplexes; HMW – high molecular weight: 1000-10000 bp duplexes) which maintains a dsRNA A-helix structure (Figure 13). PolyI:C is commonly used to mimic the responses to infection of RNA viruses by activating the interferon response. Treatment with polyI:C resulted in the same FRET increase as with 30 bp dsRNA (Figure 14). The saturation curve looked similar indicating that one long RNA molecule can

bind many KPR1 units. I tested the polyA:U mixture and the 200 bp RNA duplex of first 200 nt of Ampicillin sequence and obtained the same result.

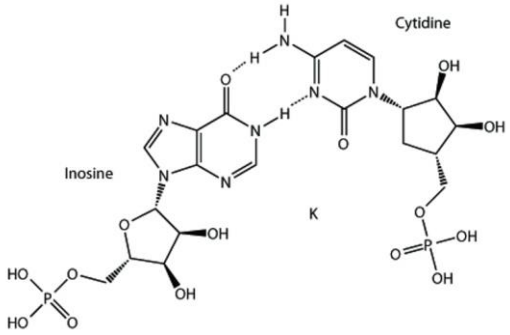

Figure 13. Structure of one I:C nucleotide pair.

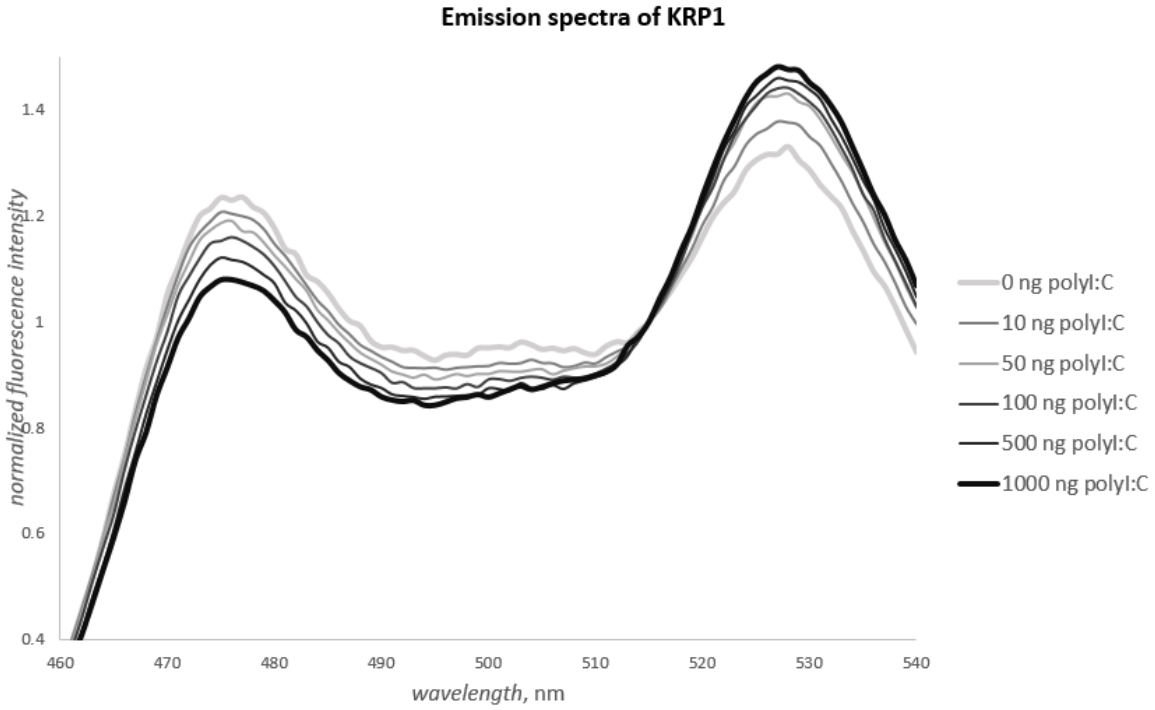

Figure 14. Emission spectra of KPR1 during the polyI:C treatment.

Specificity of the sensor

Next step was to test the specificity of KPR1 to the dsRNA substrate. Previous reports suggested that PKR is extremely specific to the dsRNA structure, able to differentiate it not only from ssRNA, ssDNA and dsDNA, but

also from RNA/DNA duplexes. We treated the lysate containing KPR1 with ssRNA, ssDNA and dsDNA of different length and observed no FRET change in the fluorescent spectra (Figure 15 and 16). As a control, dsRNA was added at the end of the experiment to induce the FRET response.

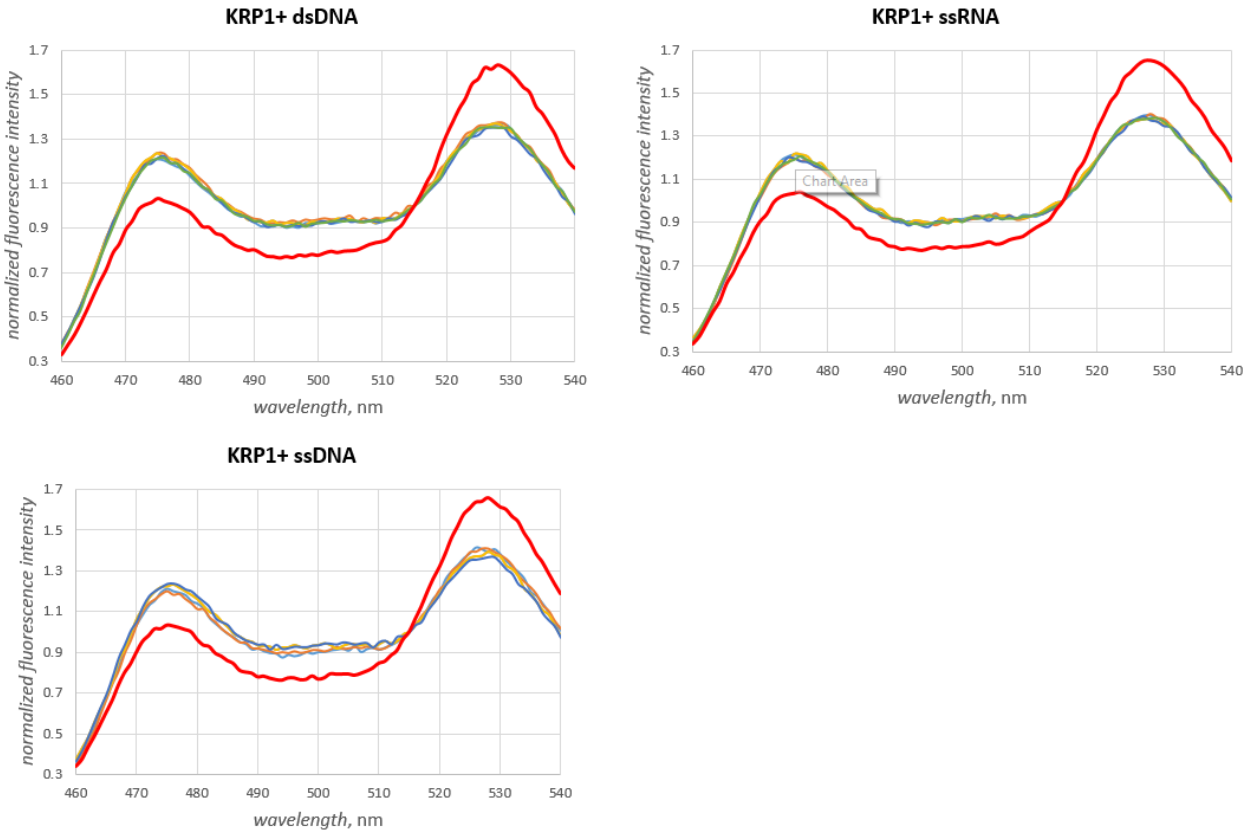

Figure 15. Emission spectra of KPR1 during titration with ssRNA, ssDNA, dsDNA, followed by treatment with dsRNA in the end of the experiment.

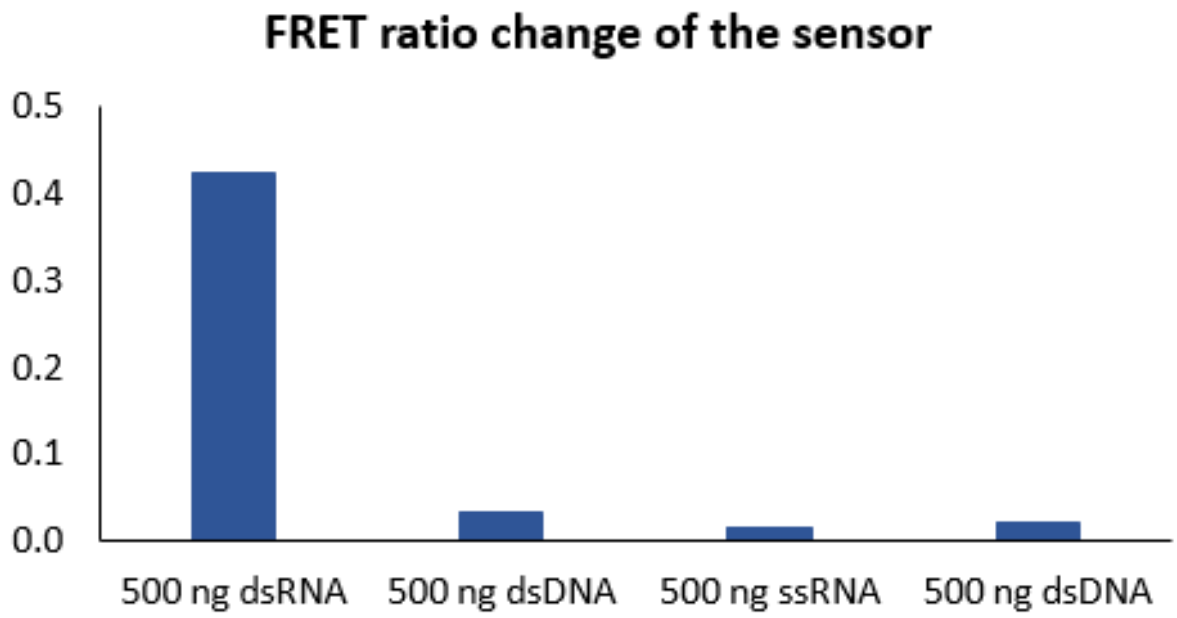

Figure 16. FRET ratio changes of the sensor depending on the substrate

Performance of the sensor in live cells

After designing the dsRNA sensor and confirming a quite good FRET response to dsRNA *in vitro* I wanted to test the performance of KRP1 in live cells against dsRNA. The difficulty of this experiment is inefficient delivery of the RNA inside the cell. dsRNA is negatively charged and cannot pass thorough the cell membrane. Among several nucleic acid delivery methods (including the electroporation and microinjection) the transfection was chosen for the experiments.

I expressed KRP1 HeLa cells. Despite the variability in the fluorescence intensity among different cells due to the transfection process, the FRET ratio in all cells was the same. The sensor localization was predominantly cytoplasmic, thus, providing the "negative" nuclear staining helping to clearly identify (and later process during the image analysis) cells during the imaging. Transfection of the short 30 bp dsRNA duplex caused cells to have a high FRET ratio compared to the cells transfected with the empty transfected reagent (Figure 17). The time

when the FRET response can be observed begins after 5h (the time needed for the RNA/transfection reagent complex to move inside the cell) (Figure 18). Acceptor photobleaching performed in some individual cells recovered the CFP fluorescence in them, while disposing of the YFP signal. This routine control confirms FRET and eliminates YFP cross-excitation and CFP bleed-through artifacts. It is hard to see cells with high FRET during the imaging of the cells later than 8h after RNA transfection. This is due to a high rate of the cell death because of both the transfection reagent and, even more so, the transfected RNA. In fact, the FRET in the cells begins to drop even below the level of the untreated cell. As surprising as it might seem, this is a common feature of many FRET sensors which respond to substrates with the FRET increase (Hochreiter et al., 2015). The activation of unspecific proteases during the apoptosis causes the digestion of the sensor and the separation of two fluorescent proteins and, hence, loss of FRET. The digestion of the fluorescent proteins themselves takes a much longer time, so individual fluorescence remains up until the cell membrane collapses.

As expected, the transfection of 200bp dsRNA, polyI:C (LMW), polyI:C (HMW) and polyA:U caused the transfected cells to have a higher FRET ratio, proving that the KRP1 response is not dependent on the sequence of the dsRNA (Figure 17). The toxicity in case of the big polyI:C molecules is much stronger than in the case of the short dsRNA duplexes which can be identified by the cell shape and the loss of FRET (very low FRET ratio).

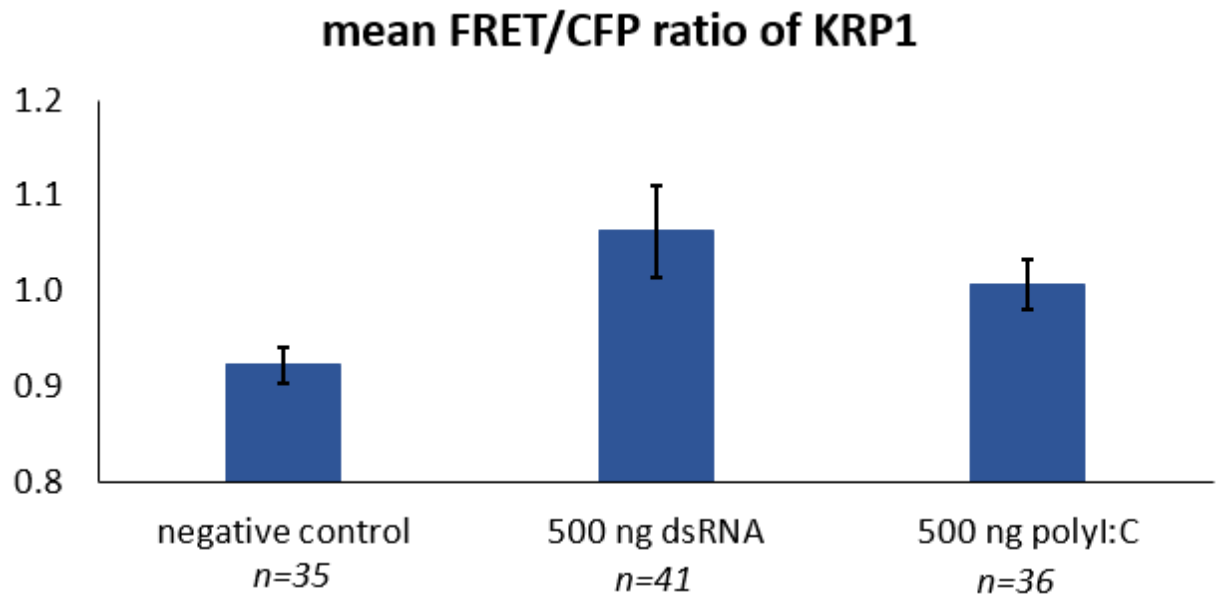

Figure 17. Mean FRET/CFP ratio across several HeLa cells expressing KRP1.

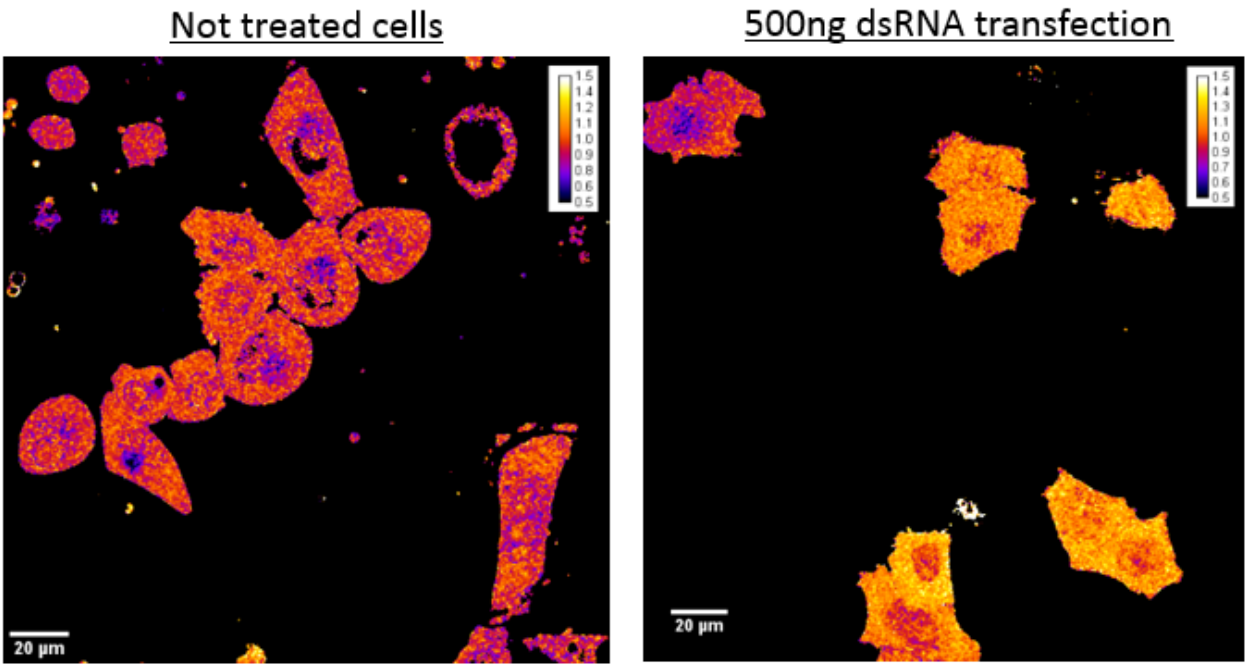

Figure 18. Example of FRET/CFP ratio images of HeLa cells expressing KRP1 in the absence or presence of dsRNA after 5h of transfection.

Optimization of the sensor

Optimization of the insert part

A standard procedure during the development of any sensor is an optimization of its performance. In KRP1 I pursued two optimization targets: RNA-binding part and fluorescent protein part.

RNA-binding part consists of the N-terminal domain of PKR (PKR 1-175). This RNA-binding domain is followed by a ~100 amino acid unstructured region before the catalytic C-terminal domain begins. The idea was to add amino acids from this unstructured region to the original PKR (1-175) with the step of 20. Effectively I was adding a long linker between the PKR part and one of the fluorescent proteins with the hope to reduce initial FRET in the resting conformation and, thus, increase the dynamic range of the sensor (Figure 5). Also I decided to take away 20 amino acids from the RNA binding domain to make the conformation stiffer with the hope of increasing the FRET change during the dsRNA binding (which would also increase the dynamic range of the sensor).

The sensors containing PKR 1-155, PKR 1-175 (KRP1, the original version), PKR 1-195, PKR 1-215, PKR 1-235, PKR 1-255 and PKR 1-275 were titrated with the increasing amount of dsRNA and the emission spectra were collected in the fluorimeter (Figure 19).

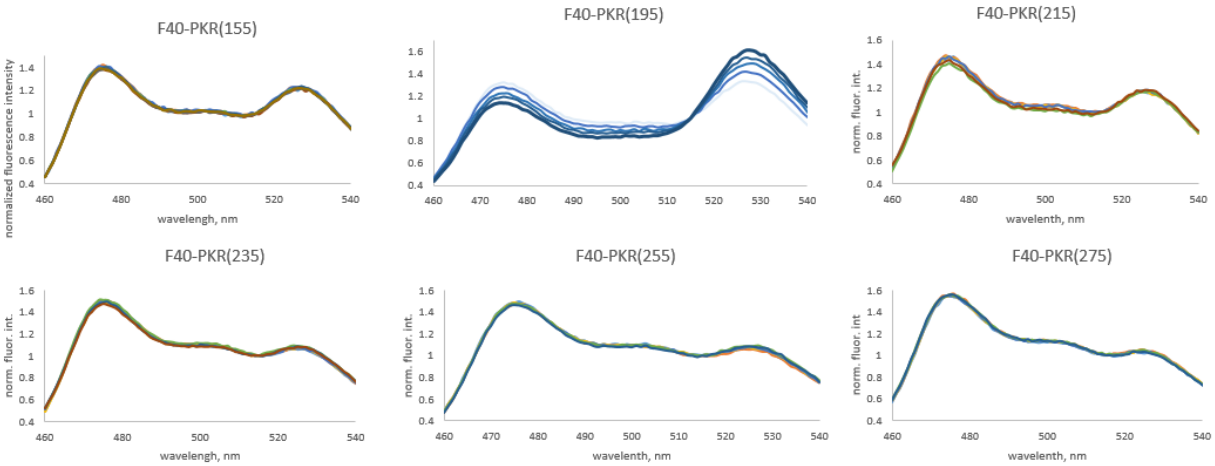

Figure 19. Emission spectra of KRP1 containing different length of the N-terminal domain of PKR upon dsRNA treatment.

The sensors with the "long linker" had indeed lower initial FRET in the absence of dsRNA (the longer the linker was – the lower FRET was detected). Unfortunately, addition of the substrate didn't result in any FRET change of the construct. The only version which showed a FRET response was the PKR(1-195) construct (20 amino acids longer N-terminal domain of PKR than in the original KRP1) with the maximum FRET ratio change of 27% (Figure 20). The dynamic range appeared to be lower than in the PKR (1-175) version, therefore the original version of the sensor had the optimal RNA sensing par. The PKR(1-155) version (lacking 20 amino acids from the C-terminal part of the dsRNA binding domain of PKR) had a significant "initial FRET" in the absence of the RNA, but didn't show any FRET change after the addition of the substrate, hence, no RNA binding. This indicates that both RNA binding motifs of the N-terminal domain of PKR are important for binding dsRNA (even partly truncating one of them prevents any interaction).

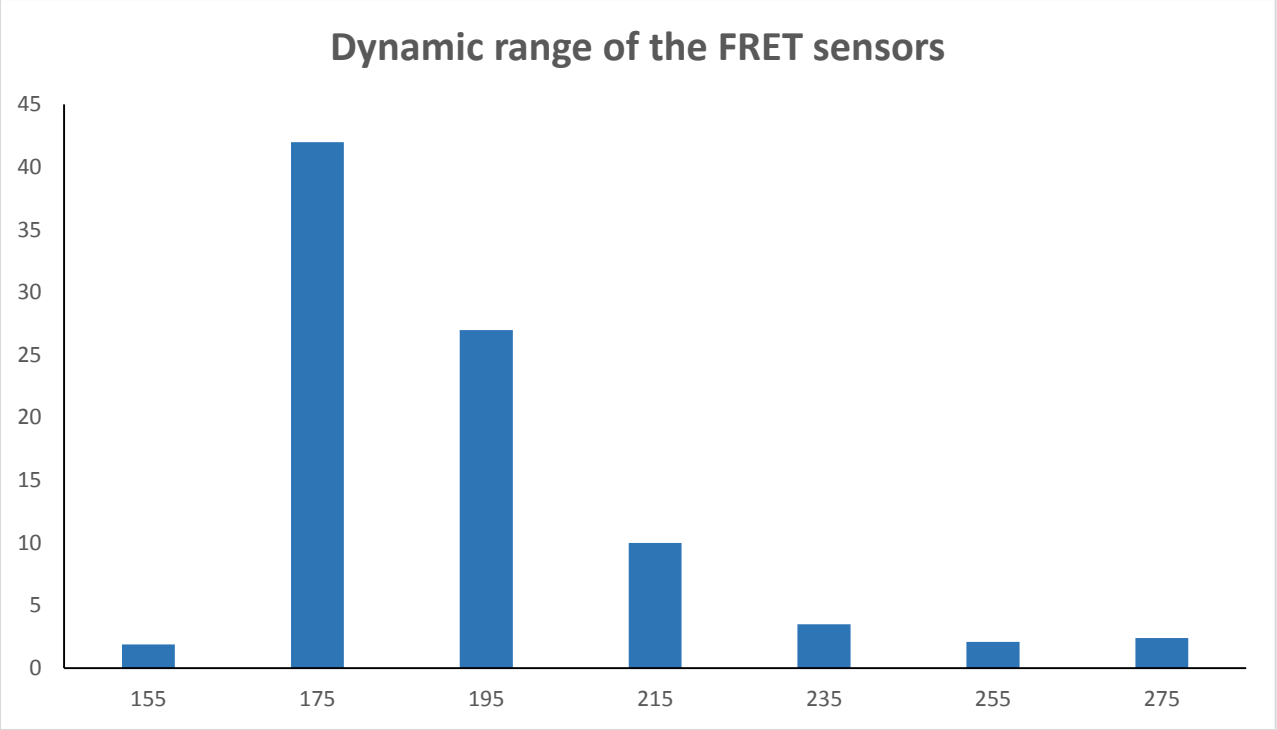

Figure 20. Max FRET ratio change of KRP1 containing different length of the N-terminal domain of PKR upon dsRNA treatment

Optimization of the Fluorescent protein FRET pair

In the sensor design I employed the most common and optimal CFP/YFP fluorescent protein FRET pair. Fluorescent proteins' proximity and orientation to each over is limited by the conformation of the sensor part of the sensor (which is the N-terminal domain of PKR). Addition of the flexibility factor in the fluorescent proteins' positioning via introduction of the linkers is not a successful strategy as concluded from the previous experiments. Alternative way to change not the proximity but the orientation of fluorescent proteins is to use their different circularly permutated versions (briefly discussed in the introduction section) in the sensor. Introduction of different circularly permutated versions of one of the fluorescent proteins can change the orientation of the fluorophore dipole moments to, hopefully, a more optimal one, and the use of different versions of the other fluorescent protein might improve the FRET efficiency.

This idea was exploited in our lab some time ago to design new and improve the existing FRET sensors (Kuchenov et al., 2016, Bulusu et al., 2017, Piljic et al., 2011, Stein et al., 2013). We cloned a library of plasmids containing different circularly permutated versions of Venus (as yellow fluorescent protein), different versions of cyan fluorescent protein and a 2-, 4- or 8-amino acid linker between them with an easy way to introduce the insert of interest.

The method is designed for a high throughput screening of FRET sensors inside the live cells. All of the cloned sensors from the library are "spotted" on the coverslip mixed with the transfection reagent followed by the reverse transfection into the cells seeded on top of the plasmids. The sensors are imaged under a fluorescent microscope (desirably with a fast stage) during the treatment with the small molecule substrate.

I cloned a set of 36 sensors (coded F02-F63, Figure 21) and tried to test them with the original protocol. Unfortunately, the live cell imaging after spotting was not suitable for comparing sensor performances. The variability in the amount of transfected RNA from cell to cell and long time-intervals of imaging (up to 8h) made it hard to clearly decide about the performance of the individual sensors compared to each other. The majority of FRET sensors (and our published optimization approach) are designed against small molecules, well diffused and easily accessible to the cells, and the time of response is rarely exceeds an hour range.

F02	**mECFP-2-(insert)-2-Venus**	**F46**	**mTuquoise-2-(insert)-2-cp49Venus**
F04	**mECFP-2-(insert)-2-cp173Venus**	**F47**	mTuquoise-4-(insert)-4-cp49Venus
F09	mECFP-4-(insert)-4-Venus	**F48**	mTuquoise-8-(insert)-8-cp49Venus
F11	mECFP-4-(insert)-4-cp173Venus	**F49**	mTuquoiseDEL-2-(insert)-2-cp49Venus
F16	mECFP-8-(insert)-8-Venus	**F50**	mTuquoiseDEL-4-(insert)-4-cp49Venus
F18	mECFP-8-(insert)-8-cp173Venus	**F51**	mTuquoiseDEL-8-(insert)-8-cp49Venus
F34	mTuquoise-2-(insert)-2-Venus	**F52**	mTuquoise-2-(insert)-2-cp157Venus
F35	mTuquoise-4-(insert)-4-Venus	**F53**	mTuquoise-4-(insert)-4-cp157Venus
F36	mTuquoise-8-(insert)-8-Venus	**F54**	mTuquoise-8-(insert)-8-cp157Venus
F37	mTuquoiseDEL-2-(insert)-2-Venus	**F55**	mTuquoiseDEL-2-(insert)-2-cp157Venus
F38	mTuquoiseDEL-4-(insert)-4-Venus	**F56**	mTuquoiseDEL-4-(insert)-4-cp157Venus
F39	mTuquoiseDEL-8-(insert)-8-Venus	**F57**	mTuquoiseDEL-8-(insert)-8-cp157Venus
F40	**mTuquoise-2-(insert)-2-cp173Venus**	**F58**	mTuquoise-2-(insert)-2-cp229Venus
F41	mTuquoise-4-(insert)-4-cp173Venus	**F59**	mTuquoise-4-(insert)-4-cp229Venus
F42	mTuquoise-8-(insert)-8-cp173Venus	**F60**	mTuquoise-8-(insert)-8-cp229Venus
F43	mTuquoiseDEL-2-(insert)-2-Venus	**F61**	mTuquoiseDEL-2-(insert)-2-cp229Venus
F44	mTuquoiseDEL-4-(insert)-4-Venus	**F62**	mTuquoiseDEL-4-(insert)-4-cp229Venus
F45	mTuquoiseDEL-8-(insert)-8-Venus	**F63**	mTuquoiseDEL-8-(insert)-8-cp229Venus

Figure 21. A list of the codes and FRET pairs used in the library (green – original KRP1, red – sensors which show a much higher FRET response).

This forced me to find another testing approach. Ultimately, I designed a high-throughput *in vitro* assay to test my sensor library. The plasmids were transfected in a high-throughput manner into the cells seeded in the 96-well plate. This was followed by the native lysis of the cells and measurement of the CFP and FRET fluorescence in the presence and the absence of dsRNA in each well with the plate-reader. In this way we determined FRET ratio change of each sensor when saturated with the dsRNA (Figure 22).

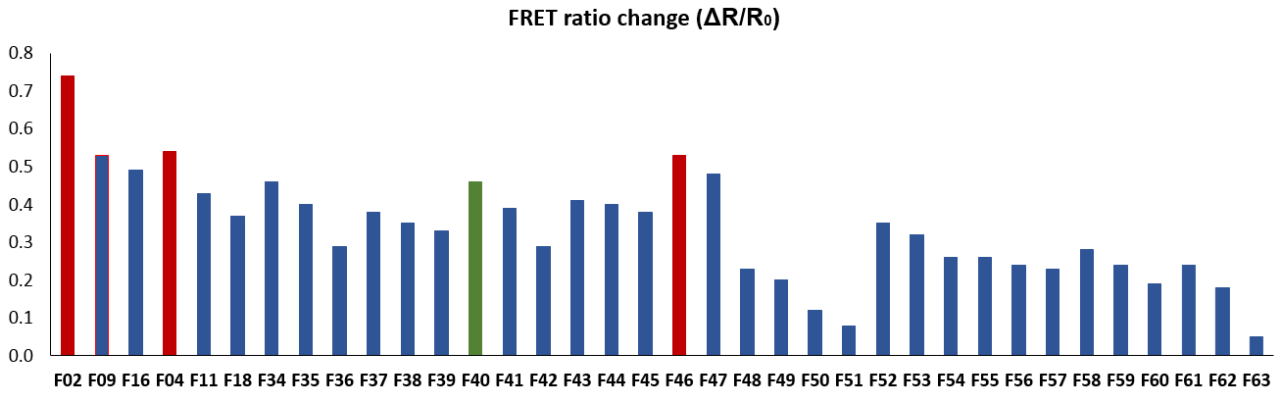

Figure 22. Dynamic range of all of the FRET sensor versions obtained from the library (green – original KRP1, red – sensors which show a much higher FRET response).

Interestingly enough, 2-amino acid linker worked best with every fluorescent protein pair while 4- and, even more so, 8- amino acid linker reduced the dynamic range. Fortunately, I identified several sensors having higher FRET ratio change in the presence of dsRNA than the original KRP1 (coded F40 in the library). Due to some margin of error of the pate-readers (because of measuring the fluorescence in small volumes) I expressed some of the best identified sensors and tested them in the cuvette (Figure 23). The best performance was observed for a sensor with the pair coded under the name F02, containing mECFP (interestingly not mTurquoise), wild type version of Venus and a two amino acid linker between them and the PKR (1-175) (Figure 24).

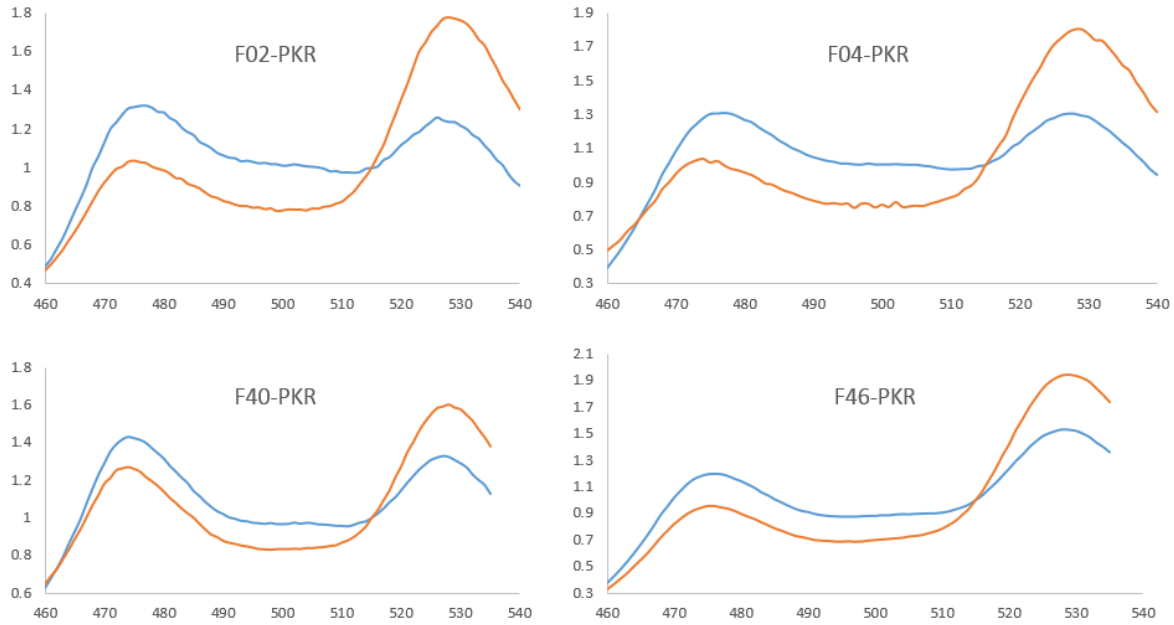

Figure 23. Emission spectra of some of the chosen FRET sensors collected in the fluorimeter (F40 – original version, F02 – the best version, blue line – before the addition of dsRNA, orange line – after the addition of dsRNA).

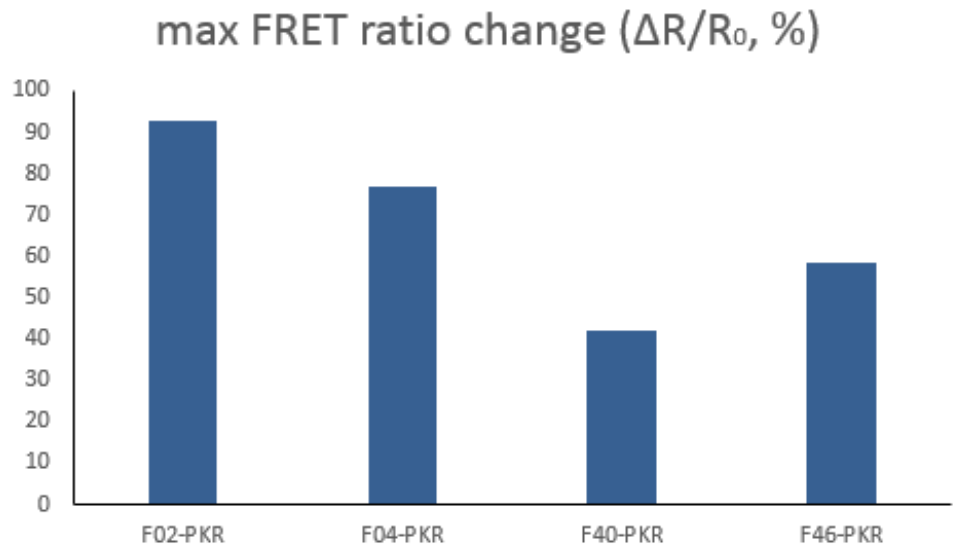

Figure 24. Dynamic range of some of the chosen FRET sensors (F40 – original version, F02 – the best version).

Performance of the improved sensor in live cells

After the optimization step I identified several fluorescent protein pairs which improved FRET response of the sensor. The best FRET efficiency in the current setup was achieved with ECFP (with the monomeric mutation) and a wild-type version of mVenus (no circular permutation). The optimized version of the sensor (with the FRET pair coded F02 in the previous figure) was called KRP2. I subjected KRP2 to the same dsRNA tests which were performed on the original version of the sensor.

The HeLa cell lysate containing expressed KRP2 was treated with the dsRNA while collecting the emission spectra of the sensor. The improved sensor has a maximum FRET ratio change of 93% when saturated with dsRNA which is more than double of the original KRP1 (Figure 25). A control treatment with trypsin destroyed FRET and recovered the original CFP intensity and treatment with different polyI:C versions resulted in identical emission spectra.

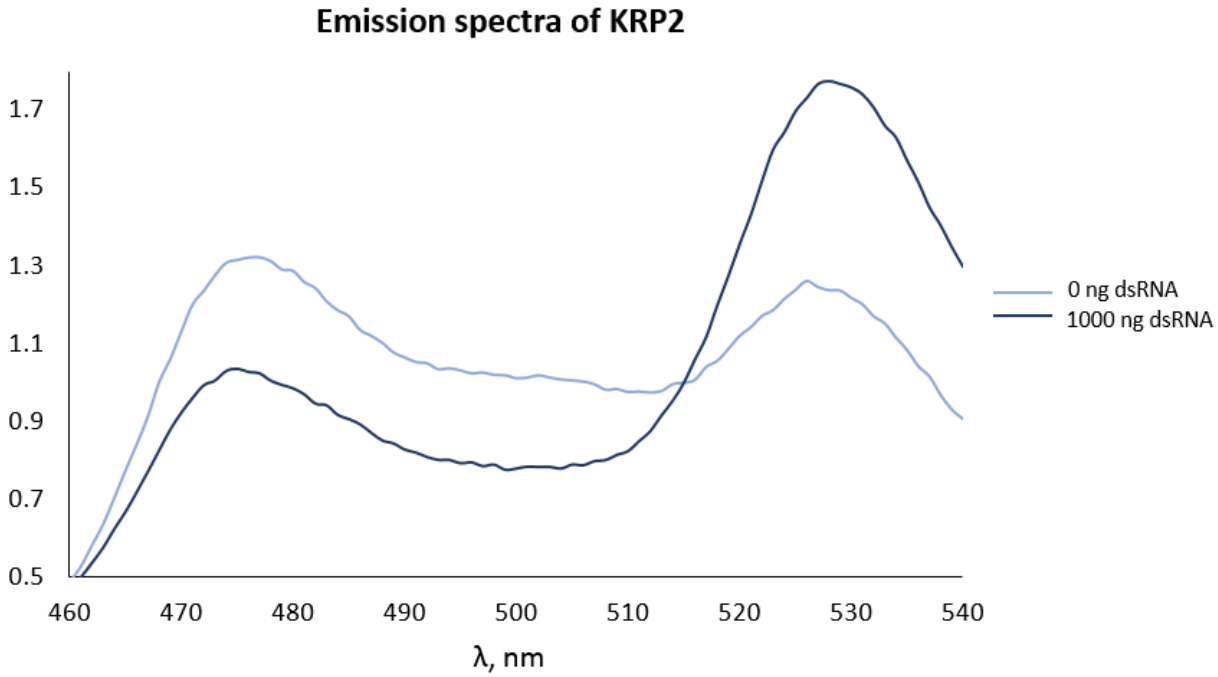

Figure 25. Emission spectra of KRP2.

The specificity of KRP2 was not expected to be different from the original version, but nevertheless was worth checking due to higher sensitivity of KRP2. The response during treatment with dsDNA, ssDNA and ssRNA was scornfully low (Figure 26).

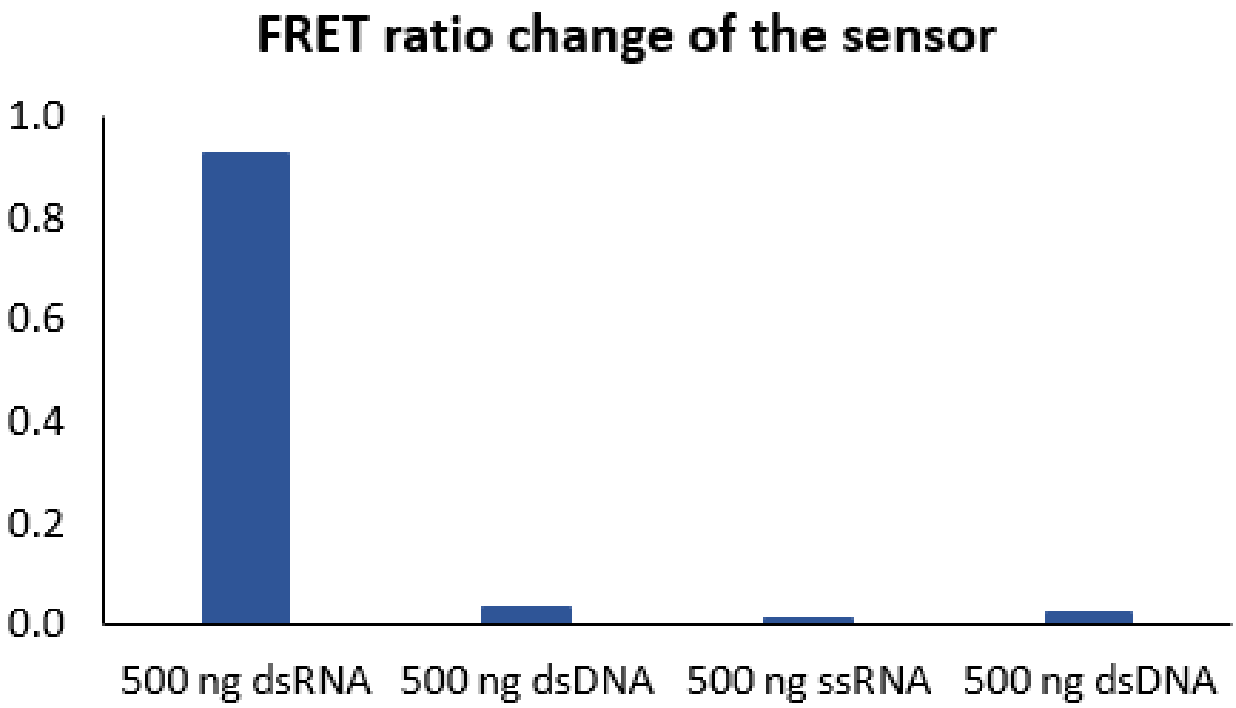

Figure 26. FRET ratio changes of the KRP2 depending on the substrate.

KRP2 was also tested in live HeLa cells under the microscope against the treatment with dsRNA. Fortunately, FRET ratio of the sensor among untreated cells was constant and didn't vary despite more than twice higher sensitivity compared to KRP1. Treatment with dsRNA resulted in many cells having a higher FRET ratio compared to the cells treated with empty transfection reagent, in often reaching maximum possible FRET ratio change. A routine acceptor photobleaching control was also performed.

Huh7 stable cell line expressing the sensor

In order to test the sensor against a viral infection it has to be introduced into the system where the replication of HCV is possible and efficient. The commonly used system for studying HCV is Huh7 cell line, which was picked for the current project.

Testing and using the sensor in the pipeline developed for HeLa or HEK cells was proven to be problematic. Huh7 cells appeared to be stiff and quite resistant to the introduction of the sensor plasmid either by transfection or electroporation. With the use of strong transfection reagents like Lipofectamine 3000 I managed to transfect Huh7 cells with KPR2 and successfully test it against dsRNA or polyI:C either in the lysate *in vitro* or on the cover slip *in vivo* (data not shown). However, high toxicity and low efficiency of this approach in the Huh7 cells forced us to develop a stable cell line expressing the sensor.

The stable cell line was produced in the Ruggieri lab and was kindly provided to me. Another potential advantage of using a stable cell line is a much lower expression level of the sensor inside the cell which would lead to a larger FRET readout in the case of low quantity of dsRNA produced during viral infection.

A quality control of the cell line was performed in a similar fashion to the one in HeLa cells. The Huh7-KPR1 or Huh7-KRP2 cells were lysed in the native conditions and the emission fluorescent spectra were obtained during the treatment with dsRNA or polyI:C (Figure 27). As expected, spectra looked the same as in the case of HeLa cell lysates, FRET ratio change was similar to what was observed in HeLa cells irrespectively of the substrate: dsRNA or polyI:C.

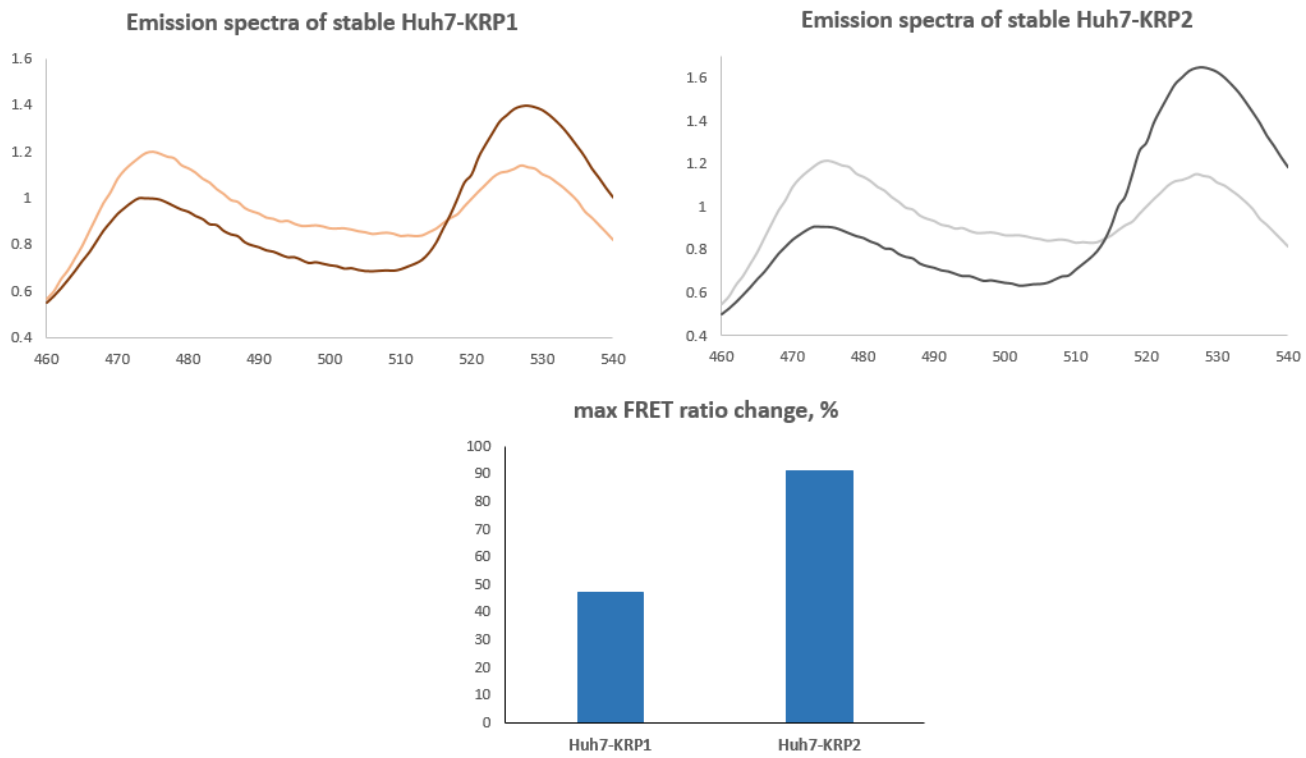

Figure 27. Emission spectra of the lysates of Huh7 stably expression KRP1 (a), KRP2 (b) and max FRET ration change upon addition of dsRNA.

Under the microscope, the fluorescent intensity and the FRET ratio were universally distributed with no cell-to-cell variability, as was observed in case of HeLa or HEK cells. Transfection of the short dsRNA resulted some cells having a higher FRET ratio (Figure 28). Unfortunately, the maximum potential of the FRET ratio change was not reached because of poor efficiency of dsRNA transfection. Increase in the amount of either the transfection reagent or dsRNA causes significant cell death. Transfection of polyI:C was also inefficient and even more toxic for the cells,, although the cells with a higher FRET ratio were still observed (Figure 29).

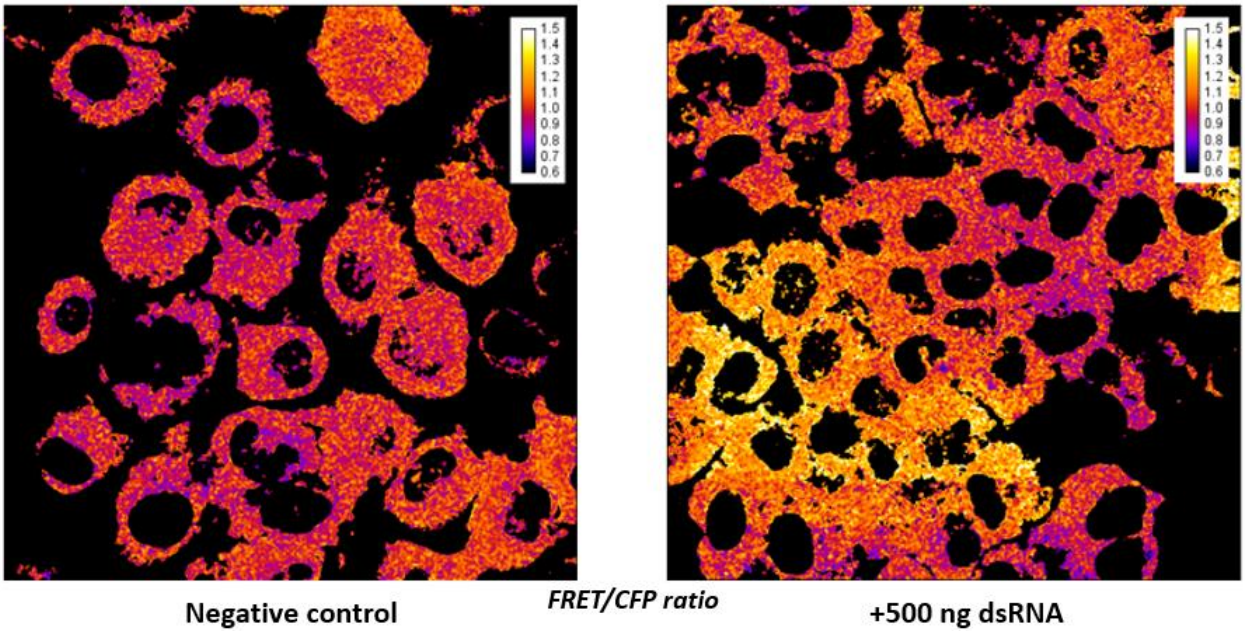

Figure 28. Example of FRET/CFP ratio images of Huh7 cells expressing the sensor in the absence or presence of dsRNA after 5h of transfection.

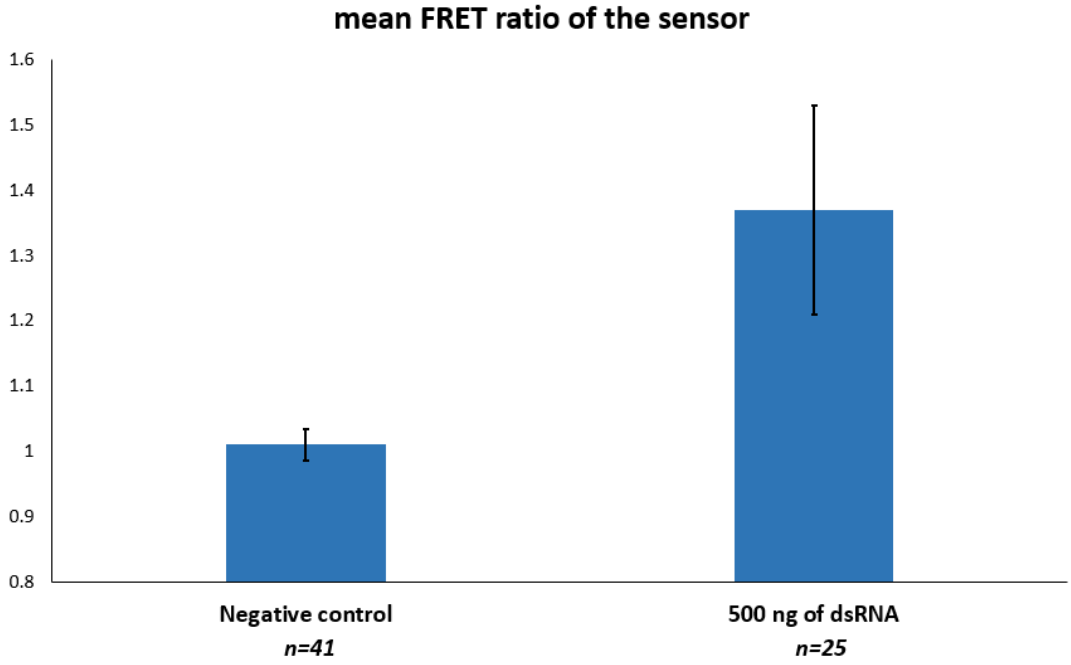

Figure 29. Mean FRET/CFP ratio across several Huh7-KRP2 cells upon the transfection of dsRNA

Worth mentioning that the dsRNA (or rather polyI:C) treatment doesn't induce the interferon response in Huh7 cells which would lead to overexpression of the endogenous PKR. While it is irrelevant in the experiments involving RNA transfection or electroporation, lower quantities of the endogenous PKR can improve the sensitivity of the sensor in the presence of low amounts of viral RNA.

Viral subgenomic RNA replicon transfection

Following the successful validation of the Huh7 stable cell line expressing the KPR1 I started to move towards the direction of viral infection. As a first step of proof-of-concept, KPR1 was tested against self-replicating subgenomic HCV replicon (Lohmann et al., 1999). This viral RNA of roughly 4.5 kb was cloned and kindly provided to me by Ruggieri lab (Figure 30). This RNA can replicate itself since it encodes HCV "replication" proteins, thus producing dsRNA intermediate during the replication. The main advantage of the use of this subgenomic replicon is inability to produce new full viral particles (due to the lack of structural genes in the RNA) hence being safe for the experiments. NS5A protein was labeled with mCherry to mark the cells where this RNA was introduced.

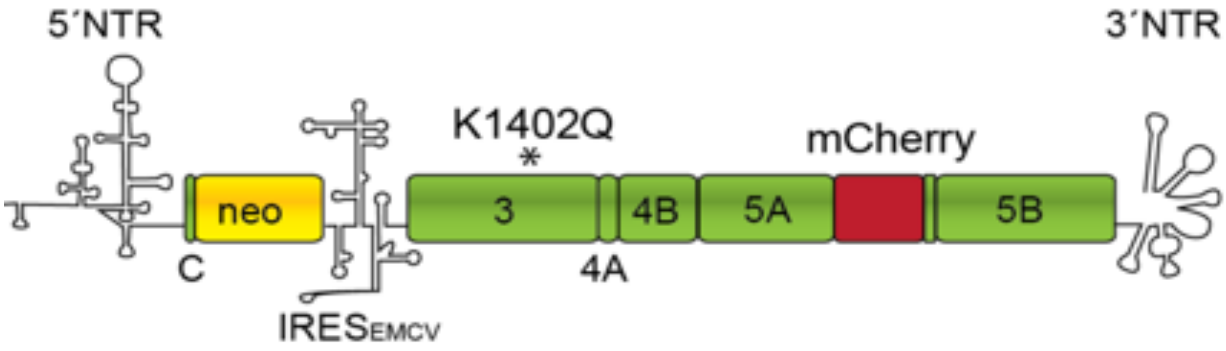

Figure 30. Schematic structure of the subgenomic RNA_{HCV} replicon used in the experiments

I transfected the stable cell line with KRP2 with moderate amount of HCV-RNA and imaged the cell on the next day. At certain period of time I could observe cells which were transfected with the HCV-RNA (and hence expressing mCherry) and having a much higher FRET ratio than the non-treated ones (up to the level of cells transfected purely with dsRNA) (Figure 31). The results were very promising, since it proves that the amount of dsRNA intermediate produced during the replication is sufficient to force the sensor response (Figure 32). Another pleasant observation was that this single-stranded viral RNA in the quantities comparable to dsRNA doesn't produce any FRET readout even though this RNA has some double-stranded hairpins structure parts. Potential reason for that is binding of host and viral proteins or ribosomes which shields these regions from the sensor. Finally, the endogenous PKR present in cells does not significantly interfere with the sensor binding to the RNA.

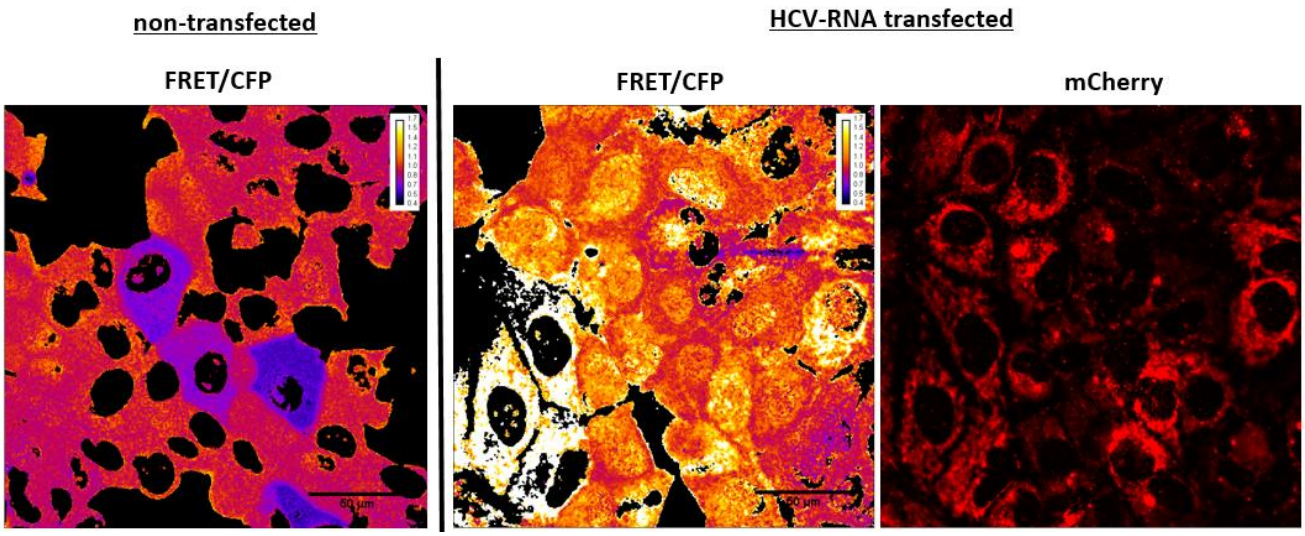

Figure 31. Example of FRET/CFP ratio images of Huh7 cells expressing the sensor after the transfection with 100 ng of the subgenomic RNA replicon (30h after transfection)

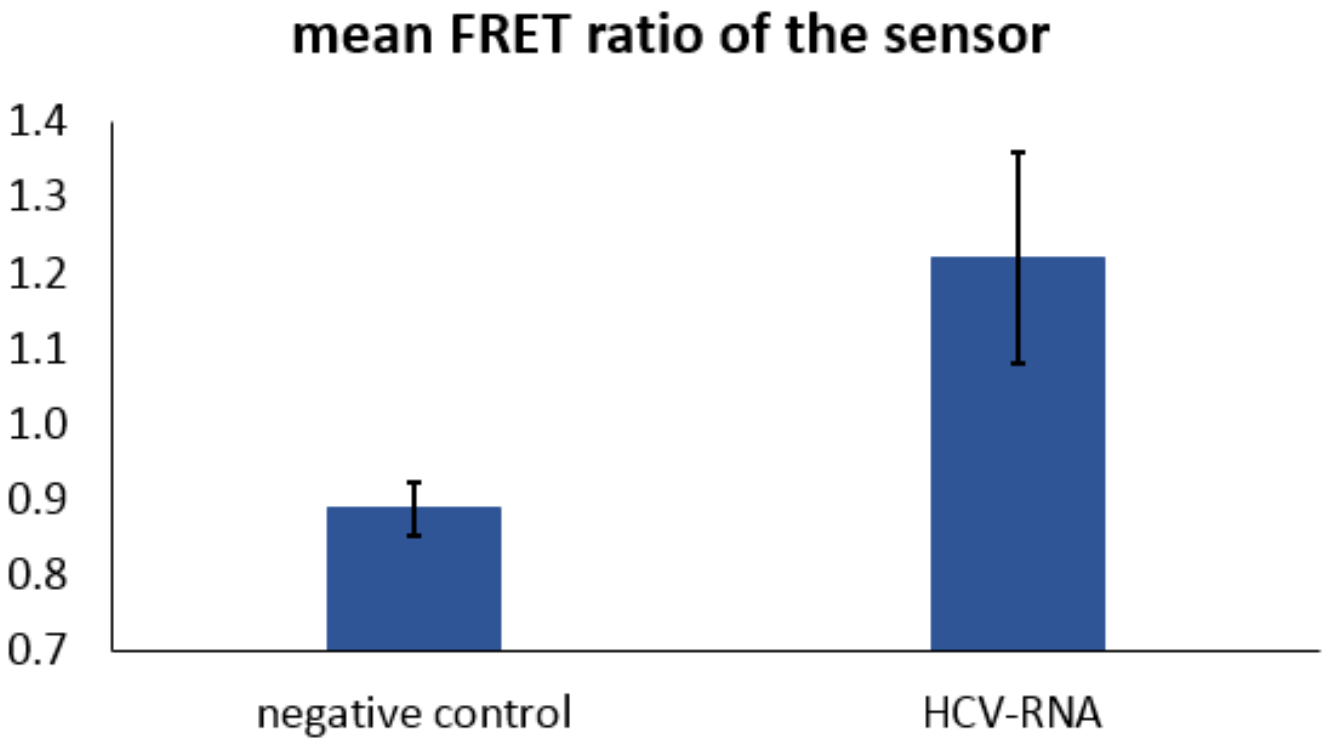

Figure 32. Mean FRET/CFP ratio across several Huh7-KRP2 cells (n=24 and n=15 respectively) after the transfection with 100 ng of the subgenomic RNA replicon (30 h after transfection).

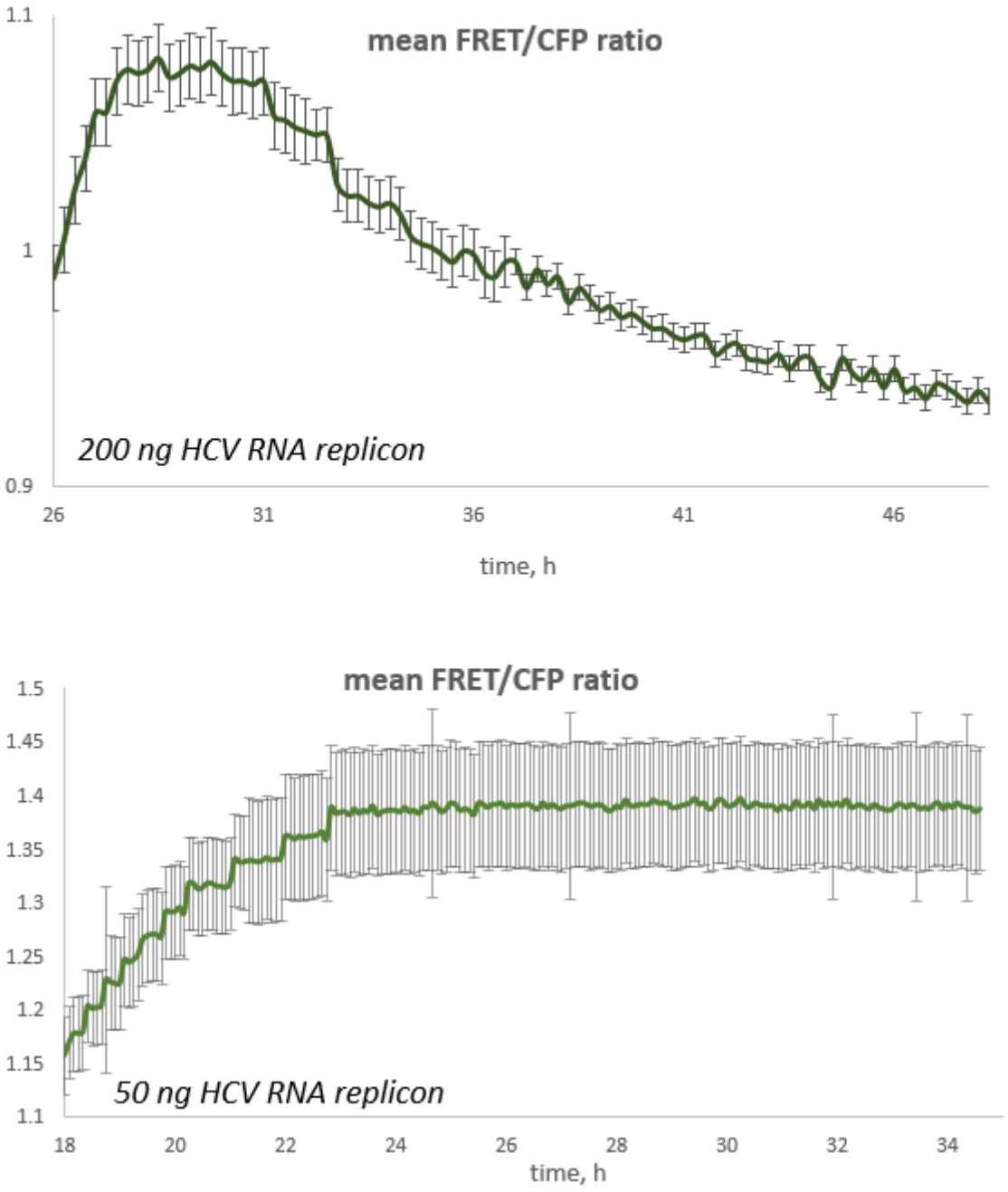

Figure 33. Mean FRET/CFP ratio of the Huh7-KRP2 cells upon transfection of different amount of the RNA_{HCV} replicon

However, there are couple of issues to mention in regard to the use of this HCV-RNA. Firstly, the FRET readout of the sensor is bell-shaped. Significant FRET ratio change can be observed only at a specific point of time around 30 h after transfection (Figure 33).

Secondly, the transfection of the cells with HCV-RNA is not simultaneous. Appearance of mCherry signal indicates the translation of the viral RNA when it is inside the host cell, and the signal appears in different cells at different time, resulting in up to 4-5 h variability. Another source of variability comes from different individual amounts of the transfected RNA form cell to cell (due to the imperfections of the transfection method). All of the sources of variability make it challenging to determine the kinetics or, rather, the precise time of optimal sensor readout.

Interestingly, transfection of the high amounts of HCV-RNA (larger than 200 ng of RNA per ~$2.5*10^4$ of cells) results in no FRET readout at all and high rate of cell death within 36h (Figure 33).

After a certain period of time (depending on the amount of RNA transfected) I can observe the cell death which is indicated by lower FRET readout compared to the non-treated cells.

Viral infection

Moving one step further, I decided to test the sensor against the infection of HCV trans-complementary particles (TCPs). These particles are a single-round infectious virus containing the truncated genome which lacks necessary structural genes to produce a new particle during the replication (Adair et al., 2009, Steinmann et al., 2008, Ishii et al., 2008). TCPs are produced by expressing HCV structural proteins in “trans” in packaging cell lines (Huh7) complemented with the HCV replicon (mentioned in the previous chapter). In simple words, TCPs are a full virus with the truncated genome and, therefore, unable to produce new particles after the infection. The advantage of using TCPs over the full virus is non-infectivity, which makes working with them more convenient. The infection with the TCP_{HCV} requires only biosafety level 2 labs (BS2) as opposed to BS3 lab requirement of the full HCV infection. After washing step on the following day, the previously infected cells are permitted to handle anywhere. The advantage of

using TCPs over the transfection of the subgenomic replicon of HCV is resemblance of the cell entry properties of the full virus. Another appealing feature of using TCPs for the infection is the potential accumulation of the replicated viral RNA (due to inability to produce new virions) and, hence, better chance of the KRP2 succeeding in sensing the dsRNA intermediate.

As was the case in the HCV replicon experiment, after the infection of the stable Huh7 cell line expressing KRP2 with TCP_{HCV} at a certain period of time I observed cells with a higher FRET ratio compared to the non-infected cells (Figure 34). Behavior of the cells and the sensor was similar to one in case of the HCV replicon experiment, although the kinetics was different. The FRET readout also was a bell-shaped curve. The time point when I observe a FRET ratio increase was around 48 h after the infection (24 h after the beginning of the imaging under the microscope) (Figure 35). As an additional control, cells were infected with the TCPs but also treated with the HCV replication inhibitor, resulted in no FRET change in the cells and no appearance of the mCherry signal.

Surprisingly, the cell-to-cell variability during the infection (which is indicated by presence and the intensity of mCherry labeled NS5A protein) was even higher than in case of the RNA transfection. Because of that, determining the precise time of the highest FRET response is problematic. This also makes catching sensor response to RNA replication difficult and forces a lot more pressure on the frequency of the imaging.

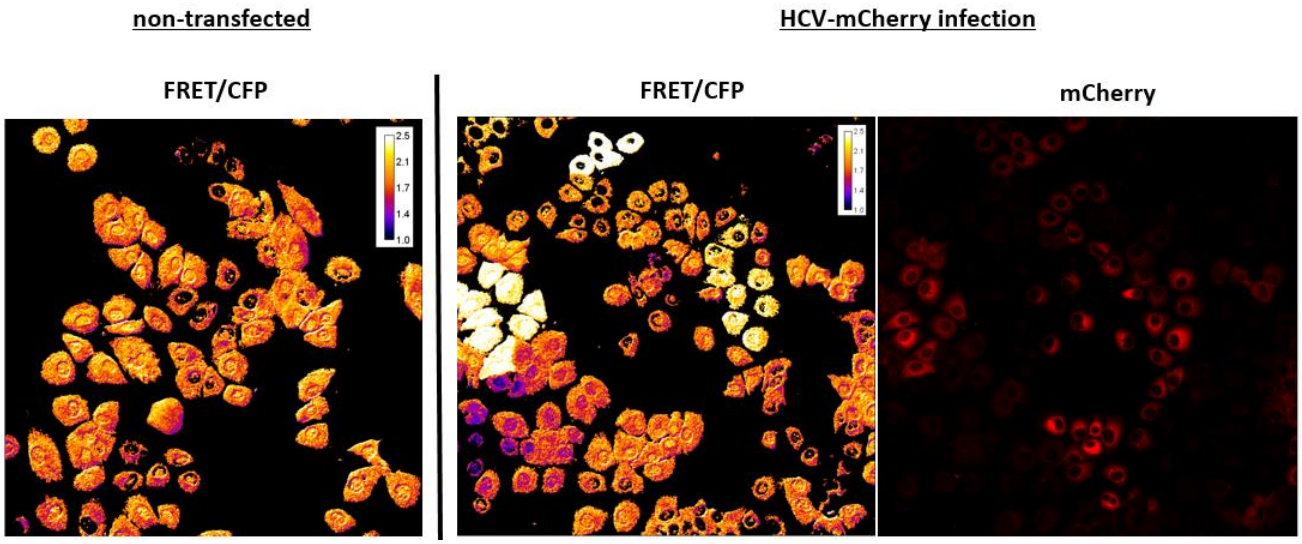

Figure 34. Example of FRET/CFP ratio images of Huh7 cells expressing the sensor after the transfection with the subgenomic RNA replicon (48h after infection)

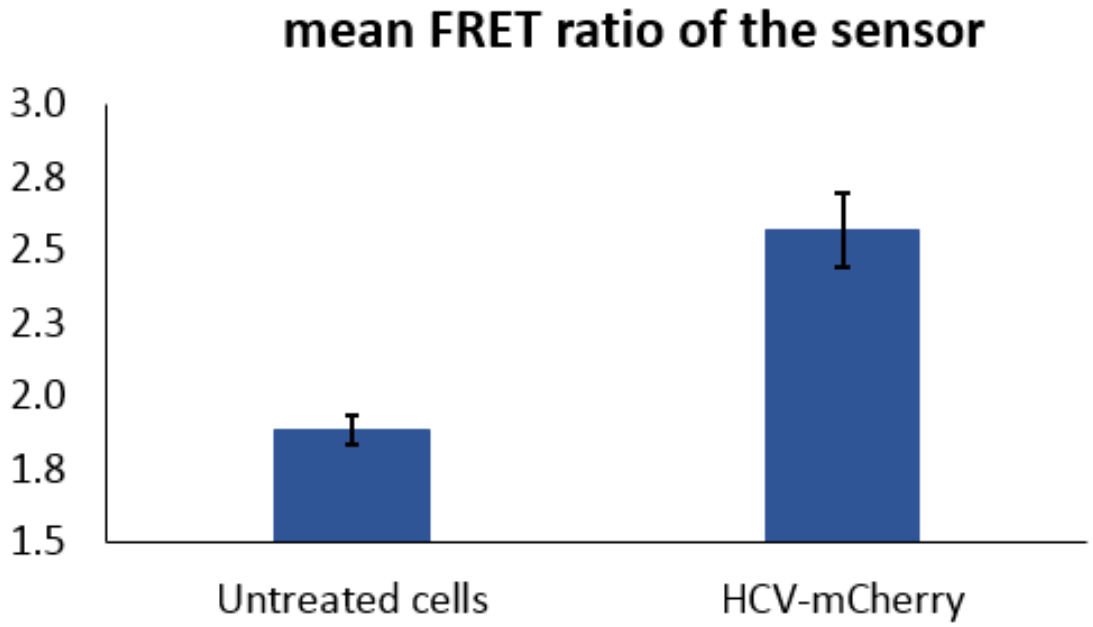

Figure 35. Mean FRET/CFP ratio across several Huh7 cells with the sensor (n=31 and n=33 respectively) after the infection with TCP_{HCV}(48 h after transfection).

Counter-intuitively, the peak response of the sensor in case of the TCP_{HCV} infection comes later, then one after the HCV replicon transfection. I expected the translation and replication of viral RNA to begin immediately after the infection, but it was not the case.

Similarly to the HCV replicon experiment, after a certain period of time I can observe the massive cell death which is indicated by lower FRET readout compared to the non-treated cells. The difference from the HCV RNA transfection experiment, though, was much a higher cell death rate. This fact makes finding the peak FRET response time or measuring the kinetics of replication even more difficult.

Application for viral infection

The fact that I can observe FRET response during a short window of time after the infection, cell-to-cell variability of the infection time and high toxicity of the produced viral RNA steered me away from using a full Hepatitis C virus for the infection. Since the infected cell will be not labeled with the wild type virus under the microscope I decided to use a similar virus with even higher replication efficiency. We decided to try Dengue virus (DENV) – also a single-stranded positive-sense RNA virus. The difference of DENV from HCV is a higher replication rate and a different mechanism of packaging newly produced RNA genome in the cell into a new particle at the ER.

Unfortunately, the results of the infection of Huh7 cell expressing KRP2 were very inconclusive. There were many cells having high FRET ratio, but also many cells rapidly dying. It was impossible to determine the peak FRET readout time point and the variability in FRET response from cell to cell was enormous.

Different color version of the FRET sensor

Following the advancements in fluorescent protein development and increased use of multiple sensors in one system, it becomes more and more

common to design a sensor in different “colors”. In a case of FRET it is usually inefficient because FRET pairs other than CFP/YFP (BFP/GFP or YFP/RFP) are less then optimal with often appearing problems of cross-excitation and/or bleedthrough. However, following the publication of the new red fluorescent protein with high quantum yield and brightness - mScarlet (Bindels et al., 2017) I decided to expand the color palette of my sensor into the red range.

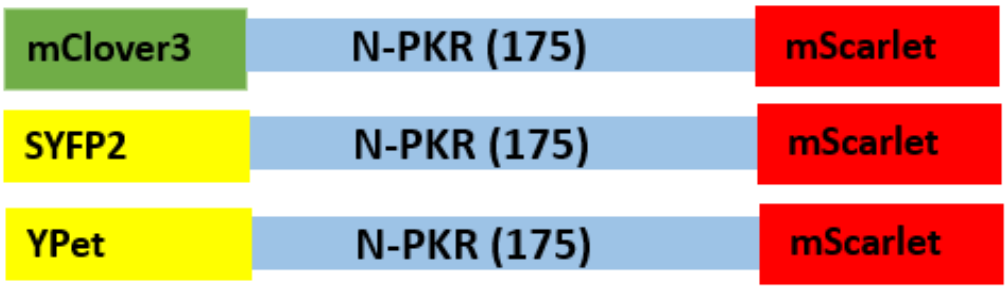

Figure 36. Schematic representation of the different color versions of the FRET sensor.

In this publication the authors not only designed a new red fluorescent protein but also successfully tested it in the FRET set up with one green (mClover3) and two yellow fluorescent proteins (SYFP2 and YPet). Consequently, I replaced CFP and YFP in my sensor with mScarlet and one of those three proteins (Figure 36) to test the FRET readout *in vitro* and in live cells.

Similarly to the original sensor, I expressed newly cloned version of KRP2 in HeLa cells and measured emission fluorescent spectra of the native lysate in the cuvette in the presence or the absence of dsRNA. The lysate of mClover3 version of the sensor was excited with 505 nm, and yellow versions – with 517 nm (Figure 37). Strictly speaking, mClover3 is not a green version, but rather an in-between version of green and yellow, with the excitation maximum shifted from 488 nm of GFP to 505 nm (which makes it more suitable for FRET with the red fluorescent protein compared to GFP). Fortunately, FRET was observed in all cases and, as expected, FRET ratio changed was observed during the titration with dsRNA (Figure 37a). The maximum FRET ratio change of the

mClover3 version was lower compared to yellow versions, and latter had lower maximum readout compared to the CFP/YFP original version (Figure 37b). There was no significant difference among SYFP2 and YPet, which is expected because SYFP2, YPet, Venus and other improved yellow fluorescent proteins have very similar spectrophotometric properties among each other. The control trypsin digestion disposed of the FRET in the same way as with the original version of the sensor.

The YPet/mScarlet version of the sensor was picked for testing against dsRNA in live cells. The sensor was expressed in HeLa cell and transfected with dsRNA the next day. As expected, I observed a FRET ratio increase in many cells transfected with dsRNA compared to the non-treated cells (Figure 38).

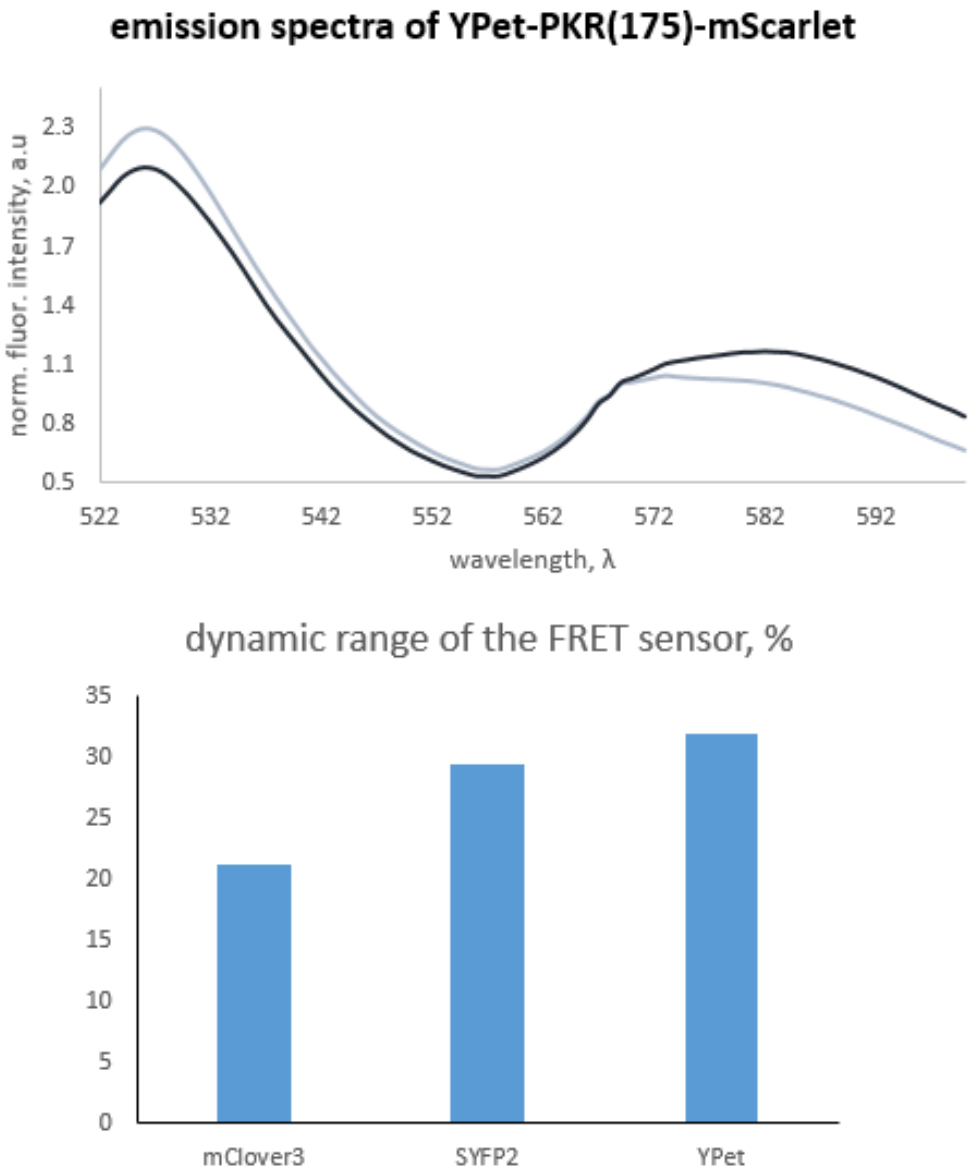

Figure 37. Example emission spectra of on the YPet/mScarlet version of the sensor before the addition (light line) and after the addition of dsRNA (darker line) (a) and max FRET ratio change of all of the version of the sensor (b)

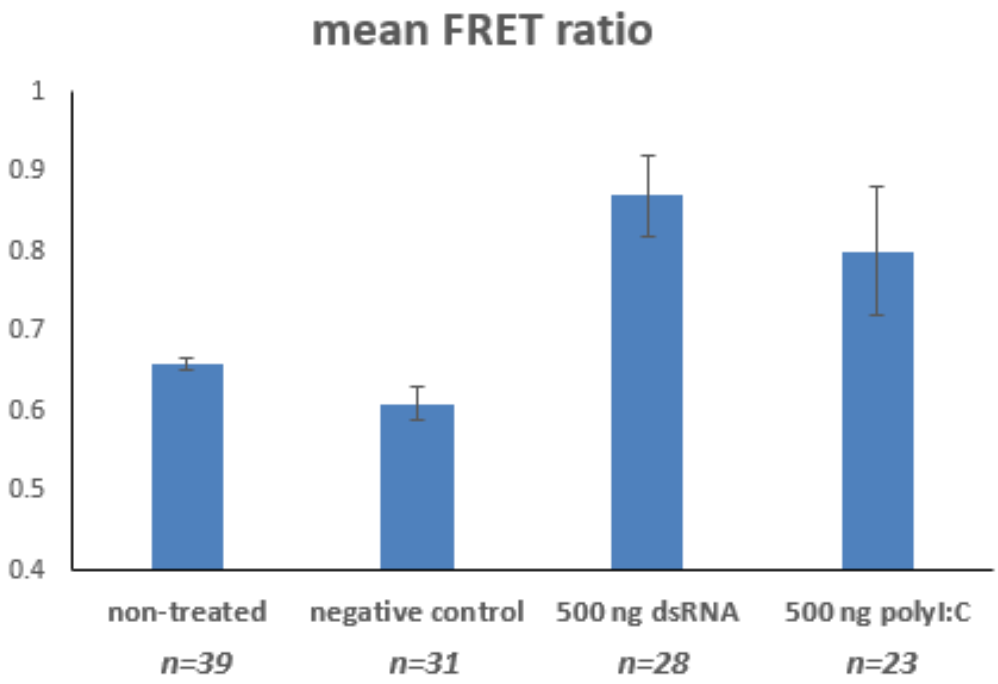

Figure 38. Mean FRET/YFP ratio across several HeLa cells expressing YPet/mScarlet version of the sensor (5h after dsRNA transfection).

Discussion

Sensor design

As mentioned before, the sensor design chosen in this work (among many others) was based the N-terminal domain of PKR placed between a fluorescent protein FRET pair. Our hypothesis was that upon binding double-stranded RNA the PKR (1-175) domain will wrap around the RNA molecule and change its conformation to a more closed one which will lead to a FRET increase between the fluorescent proteins. The hypothesis was correct as can be seen from fluorescent spectra of the sensor collected before and after addition of double-stranded RNA.

I can see that before the addition of any RNA there is some initial FRET between two fluorescent proteins in the sensor indicating that N- and C-termini are somewhat close to each other. This is expected and acceptable for the type of FRET sensors that use whole proteins or whole domains of the proteins as a sensing unit. In the case like that it is hard to influence the resting configuration of the protein or a protein domain. Ideal initial "no-FRET' state can be seen in the sensors where fluorescent protein FRET pair is separated with multiple protein domains in the sensor construct, or when the sensor consist of two separate parts each carrying a fluorescent protein which come together after the analyte presence (for example, dimerization FRET). After the addition of double-stranded RNA I clearly see a significant increase in FRET meaning that the fluorescent proteins come closer to each other. The FRET ratio change is quite high for this type of FRET sensors. The reason is that the N-terminal domain of PKR by itself consists of two subdomains separated by an unstructured region (which serves as linker between two almost symmetrical parts of the sensor) which resembles the structure of some of the FRET sensors artificially constructed out of several domains.

From the optimization experiments we can conclude that the addition of any sort of linkers between the "sensing" domain of the sensor and the fluorescent proteins impairs the readout. Flexibility in the sensor structure in this case is detrimental to the sensor response, while more rigid structure is more optimal for the FRET. Very interestingly, the orientation of the fluorophores in the sensor had a significant effect on the FRET response. By changing circularly permutated versions of one of the fluorescent proteins (the optimal version of YFP in the current sensor was "wild-type") we managed to increase the dynamic range of the sensor more than two times, while the proximity between two fluorescent protein remain the same.

Substituting the optimal CFP/YFP pair to YFP/RFP pair substantially reduced the dynamic range of KRP1 despite using a new extremely bright version of RFP as an acceptor – mScarlet (with the twice higher quantum yield than mCherry). The use of even the most novel and bright fluorescent protein still cannot match the CFP/YFP pair in terms of FRET efficiency. Still worth mentioning, though, that the continuous development in the fluorescent protein filed has permitted to have alternative color versions of FRET sensors with reasonable readout.

Sensor interaction with double-stranded RNA

Sensors is able to detect double-stranded RNA very efficiently. In this work I confirmed numerous previous reports suggested that PKR binds double-stranded RNA sequence-independently (Mayo and Cole, 2017, Husain et al., 2015, Patel et al., 2012, Nallagatla et al., 2011, Lemaire et al., 2008). During the project several dsRNAs were tested with the sensor: 30 bp RNA duplex (previously reported to be of a minimal length required for a proper PKR activity, (Lemaire et al., 2008)), different polyI:C mixtures (polymer nucleic acid mixture of relatively short or relatively long length which is commonly used to induce an interferon response and mimic viral infection), 200 bp double-stranded RNA duplex (randomly chosen, first 200 nt of the ampicillin sequence) and polyA:U

mix (alternative to polyI:C in mimicking a viral infection response, activates different receptors in the cell). In all cases, the same FRET ratio change was observed. Among these different RNA versions the response depended on the total mass of the added substrate rather than the "moles" which indicates that several PKR molecules can land on top of one RNA duplex up until it is fully covered.

Moreover, in current work I confirmed previous studies reporting extreme specificity of the PKR to dsRNA. PKR did show any significant FRET response (and therefore no binding) to any other nucleic acid molecule both *in vitro* and in the live cells. This is due to a perfect fit of the N-terminal domain of PKR to the A-helix structure of dsRNA discussed in the introduction section of this thesis. PKR can even differentiate dsRNA from the RNA/DNA duplex (Zheng and Bevilacqua, 2004), although this was not tested in this work.

Additionally, I took advantage of the observation made by many FRET sensor users which claim that the unspecific proteases can cleave the FRET sensor much quicker than the fluorescent proteins which results in the loss of FRET but the fluorescence remains. During the *in vitro* measurements in the fluorimeter I routinely added trypsin to the sensor before or after the addition of RNA to see the loss of FRET and the recovery of the CFP fluorescence as a control for CFP bleedthrough and YFP cross-excitation. The trypsin digestion indeed targeted fluorescent proteins (or at very least the fluorophores protected by the tight β-barrel structure) significantly slower.

Sensor performance in live cells

In this thesis we proved the ability to detect dsRNA with the sensor in live cells via the fluorescent microscopy. For the sensor imaging it is possible to use either widefield fluorescent microscope (high intensity, signal bleedthrough depends on the quality of the emission filters), confocal microscope (lower intensity, sharper cells for more convenient image analysis and minimal bleedthrough or cross-excitation) or any derivatives of the confocal microscope

like the “spinning-disk”. I successfully tested the sensor not only in HeLa and Huh7 cells (data shown) but also in HEK293T, COS7 and MIN6 cells (data not shown). As expected, the sensor works via direct binding to dsRNA and the biological environment is irrelevant to the sensor performance. Therefore, the sensor can be used in any cell line provided the RNA can be introduced inside the cell.

The FRET ratio of the sensor is independent of the expression level of the sensor inside the cell. This feature is very appealing since, often, FRET of the sensor in the absence of the substrate can still vary from cell to cell depending on the expression level (for example, some kinase sensors which can partly be phosphorylated by other cellular kinases).

Sensor is able to detect all types of dsRNA used in this work. The clear FRET ratio increase observed in some cells clearly indicates cells which were transfected with RNA. Individual cells might even show the maximum possible FRET ratio change, although these cells will rapidly die due to a very high amount of dsRNA present in them. The time when the FRET response can be observed begins after 5h after the RNA transfection (the time needed for the RNA/transfection reagent complex to move inside the cell), and after ~8h the cells start to rapidly undergo the apoptosis. Moreover, endogenous PKR seem to not interfere with the sensor performance even after the long dsRNAs induces overexpression of the kinase via the interferon response. This is unsurprising due to the high amount of transfected dsRNA and the overexpression of the sensor inside the cell.

Additional bonus of the sensor, clearly visible in the RNA experiments, is the ability to detect apoptotic cells via drop of FRET. This feature is fairly common in FRET sensors which experience FRET increase in the presence of the substrate. During the apoptosis unspecific proteases cleave the sensor which results in the loss of FRET, detectible under the microscope.

Sensor for the viral infection

While the cell line type is irrelevant for the sensor performance during the study, it might be important for the virus replication. In case of HCV, which was an RNA virus of interest in this work, the cell line of choice was Huh7.

Among three types of viral experiments performed here (transfection of the subgenomic RNA_{HCV} replicon, TCP infection or full viral infection) the RNA_{HCV} replicon provided the most unambiguous and clear results. The FRET response of the sensor to the viral RNA is bell-shaped. Enough quantity of the dsRNA intermediate (produced due to the self-replication of viral RNA) for KRP2 detection appears to be around 20 h after the transfection. The peak FRET response comes around 30 h after the transfection. Longer time results in FRET decay to the level of untreated cells followed by the significant drop of FRET due to the cell death.

There have been three potential obstacles for the application of KRP2 for viral infection: competition of the endogenous PKR with the sensor for RNA binding, not enough quantity of produced dsRNA during the replication, and coverage of produced viral dsRNA with other proteins which would prevent the sensor binding. The first two obstacles were proven invalid in the case of HCV – I could clearly detect the cells with high FRET after some period of time (enough to accumulate the necessary minimum amount of dsRNA). Interestingly enough, FRET of the cells seem to drop down after long period of time which is related, as we presume, with the transfer and accumulation of all viral RNA near ER wrapped in membrane-type structures (like vesicles) (El-Hage and Luo, 2003, Gosert et al., 2003, Ashfaq et al., 2011). Since the RNA cannot be released due to the lack of viral structural proteins, the cell undergoes the apoptosis which leads to the drop of FRET.

The infection with the TCPs of HCV resulted in a similar sensor response trend: rise of FRET during the accumulation of the viral RNA inside the cell

followed by a FRET decay. Curiously, the kinetics in case of TCP_{HCV} infection seemed to "lag" compared to the transfection of RNA_{HCV} replicon. The mCherry signal coming from translation of the viral RNA and peak FRET response of the sensor were observed around 10 h later (with significant cell-to-cell variability though) compared to the subgenomic replicon case. One could expect the viral cell entry to be quicker (Meertens et al., 2006) than the transfection (~2h vs ~6h) and be a determining factor deciding the beginning of viral replication and translation. However, RNA accessibility after the viral cell entry is limited for some time. I speculate the reason for to be the decapsulisation of the HCV nucleocapsid which, apparently, takes a significant amount of time. The FRET decay after a certain period of time is, probably, of the same origin as in the case of the HCV subgenomic RNA replication discussed before. The last difference between the viral RNA transfection and the TCP_{HCV} infection is a much higher toxicity of the latter to the cells (which can be concluded by monitoring cells appearing with a vanished FRET).

Potential applications of the sensor

The original motivation for the sensor design was the ability to monitor the replication of RNA viruses in live cells. However, during the sensor testing many other potential applications have emerged.

Because of the fact that the sensor has proven to be a very sensitive and extremely specific to any dsRNA, it can be used to determine levels of dsRNA both *in vitro* and *in vivo*. For the *in vitro* studies, the sensor can be expressed and purified, added to the solution potentially containing the dsRNA followed by the measurement of the emission spectra to determine FRET compared to the negative control. The examples could be a detection of produced viral dsRNA in the supernatant of the cells infected with the RNA virus or determination of the *in vitro* transcription efficiency as an alternative to agarose gel electrophoresis or northern blots. As for *in vivo* applications, spike in dsRNA levels inside the cell

can be clearly visible with the sensor under the microscope. For instance, one could monitor cells transfected with the specific siRNA in gene silencing experiments or localization of some overexpressed miRNAs during the posttranscriptional regulation of protein expression.

Another direction in which the sensor can be applied are studies of the PKR biology since the sensor is based on the N-terminal RNA-binding domain of the kinase. The most obvious use of the sensor is the study of RNA binding to PKR. During current thesis, FRET turned out to be a very convenient tool to determine the RNA-PKR binding compared to performing pull-downs/western-blots or Isothermal Titration Calorimetry assays (ITC) which were done in the previous PKR-related works. By monitoring FRET change, we confirmed previous reports of PKR binding to RNA be structurally-specific and sequence-independent and, also, sufficiency of 30 bp of dsRNA for the efficient binding of PKR. To extend the understanding of PKR-RNA interaction, the sensor can be used to determine the minimum length of dsRNA necessary for the efficient binding (hypothesized to be around 12 nt (Sambasivarao Nanduri, 1998)) or to study the impact of the nucleotide modifications in dsRNA on the PKR binding ability. Moreover, the sensor can be used to study the structure of the N-terminal domain of PKR or change in localization of PKR in response to different stimuli. Monitoring FRET change in this work I could confirm the hypothesis that the structure of the N-terminal domain of PKR bends during the dsRNA binding, "wrapping" around the molecule. Additionally, in a separate unrelated to dsRNA experiment, cells expressing the sensor were subjected to sodium arsenate treatment or UV stress. This, interestingly, caused the sensor to migrate from the cytoplasm to the nucleus (Supplementary figures S1 and S2) confirming one previously made observation that the PKR during the cellular stress unrelated to dsRNA eventually migrates to the nucleus via unknown mechanism (Hao et al., 2016).

Finally, the sensor can be applied to monitor the dsRNA production during the replication of the RNA viruses. We successfully shown that the sensor is able to detect the RNA of HCV for a short period of time. With the access to Biological safety 3 labs with the fluorescent microscope and different dsRNA- or ssRNA-viruses one can monitor dsRNA accumulation inside the cell with great sensitivity. Unfortunately, the sensor performance heavily rely on the constant accessibility of the RNA for binding which can be a major drawback. Despite a theoretically simple and straightforward mechanism of sensor performance, the biology of the virus cycle can significantly impact the ability to follow any replication. Furthermore, the toxicity of the viral infection plays a major role during the sensor performance. In this work, for example, I failed to clearly monitor Dengue virus replication despite a higher replication efficiency of Dengue compared to HCV because of the massive variability in FRET from cell-to-cell.

Challenges and failed FRET sensor designs

I uncovered many challenges during this project which should be discussed for the benefit of future related studies or application of the sensor.

The first and a major challenge in this work was the introduction of the dsRNA into the cells. The big size and the negative charge of RNA does not allow for an easy and rapid diffusion of RNA inside the cells in the live cell experiments unlike the small molecule stimuli in other published FRET sensors. The use of transfection added a variability factor to the RNA amount inside the cells and the spread from cell to cell. Moreover, the dsRNA turned out to be quite toxic for the cells and the transfection reagent only enhanced the toxicity. All that limited my ability to determine the precise kinetics of sensor's FRET response to RNA. The use of the electroporation as an alternative method wasn't successful.

In order to establish relation between the amount of RNA inside the live cells and a FRET response I attempted to use fluorescently labeled dsRNA.

Unfortunately, the hydrophobic nature of the dyes prevented the RNA to be internalized even in the presence of a transfection reagent. The labeled RNA was not able to penetrate the cellular membrane and ended up stuck in the membranes or accumulated in numerous vesicles. Alternatively, I tried to use microinjection to deliver fluorescently labeled RNA or a mixture of dsRNA with a soluble fluorescent dye. This lead to the leakage of the expressed sensor in the medium and loss of fluorescence. Waiting for the new sensor molecules to be expressed again and the fluorescence to recover was unsuccessful due to the apoptosis caused by the RNA inside the cell.

Finally, cell-to-cell variability and the toxicity of the infection, as well as shielding of the viral RNA after a certain period of time, prevented me to determine the precise kinetics of the replication of the HCV.

Separately, I will discuss some of the other FRET sensor designs which didn't work in the application to the dsRNA or viral infection. The most promising idea for a FRET sensor was based on exploiting the dimerization ability of the PKR. The PKR dimer on top of the dsRNA is expected to be symmetrical (rather than anti-symmetrical) and attaching a CFP/YFP pair of fluorescent proteins should lead to the appearance of FRET in the presence of RNA when the PKR monomers come close to each other. I cloned various PKR constructs, including full PKR with CFP or YFP on either of the N- or the C-terminal end, RNA-binding domain of PKR with CFP or YFP attached both to either N- or C-terminal end, all constructs having with various linkers lengh between the PKR part and the fluorescent protein. Addition of any type of dsRNA to the sensor both *in vitro* and in live cells did not lead to any FRET signal appearing. I can only conclude that there is something about the structure of the PKR dimer complex with dsRNA that is still unknown.

In the other sensor design I attached CFP and YFP to both ends of full PKR and check for any conformational changes (which would lead to change in FRET signal) upon dsRNA binding. Some researchers speculate that in the resting state

RNA-binding and the catalytic domains of PKR are in a closed conformation relative to each other. This conformation is expected to open up upon the binding to dsRNA and dimerization. In the sensor I didn't observe any FRET in the absence of dsRNA, therefore the fluorescent proteins were not close to each other. This leads me to believe that the previously described hypothesis about the latent PKR conformation is false. The addition of dsRNA also didn't lead to appearance of FRET making the sensor inapplicable.

Rather than detecting dsRNA presence or PKR dimerization, I attempted to design sensors to monitor the activity of PKR. The target of PKR activated via autophosphorylation is eIF2α. I cloned CFP and YFP on the both ends of eIF2α hoping that the phosphorylation of the initiation factor will lead to a conformational and, hence, FRET change. I also sandwiched the truncated versions of eIF2α between CFP/YFP pair: eIF2α (1-120) and eIF2α (13-90), both of which retained the Ser51 phosphorylation site and consisted of completed structural motifs. The phosphorylation of this sensors in both in vitro and live cell experiments did not lead to any FRET change, potentially denying the hypothesis of the conformational change in the eIF2α during the phosphorylation.

As a final attempt to detect the activity of PKR, I tried to construct an artificial sensor on the scaffold of some other popular kinase activity FRET sensors. This type of sensors contain the CFP and YFP pair on the termini, a target-peptide of phosphorylation, flexible long linker and a phosphorylated amino acid-binding (PAAB) domain (Figure 7C). I used a eIF2α(45-56) 11-amino acid peptide in this design, altering different PAAB domains and introducing single amino acid mutations in the peptide for improved the phosphorylation efficiency or PAAB domain binding efficiency. The total of 20 different combinations of the sensor were tested both in vitro and in live cells, but a significant FRET change wasn't observed (especially compared to KRP1 and KRP2 performance). I also observed the unusually high phosphorylation level of the sensor even in the absence of any stimuli, which lead me to a conclusion that

the peptide in the sensor can be efficiently phosphorylated by the abundant cellular kinases, most probably PKA (Mellor and Proud, 1991, Proud et al., 1991).

Conclusions and outlook

- In this work I designed a genetically encoded FRET sensor for the purpose of detecting the replication of RNA viruses in live cells via fluorescent microscopy.
- A FRET sensor named KRP1 consists of the N-terminal domain of protein kinase R (PKR 1-175) and mTurquoise/cp173Venus fluorescent protein pair.
- For the sensor design I exploited the ability of the N-terminal domain of PKR to bind dsRNA followed by a change of its conformation.
- *In vitro* experiments showed that the sensor binds dsRNA very efficiently, structure specifically and sequence –independently. The dynamic range (the maximum FRET ratio change) of this version of the sensor was 42%, which is quite high for this type of FRET sensors.
- I successfully optimized the sensor using the FRET sensor optimization library previously developed in our lab. A version named KRP2 consists of mECFP, Venus (WT) and PKR (1-175) with a more than twice higher dynamic range of 92%.
- The sensor was proven to work for the detection of dsRNA in various types of live cells with the help of widefield or confocal fluorescent microscopy.
- I created an alternative yellow/red version of the sensor with the reduced but still acceptable dynamic range (possible due to the development of the new version of mCherry – mScarlet).
- KRP2 was able to detect viral RNA produced during the HCV replication.
- Cell-to-cell variability and the toxicity of the infection, as well as shielding of the viral RNA after a certain period of time, prevented me to determine the precise kinetics of the replication of the HCV.
- Due to the simplicity of the working mechanism and the efficiency of RNA binding, KRP2 can have a wide range of potential application, including

studies of the PKR biology, detection of dsRNA or potentially monitoring replication of different RNA viruses (especially promising for the dsRNA viruses).

References

ADAIR, R., PATEL, A. H., CORLESS, L., GRIFFIN, S., ROWLANDS, D. J. & MCCORMICK, C. J. 2009. Expression of hepatitis C virus (HCV) structural proteins in trans facilitates encapsidation and transmission of HCV subgenomic RNA. *J Gen Virol,* 90**,** 833-42.

ANSBACHER, T., SRIVASTAVA, H. K., STEIN, T., BAER, R., MERKX, M. & SHURKI, A. 2012. Calculation of transition dipole moment in fluorescent proteins--towards efficient energy transfer. *Phys Chem Chem Phys,* 14**,** 4109-17.

APPLEBY, T. C., PERRY, J. K., MURAKAMI, E., BARAUSKAS, O., FENG, J., CHO, A., FOX, D., 3RD, WETMORE, D. R., MCGRATH, M. E., RAY, A. S., SOFIA, M. J., SWAMINATHAN, S. & EDWARDS, T. E. 2015. Viral replication. Structural basis for RNA replication by the hepatitis C virus polymerase. *Science,* 347**,** 771-5.

ASHFAQ, U. A., JAVED, T., REHMAN, S., NAWAZ, Z. & RIAZUDDIN, S. 2011. An overview of HCV molecular biology, replication and immune responses. *Virol J,* 8**,** 161.

BANDO, Y., ONUKI, R., KATAYAMA, T., MANABE, T., KUDO, T., TAIRA, K. & TOHYAMA, M. 2005. Double-strand RNA dependent protein kinase (PKR) is involved in the extrastriatal degeneration in Parkinson's disease and Huntington's disease. *Neurochem Int,* 46**,** 11-8.

BARTENSCHLAGER, R. & LOHMANN, V. 2000. Replication of hepatitis C virus. *J Gen Virol,* 81**,** 1631-48.

BINDELS, D. S., HAARBOSCH, L., VAN WEEREN, L., POSTMA, M., WIESE, K. E., MASTOP, M., AUMONIER, S., GOTTHARD, G., ROYANT, A., HINK, M. A. & GADELLA, T. W., JR. 2017. mScarlet: a bright monomeric red fluorescent protein for cellular imaging. *Nat Methods,* 14**,** 53-56.

BOLBAT, A. & SCHULTZ, C. 2017. Recent developments of genetically encoded optical sensors for cell biology. *Biol Cell,* 109**,** 1-23.

BULLIDO, M. J., MARTINEZ-GARCIA, A., TENORIO, R., SASTRE, I., MUNOZ, D. G., FRANK, A. & VALDIVIESO, F. 2008. Double stranded RNA activated EIF2 alpha kinase (EIF2AK2; PKR) is associated with Alzheimer's disease. *Neurobiol Aging,* 29**,** 1160-6.

BULUSU, V., PRIOR, N., SNAEBJORNSSON, M. T., KUEHNE, A., SONNEN, K. F., KRESS, J., STEIN, F., SCHULTZ, C., SAUER, U. & AULEHLA, A. 2017. Spatiotemporal Analysis of a Glycolytic Activity Gradient Linked to Mouse Embryo Mesoderm Development. *Dev Cell,* 40**,** 331-341 e4.

BURWICK, N. & AKTAS, B. H. 2017. The eIF2-alpha kinase HRI: a potential target beyond the red blood cell. *Expert Opin Ther Targets,* 21**,** 1171-1177.

CASTILHO, B. A., SHANMUGAM, R., SILVA, R. C., RAMESH, R., HIMME, B. M. & SATTLEGGER, E. 2014. Keeping the eIF2 alpha kinase Gcn2 in check. *Biochim Biophys Acta,* 1843**,** 1948-68.

CHATEL-CHAIX, L., CORTESE, M., ROMERO-BREY, I., BENDER, S., NEUFELDT, C. J., FISCHL, W., SCATURRO, P., SCHIEBER, N., SCHWAB, Y., FISCHER, B., RUGGIERI, A. & BARTENSCHLAGER, R. 2016. Dengue Virus Perturbs Mitochondrial Morphodynamics to Dampen Innate Immune Responses. *Cell Host Microbe,* 20**,** 342-356.

CHEN, K. X. & NJOROGE, F. G. 2009. A review of HCV protease inhibitors. *Curr Opin Investig Drugs,* 10**,** 821-37.

DAR, A. C., DEVER, T. E. & SICHERI, F. 2005. Higher-order substrate recognition of eIF2alpha by the RNA-dependent protein kinase PKR. *Cell,* 122**,** 887-900.

DE HARO, C., MENDEZ, R. & SANTOYO, J. 1996. The eIF-2alpha kinases and the control of protein synthesis. *FASEB J,* 10**,** 1378-87.

DEY, M., CAO, C., DAR, A. C., TAMURA, T., OZATO, K., SICHERI, F. & DEVER, T. E. 2005. Mechanistic link between PKR dimerization, autophosphorylation, and eIF2alpha substrate recognition. *Cell,* 122**,** 901-13.

DZANANOVIC, E., MCKENNA, S. A. & PATEL, T. R. 2018. Viral proteins targeting host protein kinase R to evade an innate immune response: a mini review. *Biotechnol Genet Eng Rev,* 34**,** 33-59.

EL-HAGE, N. & LUO, G. 2003. Replication of hepatitis C virus RNA occurs in a membrane-bound replication complex containing nonstructural viral proteins and RNA. *J Gen Virol,* 84**,** 2761-9.

GARCIA-ORTEGA, M. B., LOPEZ, G. J., JIMENEZ, G., GARCIA-GARCIA, J. A., CONDE, V., BOULAIZ, H., CARRILLO, E., PERAN, M., MARCHAL, J. A. & GARCIA, M. A. 2017. Clinical and therapeutic potential of protein kinase PKR in cancer and metabolism. *Expert Rev Mol Med,* 19**,** e9.

GARCIA, M. A., MEURS, E. F. & ESTEBAN, M. 2007. The dsRNA protein kinase PKR: virus and cell control. *Biochimie,* 89**,** 799-811.

GOSERT, R., EGGER, D., LOHMANN, V., BARTENSCHLAGER, R., BLUM, H. E., BIENZ, K. & MORADPOUR, D. 2003. Identification of the hepatitis C virus RNA replication complex in Huh-7 cells harboring subgenomic replicons. *J Virol,* 77**,** 5487-92.

HAO, C., SHAO, R., RAJU, U., FANG, B., SWISHER, S. G. & PATAER, A. 2016. Accumulation of RNA-dependent protein kinase (PKR) in the nuclei of lung cancer cells mediates radiation resistance. *Oncotarget,* 7**,** 38235-38242.

HOCHREITER, B., GARCIA, A. P. & SCHMID, J. A. 2015. Fluorescent Proteins as Genetically Encoded FRET Biosensors in Life Sciences. *Sensors (Basel),* 15**,** 26281-314.

HUSAIN, B., HESLER, S. & COLE, J. L. 2015. Regulation of PKR by RNA: formation of active and inactive dimers. *Biochemistry,* 54**,** 6663-72.

IRSHAD, M., KHUSHBOO, I., SINGH, S. & SINGH, S. 2008. Hepatitis C virus (HCV): a review of immunological aspects. *Int Rev Immunol,* 27**,** 497-517.

ISHII, K., MURAKAMI, K., HMWE, S. S., ZHANG, B., LI, J., SHIRAKURA, M., MORIKAWA, K., SUZUKI, R., MIYAMURA, T., WAKITA, T. & SUZUKI, T. 2008. Trans-encapsidation of hepatitis C virus subgenomic replicon RNA with viral structure proteins. *Biochem Biophys Res Commun,* 371**,** 446-50.

KAUFMANN, S. H. E., DORHOI, A., HOTCHKISS, R. S. & BARTENSCHLAGER, R. 2018. Host-directed therapies for bacterial and viral infections. *Nat Rev Drug Discov,* 17**,** 35-56.

KING, A. M. Q., LEFKOWITZ, E. J., MUSHEGIAN, A. R., ADAMS, M. J., DUTILH, B. E., GORBALENYA, A. E., HARRACH, B., HARRISON, R. L., JUNGLEN, S., KNOWLES, N. J., KROPINSKI, A. M., KRUPOVIC, M., KUHN, J. H., NIBERT, M. L., RUBINO, L., SABANADZOVIC, S., SANFACON, H., SIDDELL, S. G., SIMMONDS, P., VARSANI, A., ZERBINI, F. M. & DAVISON, A. J. 2018. Changes to taxonomy and the International Code of Virus Classification and Nomenclature ratified by the International Committee on Taxonomy of Viruses (2018). *Arch Virol*.

KOHLI, A., SHAFFER, A., SHERMAN, A. & KOTTILIL, S. 2014. Treatment of hepatitis C: a systematic review. *JAMA,* 312**,** 631-40.

KOMATSU, N., AOKI, K., YAMADA, M., YUKINAGA, H., FUJITA, Y., KAMIOKA, Y. & MATSUDA, M. 2011. Development of an optimized backbone of FRET biosensors for kinases and GTPases. *Mol Biol Cell,* 22**,** 4647-56.

KOONIN, E. V. & DOLJA, V. V. 1993. Evolution and taxonomy of positive-strand RNA viruses: implications of comparative analysis of amino acid sequences. *Crit Rev Biochem Mol Biol,* 28**,** 375-430.

KUCHENOV, D., LAKETA, V., STEIN, F., SALOPIATA, F., KLINGMULLER, U. & SCHULTZ, C. 2016. High-Content Imaging Platform for Profiling Intracellular Signaling Network Activity in Living Cells. *Cell Chem Biol,* 23**,** 1550-1559.

LEMAIRE, P. A., ANDERSON, E., LARY, J. & COLE, J. L. 2008. Mechanism of PKR Activation by dsRNA. *J Mol Biol,* 381**,** 351-60.

LI, C. X., SHI, M., TIAN, J. H., LIN, X. D., KANG, Y. J., CHEN, L. J., QIN, X. C., XU, J., HOLMES, E. C. & ZHANG, Y. Z. 2015. Unprecedented genomic diversity of RNA viruses in arthropods reveals the ancestry of negative-sense RNA viruses. *Elife,* 4.

LIU, Z., LV, Y., ZHAO, N., GUAN, G. & WANG, J. 2015. Protein kinase R-like ER kinase and its role in endoplasmic reticulum stress-decided cell fate. *Cell Death Dis,* 6**,** e1822.

LOHMANN, V., KORNER, F., KOCH, J., HERIAN, U., THEILMANN, L. & BARTENSCHLAGER, R. 1999. Replication of subgenomic hepatitis C virus RNAs in a hepatoma cell line. *Science,* 285**,** 110-3.

LU, J., O'HARA, E. B., TRIESELMANN, B. A., ROMANO, P. R. & DEVER, T. E. 1999. The interferon-induced double-stranded RNA-activated protein kinase PKR will phosphorylate serine, threonine, or tyrosine at residue 51 in eukaryotic initiation factor 2alpha. *J Biol Chem,* 274**,** 32198-203.

LUXENBURGER, H., NEUMANN-HAEFELIN, C., THIMME, R. & BOETTLER, T. 2018. HCV-Specific T Cell Responses During and After Chronic HCV Infection. *Viruses,* 10.

MATTHEWS, R. E. & MAURIN, J. 1979. [Virus classification and nomenclature. Summarized proceedings of the international committee on taxonomy of viruses. Lay Haye, September, 1978]. *Ann Microbiol (Paris),* 130 A**,** 133-6.

MAYO, C. B. & COLE, J. L. 2017. Interaction of PKR with single-stranded RNA. *Sci Rep,* 7**,** 3335.

MEERTENS, L., BERTAUX, C. & DRAGIC, T. 2006. Hepatitis C virus entry requires a critical postinternalization step and delivery to early endosomes via clathrin-coated vesicles. *J Virol,* 80**,** 11571-8.

MELLOR, H. & PROUD, C. G. 1991. A synthetic peptide substrate for initiation factor-2 kinases. *Biochem Biophys Res Commun,* 178**,** 430-7.

MEMON, M. I. & MEMON, M. A. 2002. Hepatitis C: an epidemiological review. *J Viral Hepat,* 9**,** 84-100.

MEURS, E., CHONG, K., GALABRU, J., THOMAS, N. S., KERR, I. M., WILLIAMS, B. R. & HOVANESSIAN, A. G. 1990. Molecular cloning and characterization of the human double-stranded RNA-activated protein kinase induced by interferon. *Cell,* 62**,** 379-90.

MODI, A. A. & LIANG, T. J. 2008. Hepatitis C: a clinical review. *Oral Dis,* 14**,** 10-4.

NALLAGATLA, S. R., TORONEY, R. & BEVILACQUA, P. C. 2011. Regulation of innate immunity through RNA structure and the protein kinase PKR. *Curr Opin Struct Biol,* 21**,** 119-27.

NGUYEN, M. & HAENNI, A. L. 2003. Expression strategies of ambisense viruses. *Virus Res,* 93**,** 141-50.

PATEL, S., BLOSE, J. M., SOKOLOSKI, J. E., POLLACK, L. & BEVILACQUA, P. C. 2012. Specificity of the double-stranded RNA-binding domain from the RNA-activated protein kinase PKR for double-stranded RNA: insights from thermodynamics and small-angle X-ray scattering. *Biochemistry,* 51**,** 9312-22.

PEEL, A. L., RAO, R. V., COTTRELL, B. A., HAYDEN, M. R., ELLERBY, L. M. & BREDESEN, D. E. 2001. Double-stranded RNA-dependent protein kinase, PKR, binds preferentially to Huntington's disease (HD) transcripts and is activated in HD tissue. *Hum Mol Genet,* 10**,** 1531-8.

PILJIC, A., DE DIEGO, I., WILMANNS, M. & SCHULTZ, C. 2011. Rapid development of genetically encoded FRET reporters. *ACS Chem Biol,* 6**,** 685-91.

PROUD, C. G., COLTHURST, D. R., FERRARI, S. & PINNA, L. A. 1991. The substrate specificity of protein kinases which phosphorylate the alpha subunit of eukaryotic initiation factor 2. *Eur J Biochem,* 195**,** 771-9.

ROTH, H., MAGG, V., UCH, F., MUTZ, P., KLEIN, P., HANEKE, K., LOHMANN, V., BARTENSCHLAGER, R., FACKLER, O. T., LOCKER, N., STOECKLIN, G. & RUGGIERI, A. 2017. Flavivirus Infection Uncouples Translation Suppression from Cellular Stress Responses. *MBio,* 8.

RUGGIERI, A., DAZERT, E., METZ, P., HOFMANN, S., BERGEEST, J. P., MAZUR, J., BANKHEAD, P., HIET, M. S., KALLIS, S., ALVISI, G., SAMUEL, C. E., LOHMANN, V., KADERALI, L., ROHR, K., FRESE, M., STOECKLIN, G. & BARTENSCHLAGER, R. 2012. Dynamic oscillation of translation and stress granule formation mark the cellular response to virus infection. *Cell Host Microbe,* 12**,** 71-85.

SAINZ, B., JR., TENCATE, V. & UPRICHARD, S. L. 2009. Three-dimensional Huh7 cell culture system for the study of Hepatitis C virus infection. *Virol J,* 6**,** 103.

SAMBASIVARAO NANDURI, B. W. C., YANWU YANG, BRYAN R.G.WILLIAMS AND JUN QIN 1998. Structure of the double-stranded RNA-binding domain of the protein kinase PKR reveals the molecular basis of its dsRNA-mediated activation. *The EMBO Journal,* 17**,** 5458-5465.

SCHULT, P., ROTH, H., ADAMS, R. L., MAS, C., IMBERT, L., ORLIK, C., RUGGIERI, A., PYLE, A. M. & LOHMANN, V. 2018. microRNA-122 amplifies hepatitis C virus translation by shaping the structure of the internal ribosomal entry site. *Nat Commun,* 9**,** 2613.

SEGEV, Y., BARRERA, I., OUNALLAH-SAAD, H., WIBRAND, K., SPORILD, I., LIVNE, A., ROSENBERG, T., DAVID, O., MINTS, M., BRAMHAM, C. R. & ROSENBLUM, K. 2015. PKR Inhibition Rescues

Memory Deficit and ATF4 Overexpression in ApoE epsilon4 Human Replacement Mice. *J Neurosci,* 35**,** 12986-93.

SEGEV, Y., LIVNE, A., MINTS, M. & ROSENBLUM, K. 2016. Concurrence of High Fat Diet and APOE Gene Induces Allele Specific Metabolic and Mental Stress Changes in a Mouse Model of Alzheimer's Disease. *Front Behav Neurosci,* 10**,** 170.

SEGEV, Y., MICHAELSON, D. M. & ROSENBLUM, K. 2013. ApoE epsilon4 is associated with eIF2alpha phosphorylation and impaired learning in young mice. *Neurobiol Aging,* 34**,** 863-72.

SEIPP, S., MUELLER, H. M., PFAFF, E., STREMMEL, W., THEILMANN, L. & GOESER, T. 1997. Establishment of persistent hepatitis C virus infection and replication in vitro. *J Gen Virol,* 78 (Pt 10)**,** 2467-76.

STEIN, F., KRESS, M., REITHER, S., PILJIC, A. & SCHULTZ, C. 2013. FluoQ: a tool for rapid analysis of multiparameter fluorescence imaging data applied to oscillatory events. *ACS Chem Biol,* 8**,** 1862-8.

STEINMANN, E., BROHM, C., KALLIS, S., BARTENSCHLAGER, R. & PIETSCHMANN, T. 2008. Efficient trans-encapsidation of hepatitis C virus RNAs into infectious virus-like particles. *J Virol,* 82**,** 7034-46.

TARGETT-ADAMS, P., BOULANT, S. & MCLAUCHLAN, J. 2008. Visualization of double-stranded RNA in cells supporting hepatitis C virus RNA replication. *J Virol,* 82**,** 2182-95.

TELESNITSKY, A. 2010. Retroviruses: Molecular Biology, Genomics and Pathogenesis. *Future Virol,* 5**,** 539-543.

WEBER, F., WAGNER, V., RASMUSSEN, S. B., HARTMANN, R. & PALUDAN, S. R. 2006. Double-stranded RNA is produced by positive-strand RNA viruses and DNA viruses but not in detectable amounts by negative-strand RNA viruses. *J Virol,* 80**,** 5059-64.

WICKNER, R. B. 1993. Double-stranded RNA virus replication and packaging. *J Biol Chem,* 268**,** 3797-800.

ZHENG, X. & BEVILACQUA, P. C. 2004. Activation of the protein kinase PKR by short double-stranded RNAs with single-stranded tails. *RNA,* 10**,** 1934-45.

Acknowledgments

I am very thankful to EMBL for giving me an opportunity to do my PhD here, gather indescribable experience and incredible scientists and research. I am also thankful to Carsten Schultz for having me in the lab and giving me the project. I want to thank my Thesis Advisory Committee members for discussions.

I want to thank my girlfriend Sinja for all the indescribable help and support from her.

I would like to thank Dr. Dmytro Yushchenko for constructive discussions and a positive attitude. I learned a lot about focusing on the right thing, managing a project and looking at the bigger picture.

Furthermore, I would like to thank Alessia Ruggieri and a PhD student from her lab Philipp Klein for all the help and time with the virology part of the project.

I want to separately thank Carsten for the incredible patience.

Finally, I want to acknowledge the big help of Susanne Ficht-Redmer in the lab.

Supplementary material

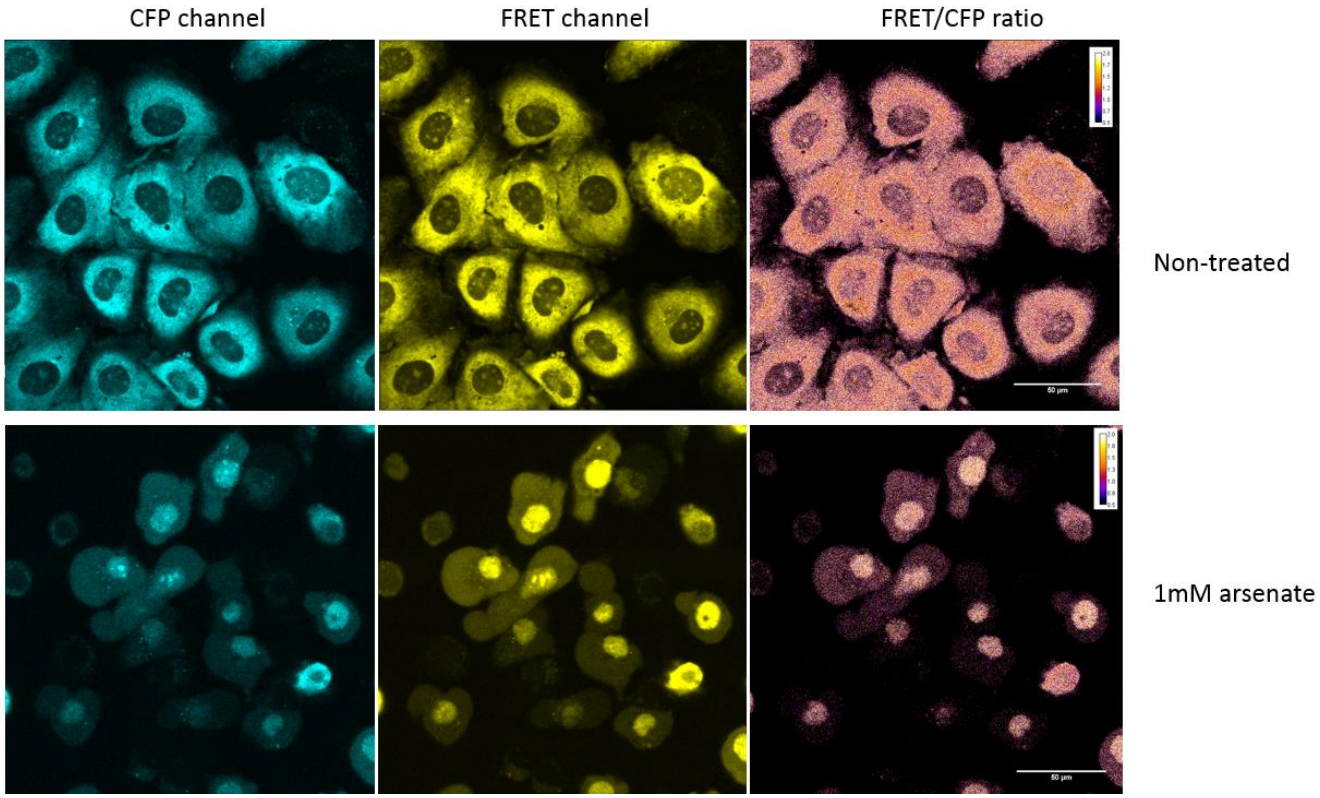

Figure S1. HeLa cells expressing KRP2 during stress.

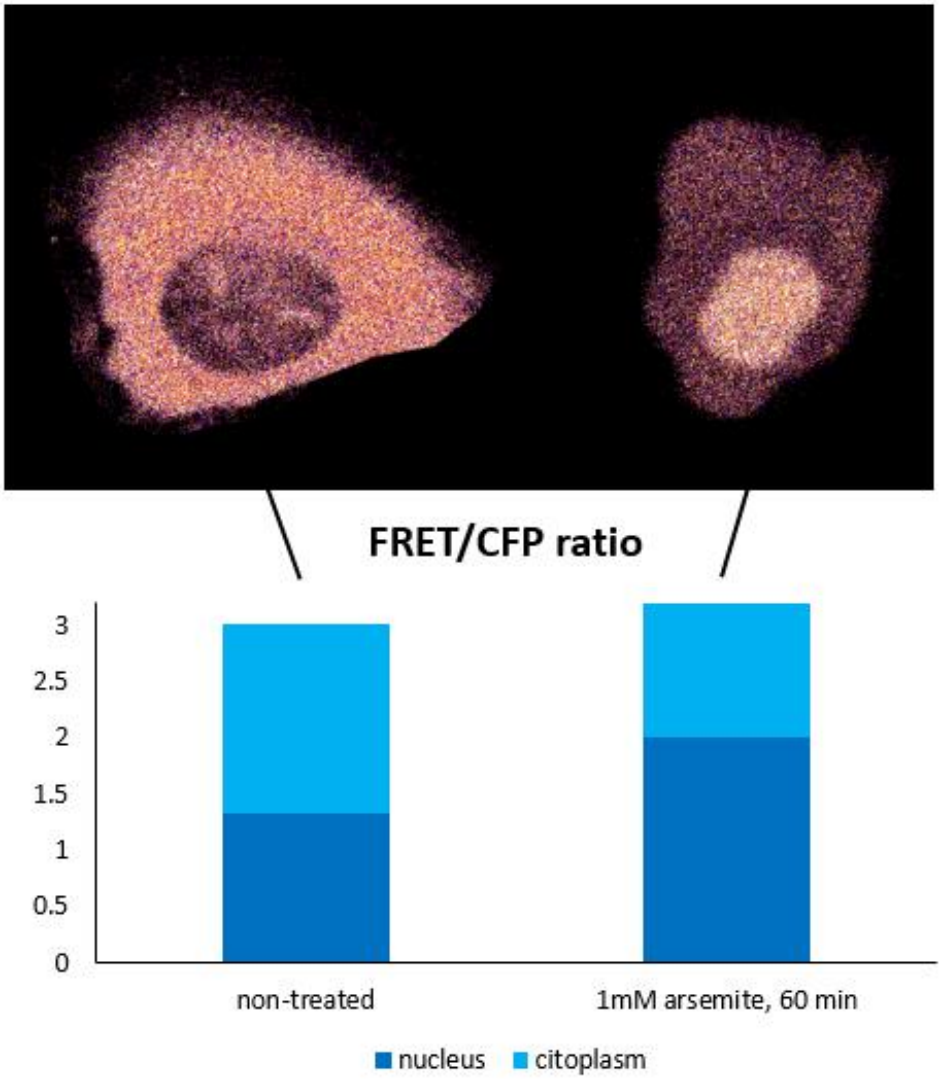

Figure S2. FRET ratio in the cytoplasm and the nucleus of HeLa cells expressing KRP2 before and after the stress.